SAPIENZA
UNIVERSITÀ DI ROMA

Ph.D. School in Environmental and Hydraulic Engineering

Curriculum: Environmental Engineering

Cycle XXX

# Back-Diffusion phenomena from low permeability layers of aquifers: laboratory investigations and numerical model

Tutor
Prof. Ing. Paolo Viotti

Ph.D. Student
Fabio Tatti

A.A. 2016-2017

# Contents

# ABSTRACT

The aim of this thesis is to study the redistribution process of contaminants from low to high-permeability zones of aquifers in order to improve groundwater remediation. When the plume emitted by the primary source of contamination encounters low permeability layers of aquifer generates a concentration gradient between the high and low aquifer permeability zones. A molecular diffusive flux hence is induced causing pollutant accumulation in the low permeable layers (Forward-Diffusion). After the primary source of contamination is reduced, the pollutant concentration in the transmissive zone decreases and the concentration gradient reverses. Previously stored contaminant is released by the so-called “Back-Diffusion” process, which causes a long plume tail. Thus, contaminated low permeability zones of aquifer represent long-term sources of contamination, today considered as one of the main obstacles to effective groundwater remediation.

The Back-Diffusion phenomenon was reproduced at laboratory scale reconstructing an aquifer characterized by a high-permeability layer and three different low-permeability zones. The measurement of contaminant fluxes released from the low permeability lenses by image analysis technique permitted to evaluate the influence of the lenses granulometry on the pollutant redistribution process. The results show that the lower the average grain dimension of the formation is, the higher the flux is and the longer the time for which the values of the released concentration can constitute a source of contamination.

It is known the large use of pumping technologies to restore groundwater, so the efficiency of the traditional pumping technology to remediate contaminated low permeability zones of aquifer was investigated by laboratories tests. The remediation time of the three lenses were calculated under different groundwater velocities using the diffusive flux values obtained by image analysis.  In this way, a relation between “groundwater velocity” and “remediation time” was determined for each lens. This relation shows the low efficiency of the traditional pumping system to restore contaminated low permeability zones of aquifers, demonstrating the need to use alternative technologies. The Groundwater Circulation Well (GCW) system was investigated as an alternative remediation technology. The GCW system creates vertical groundwater circulation cells by drawing groundwater through a one screened section of a multiscreen well and discharging it through another screened section. The suitability of this technology to restore contaminated low permeability layers was investigated by laboratory test. The collected data were used to calibrate a model created to simulate the Back-Diffusion process and to evaluate the effect of pumping technologies on the depletion time of that process. Results show that GCW develops a hydraulic gradient inside the aquifer, which supports the diffusive flow into the lenses and increases the concentration gradient at the interface between low and high permeability zones of aquifers. The efficiency of the GCW system appears dependent on the position of the low permeability zones, but it seems always higher than traditional pumping technology one.

# INTRODUCTION

The issue of groundwater remediation emerged in the 1970s because synthetic organic contaminant began to be observed in supply wells in United States. The first conceptual model used to describe the contamination source and the pollutant's redistribution through the unsaturated/saturated porous media was based on existing agricultural models and on assumptions of isotropic and homogeneous aquifer. In particular, the first conceptual model assumed that the source was located in the unsaturated zone, contaminants have been released mostly in dissolved form and all pollutants were dissolved in groundwater or adsorbed by the aquifer material (Hadley and Newell 2014). The transport of contaminants in the saturated zone was explained using the advection-dispersion equation and for many years it represented the main approach used to simulate the dispersion of contamination plume into groundwater. In the 1980s many Pump and Treat systems were constructed based on the described conceptual model to remediate contaminated groundwater. However, in the late 1980s some Pump and Treat systems had removed more mass of pollutants than what was initially estimated to be present in the aquifer. Sometimes also contamination rebounded after the pumping systems were turned off (Simon et al.). These two unexpected phenomena caused a slower complete aquifer restoration than expected. The application of Pump and Treat technology to restore sites contaminated by fuel allowed to understand that contamination by hydrocarbons was often distributed as a distinct and persistent phase at water surface (Hadley and Newell 2014). Soon, the scientific community recognized that Light Non Aqueous Phase Liquid (LNAPL) contamination causes long-term plumes that are very difficult to remove completely or isolate. This idea was also quickly applied to Dense Non Aqueous Phase Liquid (DNAPL) contaminants as the chlorinated solvent. Therefore, NAPLs became an important component of the groundwater remediation conceptual model and for many years their presence dominated the remediation discussion. In recent years the attention of the scientific community has been focused on the low permeability zones of aquifer and the so called "Back-Diffusion" phenomenon. In 2011, the papers in literature about "Diffusion" matched the number of manuscripts about "NAPLs" (Hadley and Newell 2014). Several authors (Wilson 1997, Adamson et al. 2016, Mackay and Cherry 1989), showed that the presence of NAPL is not the only cause of persistent plumes of dissolved contaminants. They can persist in groundwater due to a further process linked to the diffusion of contaminants from low-permeability zones encountered within the aquifer. The plume emitted by the primary source of contamination generates a concentration gradient between the high and low aquifer permeability zones that induces a molecular diffusive flux, causing pollutant accumulation in the low permeable layers (Forward-Diffusion). When the primary source of contamination is reduced due to natural source depletion processes or active remediation efforts, the pollutant dissolved concentration in the transmissive zone decreases and the concentration gradient reverses. Previously stored contaminant starts to be released by the so-called “Back-Diffusion” process which causes a plume tail that can considerably increase the aquifer remediation timeframe (Sale et al., 2008, Parker et al., 2008, Carey et al., 2015). Therefore, the “Back Diffusion” process is expected to occur when the contaminant flux from a source zone that passes directly into the ground waters is strongly reduced. This aspect can indicate the similarity of behavior between this type of source and others that have as a fundamental characteristic a long-lasting release, such as those derived from NAPL contamination. The main difference can be observed in that the separated phases release directly in the flow from their pooled or residual status; thus, the flux is mostly dependent on the solubility of the substance/substances in the solvent phase (Falta et al., 2005, Seyedabbasi et al., 2012). In contrast, in the examined cases, the driving force of the release is the diffusion that is governed from gradient, and the resulting flux is thus influenced by mechanical parameters such as the grain size and molecular diffusion (Rolle et al., 2013).

Back-Diffusion was previously recognized as an important process in aquifers with silty or clayey layers by Mackay and Cherry (1989). They discussed the problem of dissolved contaminants stored inside the low-permeability zones due to forward diffusion and their subsequent slow release by reverse diffusion during Plump &Treat (P&T). Liu and Ball (2002) and Parker et al., 2008 demonstrated the Back-Diffusion process with field measurements after the hydraulic isolation of the primary source. These studies considered low-permeability zones as active and persistent secondary sources. Carey et al., 2014 numerically simulated the duration of Back-Diffusion from an aquitard contaminated by Trichloroethene (TCE) and the results showed a much higher groundwater remediation time than that necessary for the depletion of the DNAPL source. Seyedabbasi et al., 2012 investigated the relative contribution of DNAPL dissolution versus Back-Diffusion phenomenon to the longevity of a chlorinated source. A coupled dissolution–diffusion model was developed to facilitate diffusion into low-permeability layers while in contact with DNAPL followed by Back-Diffusion out of these same layers after complete DNAPL dissolution. Simulations indicated that Back-Diffusion caused from

17% to 97% of the total source longevity based on the different contaminant properties. Therefore, contaminant redistribution from low to high permeability zones can be considered an obstacle to complete groundwater restoration like in the case of the presence of a NAPL source.

The Back-Diffusion process has been widely studied at laboratory scale due to the difficulty of collecting data in field studies (Sale et al., 2008, Chapman et al., 2012, Wilking et al., 2013, Yang et al., 2014). In laboratory tests, aquifer models were reconstructed in tanks with thin clay lenses or with aquitard layers at the bottom. In most of the laboratory experiments tracers were used with the aim of observing the processes of storage and release of contaminant from low-permeability zones, paying particular attention to the consequent possible plume tailing.

In recent years, several laboratory experiments were carried out using image analysis as contaminant concentration could be estimated without recourse to invasive instruments (Cenedese et al., 1996, Citarella et al., 2015, Cupola et al., 2015, Huang Wei et al., 2002, Luciano et al., 2010, McNeil et al., 2006, Theodoropoulou et al., 2003, Werth et al., 2010, Zinn et al., 2004,). Different image analysis methods can be used to measure the tracer concentrations: they can be roughly re-conducted according to the light transmission technique (Zinn et al. 2004, Catania et al., 2008, Konz et al., 2008, Wang et al., 2008, Jaeger et al., 2009) or the reflection light technique (Konz et al., 2009). This technique has also been used to investigate the Back-Diffusion phenomenon while improving the practical approaches and numerical models used for its management during restoration treatments. For this reason, in several studies different types of numerical models were validated using experimental results from laboratory tests. The numerical approaches range from analytical solutions for the simplest scenarios (Sale et al., 2008, Brown et al., 2012 and Yang et al., 2014) to numerical solutions based on finite-element techniques (Parker and Chapman 2005, Parker et al., 2008, Chapman et al., 2012) or finite-difference techniques (Chapman et al., 2012) for more complicated situations.

Laboratory tests were also carried out to investigate the effect of different remediation technologies for contaminated low-permeability zones. Some of these studies focused on the reduction of the contaminant flux released from low-permeability lenses using electrokinetic migration (Chowdhury et al., 2017, Gill et al., 2015), low k zone treatment with dissolved Oxygen (Clifton et al., 2014), Sodium Persulfate (Cavanagh et al., 2014), Permanganate (Chokejaroenrat et al., 2014), and testing the effect of Groundwater Circulation Wells (Mohrlok et al., 2010). Although efforts of the scientific community, the restoration of low contaminated low permeability layers is a problem which is not solved today. The presence of contaminants in these zones represents a real limitation for a complete and effective groundwater remediation.

The aim of this thesis is the reproduction of the Back-Diffusion process at laboratory scale, to study this phenomenon and to improve the remediation of contaminated low permeability layers of aquifers.

In the first chapter, the Back-Diffusion process was reproduced at laboratory scale reconstructing an aquifer with three low permeability lenses inside it and using a fluorescent tracer to enhance the visibility of the phenomenon. An image analysis procedure was elaborated to estimate the diffusive fluxes of tracer released from the lenses during the Back-Diffusion process and to evaluate the influence of the lenses granulometry on this phenomenon.

In the second chapter, the effect of pumping water on the remediation time of these contaminated low-permeability layers was investigated. Three laboratory experiments were carried out to study the Back-Diffusion phenomenon under three different groundwater velocities. The remediation time of the lenses were calculated using the diffusive flux values obtained by image analysis for each test. Results were used to determine a relation between “groundwater velocity” and “remediation time” for each lens. The coefficients of the relations obtained were matched with the grain size of the low-permeability lenses. The results show the low efficiency of the traditional pumping system to restore contaminated low permeability zones of aquifers. This clearly demonstrates the need to use alternative technologies.

In the third chapter, the effect of the Groundwater Circulation Well (GCW) on the Back-Diffusion process was investigated. The GCW system is an in-situ remediation technology that creates vertical groundwater circulation cells by drawing groundwater from an aquifer through a one screened section of a multiscreen well and discharging it through another screened section. GCW can be configured with upward or downward in well flow depending on site requirements. Groundwater circulation wells can be used in conjunction with other technologies such as bioremediation, bioventing, soil vapor extraction, surfactant, and oxidation (EPA, 1995). GCW was employed at field scale to remediate groundwater contaminated by NAPL (Scholz et al., 1998), by volatile organic compounds (Allmon et al., 1999) and to enhance bioventing (EPA, 1998). In literature, many studies were performed to numerically evaluate the flow developed in a porous media by a Groundwater Circulation Well (Jonhson et al., 2007, Ross and Gary, 1992, Elmore et al., 2001, Miller et al., 2005).

In this thesis, an innovative application of GCW was studied. A laboratory test was performed to evaluate the suitability of this technology to restore contaminated low permeability layers. An aquifer with two low permeability lenses saturated with a Fluorescein solution was reconstructed. A GCW model was inserted inside the aquifer and water was extracted from the upper screen section and injected from the lower screen until the Back-Diffusion process was depleted. During the test the tracer mass contained inside the lenses was estimated using the image analysis technique. The obtained values were used to calibrate a model created to simulate the Back-Diffusion process and to evaluate the effect of pumping technologies on the depletion time of that process. In particular, the model was used to numerically investigate the efficiency of two GCW models (with two and three screen sections) and their ability to restore contaminated low permeability zones of aquifers.

# CHAPTER 1

## BACK-DIFFUSION PROCESS: REPRODUCTION AT LABORATORY SCALE AND INVESTIGATION OF THE PHENOMENON BY IMAGE ANALYSIS TECHNIQUE

### 1.1 Laboratory test: Experimental apparatus

Back-Diffusion phenomenon was reproduced at laboratory scale reconstructing an aquifer inside a box model. The entire experimental apparatus is shown in Fig. 1 and consisted of a box, two peristaltic pumps connected to the inlet and the outlet of the tank, a reservoir for the storage of Fluorescein, a UV lamp positioned in front of the tank and a 3CCD camera.

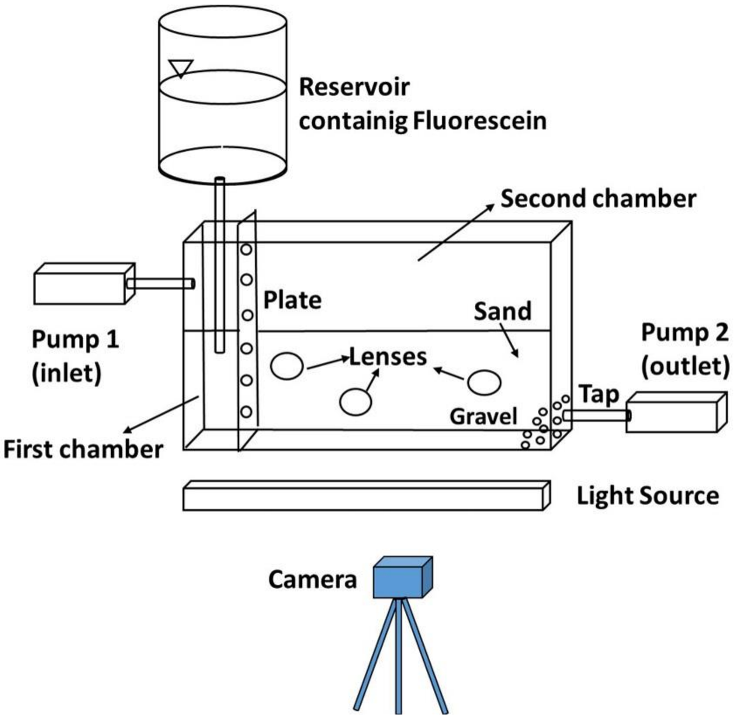

**Fig.1:** Experimental apparatus used for laboratory tests (Tatti et al., 2016).

The box, made of Plexiglass, is characterized by a horizontal length of 68 cm, a height of 40 cm and a depth of 7 cm. The Plexiglass tank was divided into two parts: the smaller part was used to control the water level and limit the turbulence effects, the other one was utilized to reconstruct the aquifer model. The two parts of the box were connected by a punched plate to allow water flow. Two peristaltic pumps were used to control the flux through the aquifer during the experiment, one connected to the smaller chamber of the box and the other one to the outlet of the tank. To prevent material from escape, a gravel layer was located before the outlet. The model of the aquifer reconstructed consists of a high-permeability layer in which three low permeability lenses are inserted (Fig. 2).

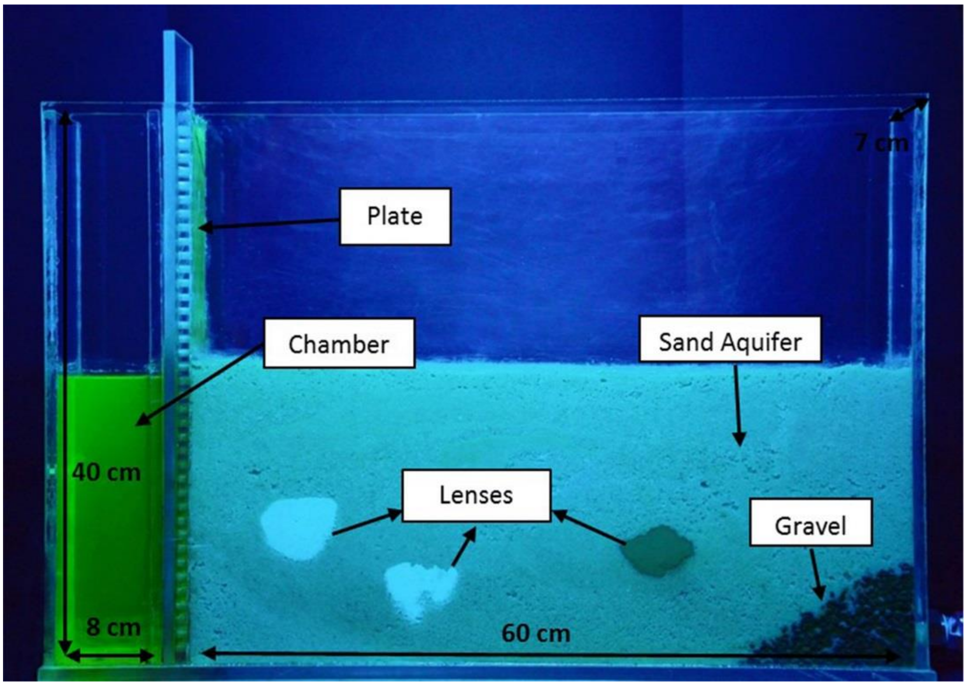

**Fig.2:** The model of aquifer reconstructed (Tatti et al., 2016).

The high-permeability layer was realized using quartz sand. The first two low permeability lenses were composed of the quartz flour (Silverbond SA 12S and Silverbond SA 4K), and the third lens was composed of Sodium Bentonite. The quartz flours were chosen to simulate the low-permeability media due to their insolubility in water, low reactivity and light color; this last property allows to observe clearly the diffusion of a colored tracer inside the lenses.

Laboratory measurements were performed to estimate the particle size and porosity of each material. The particle size analyses of quartz flours and Sodium Bentonite were performed using a Sedigraph. The method of measurement utilizing by the instrument is based on Stokes' law and on the absorption of X-rays as functions of the concentration of sediment in the liquid dispersant. As Table 1 shows, Sodium Bentonite is characterized by a medium grain size ($D_{50}$) an order of magnitude smaller than those of lenses 1 and 2, which have $D_{50}$ values of 15 µm and 12 µm, respectively. The particle size analysis of quartz sand was performed by sieving, according to the ASTM standards. The medium grain size of the sand was estimated to be 700 µm (Table 1).

**Table 1:** Characteristics of materials used for constructing the aquifer model.

| | Materials | $\gamma s$ (kg/dm$^3$) | $D_{50}$ (µm) | $D_{10}$ (µm) | Porosity | Hydraulic Conductivity (m/s) |
|---|---|---|---|---|---|---|
| Sand | Quartz | 2.65 | 700 | 430 | 0.40 | $2.7*10^{-3}$ |
| Lens 1 | Quartz Flour | 2.65 | 15 | 1.8 | 0.40 | $1.4*10^{-6}$ |
| Lens 2 | Quartz Flour | 2.65 | 12 | 1.4 | 0.42 | $5*10^{-7}$ |
| Lens 3 | Sodium Bentonite | 2.35 | 1.4 | 0.1 | 0.60 | $6.8*10^{-8}$ |

To determine the porosity of sand, quartz flours and Sodium Bentonite, the following relation was used:

$$\eta = 1 - \frac{Ps}{V_{Tot} * \gamma_s} \tag{1}$$

where η is the porosity, Ps the dry weight of the material, $V_{Tot}$ the sample volume and $\gamma_s$ the density of the material. To estimate the value of sand Ps, the Sand-Cone Method was used, according to the ASTM standards. To determine the Sodium Bentonite Ps, three samples with known volumes were filled with the saturated material and then weighed. The samples were dried at a temperature of 110 °C for 24 hours and after they were weighed again. In this way, Ps was determined and, using (1), the water moisture of samples were estimated. The same laboratory procedure was used to determine the value of the quartz flours' Ps. Table 1 presents the porosity value for each material obtained from the average of the three samples' values. The hydraulic conductivity of each material was estimated using theoretical approaches. The sand hydraulic conductivity was estimated using the formula proposed by Hazen:

$$k = \frac{g}{v} * 6 * 10^4 * (1 + 10 * (\eta - 0.26)) * D_{10}^2 \qquad (2)$$

where g is the acceleration due to gravity, υ the kinematic viscosity of water, η the porosity and $D_{10}^2$ the grain diameter for which 10% of the material has a lower dimension.

The hydraulic conductivities of the two lenses were calculated using the semi-empirical approach proposed by Kozeny and Carman:

$$k = \frac{\gamma_s}{\mu} * \frac{1}{C_{k-C}} * \frac{1}{S_0^2} * \frac{e^3}{1+e} \qquad (3)$$

where $\gamma_s$ is the density and μ the dynamic viscosity of water, $C_{k-C}$ an empirical coefficient equal to 5, $S_0$ the grains specific surface per unit of volume and e the void ratio. $S_0$ was estimated using the specific surface of grains measured utilizing laser diffraction (expressed as $cm^2/g$). As Table 1 shows, the lower the grain size, the lower the hydraulic conductivity and the higher the porosity is. Thus, lens 1 is characterized by the biggest grain size and by the highest permeability, lens 3 has the smallest grain size and the lowest hydraulic conductivity.

Sodium Fluorescein was used as a colored tracer to simulate a contaminant. Fluorescein is a non-toxic and non-reactive compound. It was chosen because it emits a light that varies from green to orange as a function of its concentration when it is excited by UV light (Sabatini and Austinal, 1991). In this way, the tracer appears clearly visible in porous media and thus image analysis technique results a suitable method to estimate tracer concentration in the aquifer. In the experiments described, the fluorescence was stimulated using an ultraviolet light bulb (Philips Actinic BL TL-D 18W-10 UV-A G13).

## 1.2 Test Procedure

In the first step of the experiment, the tank was saturated with clean water and a constant groundwater velocity was reached setting the two pumps to a fixed flow rate of about 26 mL/min. Subsequently, in order to simulate a contamination, a solution containing 2 g/L of dissolved Fluorescein was slowly injected into the first chamber of the tank. Fluorescein quickly advanced into the sand layer, generating a concentration gradient between low and high-permeability zones of the aquifer (Fig.3).

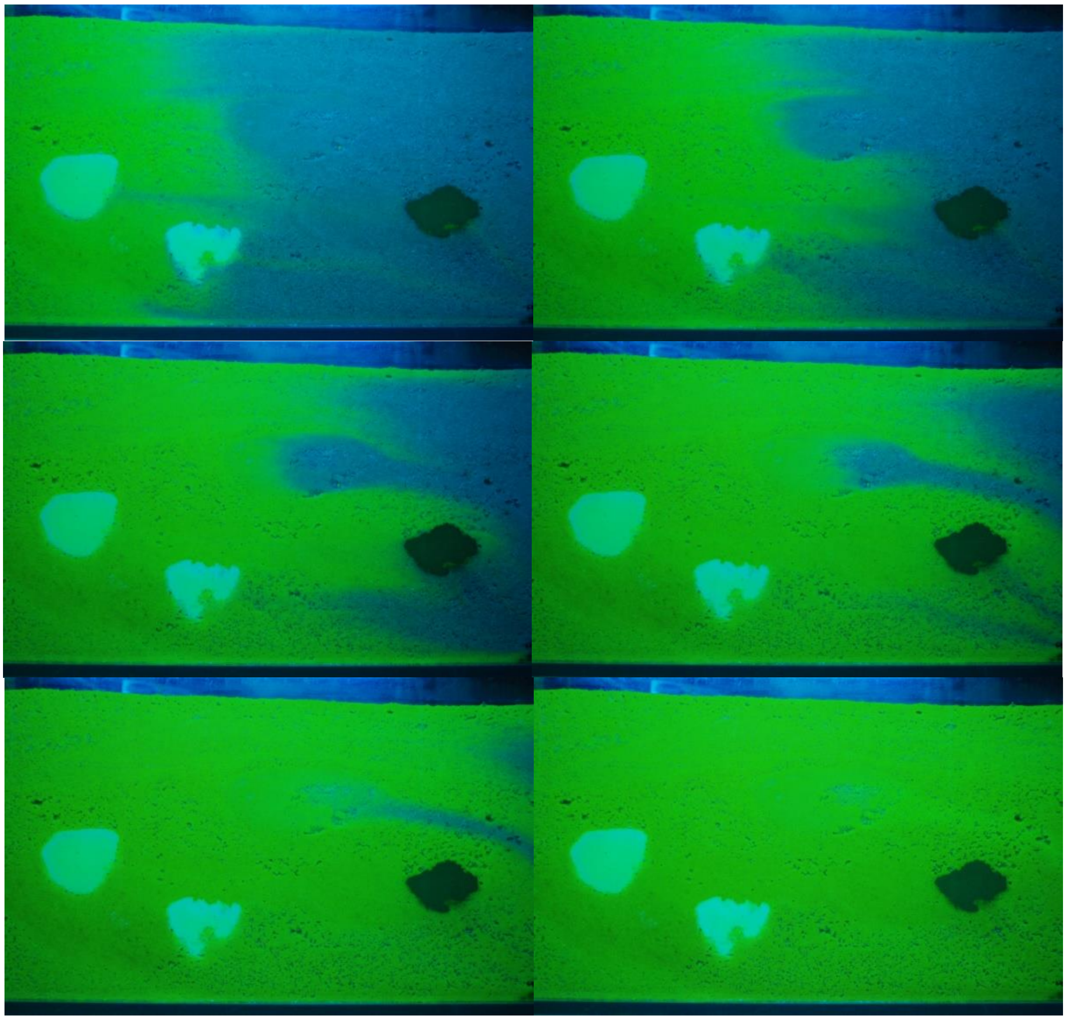

**Fig.3:** The advancement of Fluorescein in sand layer.

The concentration of the solution in the sand layer was monitored collecting water samples at the outlet of the box. The Sodium Fluorescein concentration in every sample was estimated by measuring the intensity of the tracer’s fluorescence. Each water sample was excited by UV light at 254 nm and the intensity of the emitted light (fluorescence) by Fluorescein was measured using a fluorometer.

Based on the fluorescence intensity of samples with known tracer concentrations, a relationship was determined between the intensity of fluorescence and the Fluorescein concentration. That relationship was used to match the measured fluorescence of the samples to the respective concentration.

When the sample concentration reached a plateau of 2 g/L, this concentration was considered to exist in the whole tank. At that time, the injection of the Fluorescein solution was stopped, the top of the tank was sealed to avoid evaporation and the aquifer was kept in a saturated condition for three weeks with null velocity. During that time, dissolved Fluorescein advanced visibly in the lenses by molecular diffusion (Fig. 4).

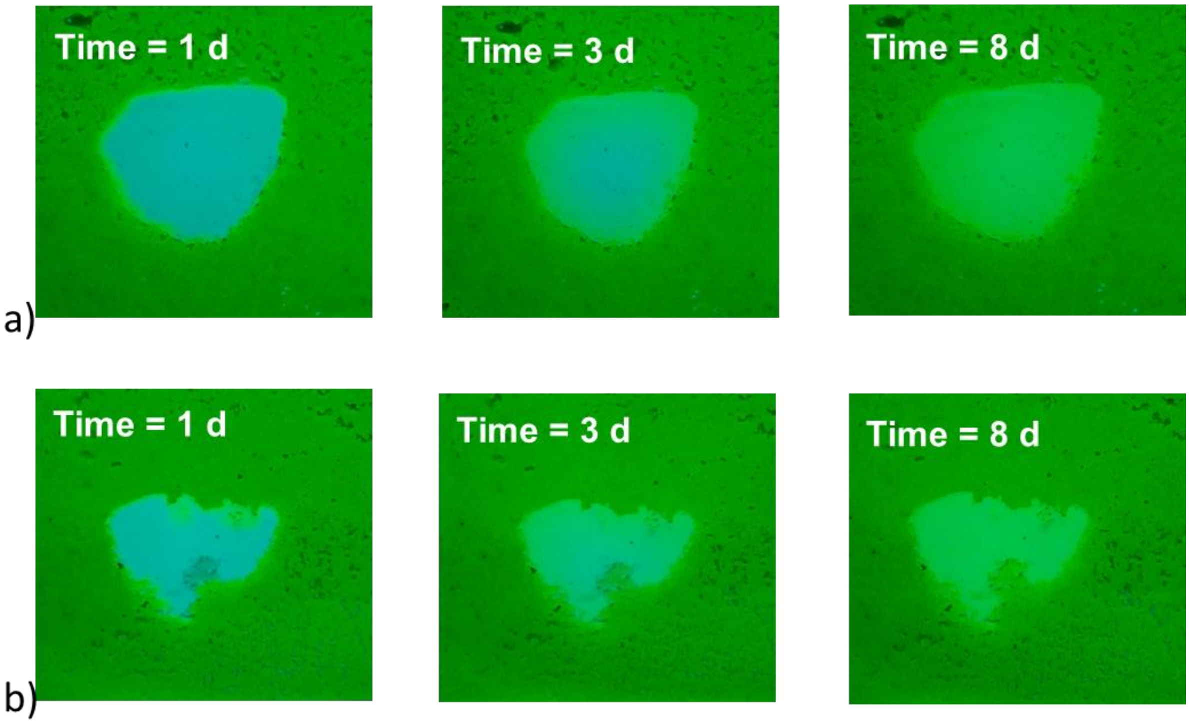

**Fig.4:** Fluorescein advancement by Forward-Diffusion in lens 1 (a) and lens 2 (b).

At the end of three weeks, the removal of the primary contamination source was simulated flushing clean water for 14 days using the previously mentioned flow rate of 26 mL/min. For the first 5 days, two pore volumes were flushed daily, and for the remaining 9 days, only one pore volume of water (about four liters) was flushed. The daily flushing phase was conducted during the daytime hours, and during the night, the flow was stopped and then re-started on the following morning. In this way, periods of enhanced groundwater velocity due to pumping activity and periods of rest were simulated. As the Fig. 5 shows, during the flushing phase an advective component of transport removed Fluorescein from the sand layer quickly and the concentration gradient between low and high permeability layer reverses.

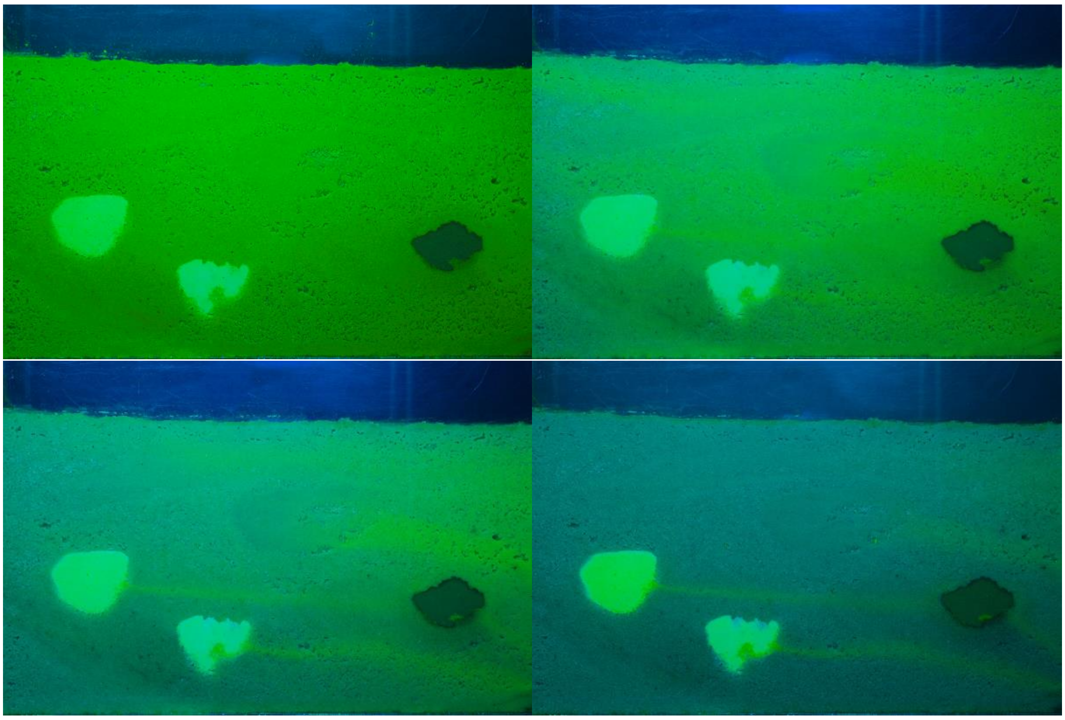

**Fig.5:** Fluorescein removal from sand layer by advective transport.

The diffusion phenomenon from the low-permeability zones was clearly visible during both flushing and non flushing phases. Figure 6 shows the solute that was released from the low-permeability lenses during the night phase and redistributed via diffusion in the higher-permeability layer. Figure 7 shows the tails of the released dye during water flushing. During the experiment images of the aquifer were collected continuously with a prefixed time interval from an automatic acquisition system. To take images a CCD camera was used and to increase their clarity, a UV filter (Hoya Pro1 Digital Filter UV) was applied on the camera lens.

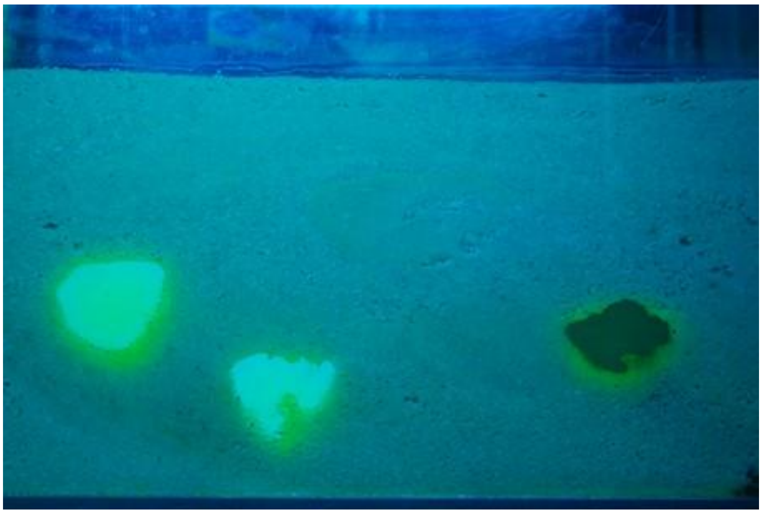

**Fig.6:** Fluorescein released by low permeability lenses at the end of the daily non flushing phase (Tatti et al., 2016).

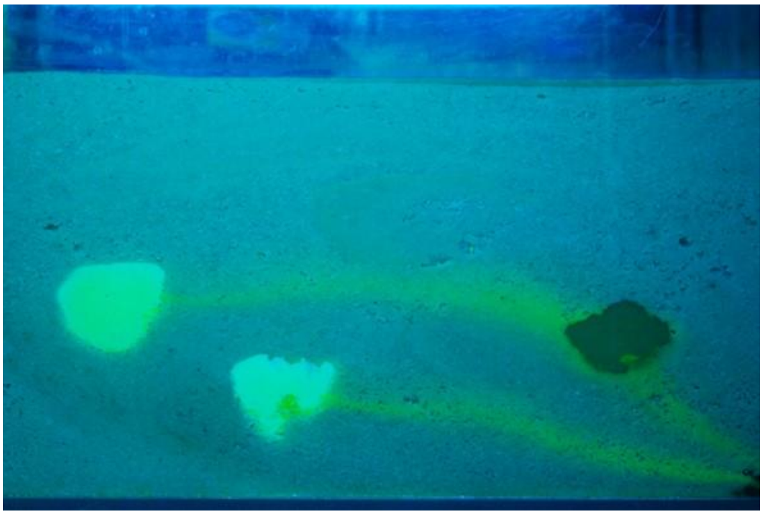

**Fig.7:** Tail of Fluorescein released by low permeability lenses during the flushing phase (Tatti et al., 2016).

## 1.3 Image analysis technique

The fluorescence of the tracer allows the use of an image analysis technique to determine the Fluorescein concentration released by the low-permeability lenses. The source of UV light placed in front of the tank excites the dissolved Fluorescein, which subsequently reemits light. The image analysis procedure used to elaborate the images of the aquifer is based on the intensity of that light. The small thickness of the aquifer (7 cm) compared with the other dimensions (60 cm of horizontal length and 20 cm of high) allowed a 2D approach to be used for the analysis, considering the dye distribution to be uniform in the third dimension.

At first, image analysis was applied to evaluate the trend of effluent concentration in order to demonstrate the suitability of the image analysis technique to estimate the tracer concentration in the reconstructed aquifer. Subsequently, an image analysis procedure was elaborated to estimate the diffusive flux released by lenses during the Back-Diffusion process.

### *1.3.1 Calibration phase*

To estimate the effluent concentration, a calibration procedure was conducted using an additional small Plexiglass tank filled with quartz sand and saturated with solutions at different known concentrations of Fluorescein. Due to the phenomenon of brightness attenuation far from the central area of the image (M. Yang et al., 2014), the behaviour for each colour was investigated locating the calibration tank once at the central part of the box model and once relatively close to the outlet (Fig.8). In both positions, images of the small tank containing solutions at known tracer concentrations were collected.

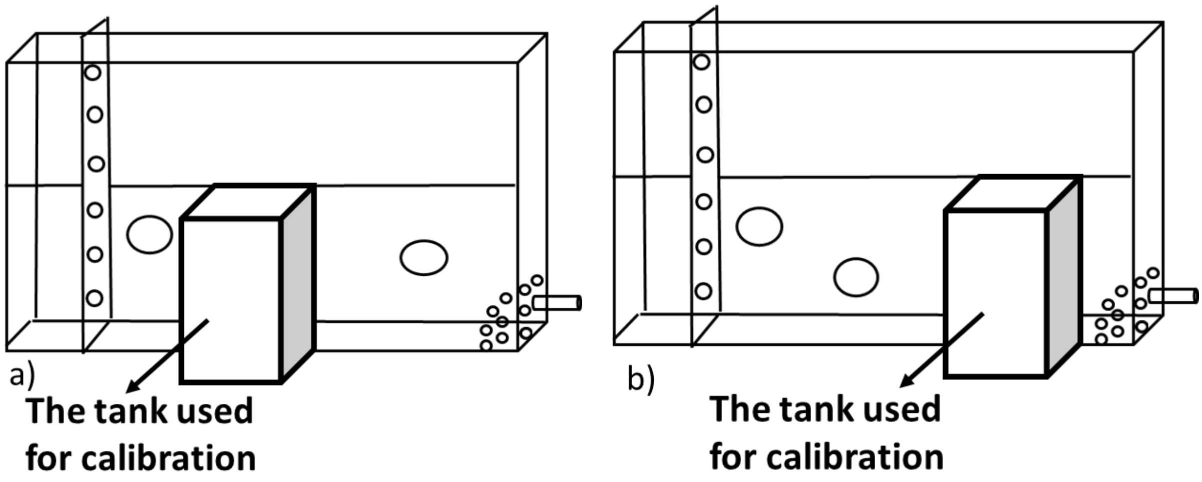

**Fig.8:** The locations of the small tank utilized for calibration.

Each pixel of the pictures displays a colour due to the combination of Red, Green and Blue (RGB colour system). For each image the three colours were separated, transforming every picture in three different images in grey scale. In this manner, each pixel assumes integer values from 0 (Black) to 255 (White), thereby enabling the measurement of the pixel intensity of the whole image in each channel. Elaborating the collected picture using this image analysis procedure, Red values resulted in negligible intensity, and thus only the intensities of the Blue and Green light were measured (Fig. 9).

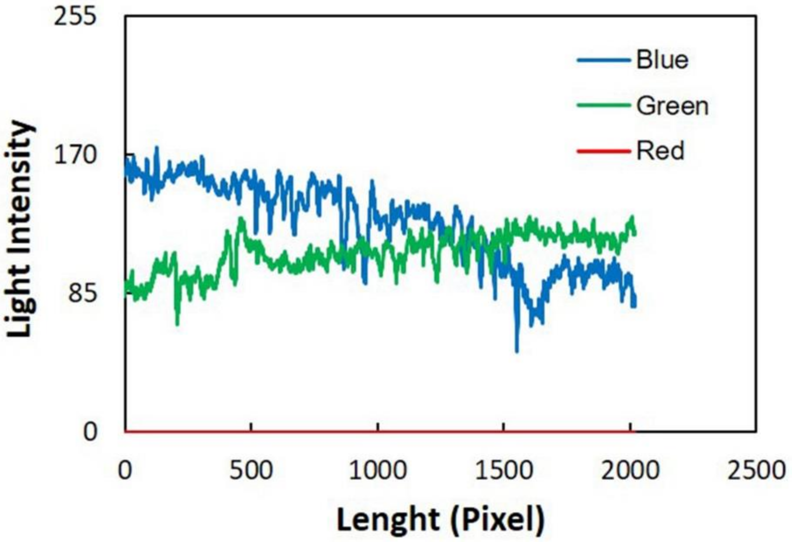

**Fig.9:** Intensities of the three colours (RGB) in a section of the aquifer (Tatti et al., 2016).

The colour intensity values obtained by image elaboration matched to the respective concentrations were interpolated to determine the analytical relations between the Fluorescein concentration and the Green and Blue intensities. A polynomial relation based on exponential functions is found for Blue colour (Fig. 10a, c); this result agrees with studies by Yang et al., 2014 Catania et al., 2008, Konz et al., 2008 and Jones and Smith. Conversely, a simple exponential function fits the relation between the Green colour intensity and the concentrations (Fig. 10b, d) for both positions. This result is valid for concentrations lower than 0.2 g/L because for higher concentration values, an over-saturation intensity is observed. This observation is in agreement with the study performed by Konz et al., 2008. The high value of correlation coefficient ($R^2$) and the low values of the Root Mean Square Error (RMSE) demonstrate the good compatibility between the experimental points and the interpolating relations. $R^2$ is greater than 0.99 for both the positions analysed, and these values are similar for the Blue and Green colours. The RMSE result to be on the order of $10^{-2}$ for Blue functions and $10^{-3}$ for Green functions.

The good fitting of the analytical relations to the experimental data is an important result for successfully estimating the tracer concentration in the box model using the image analysis technique.

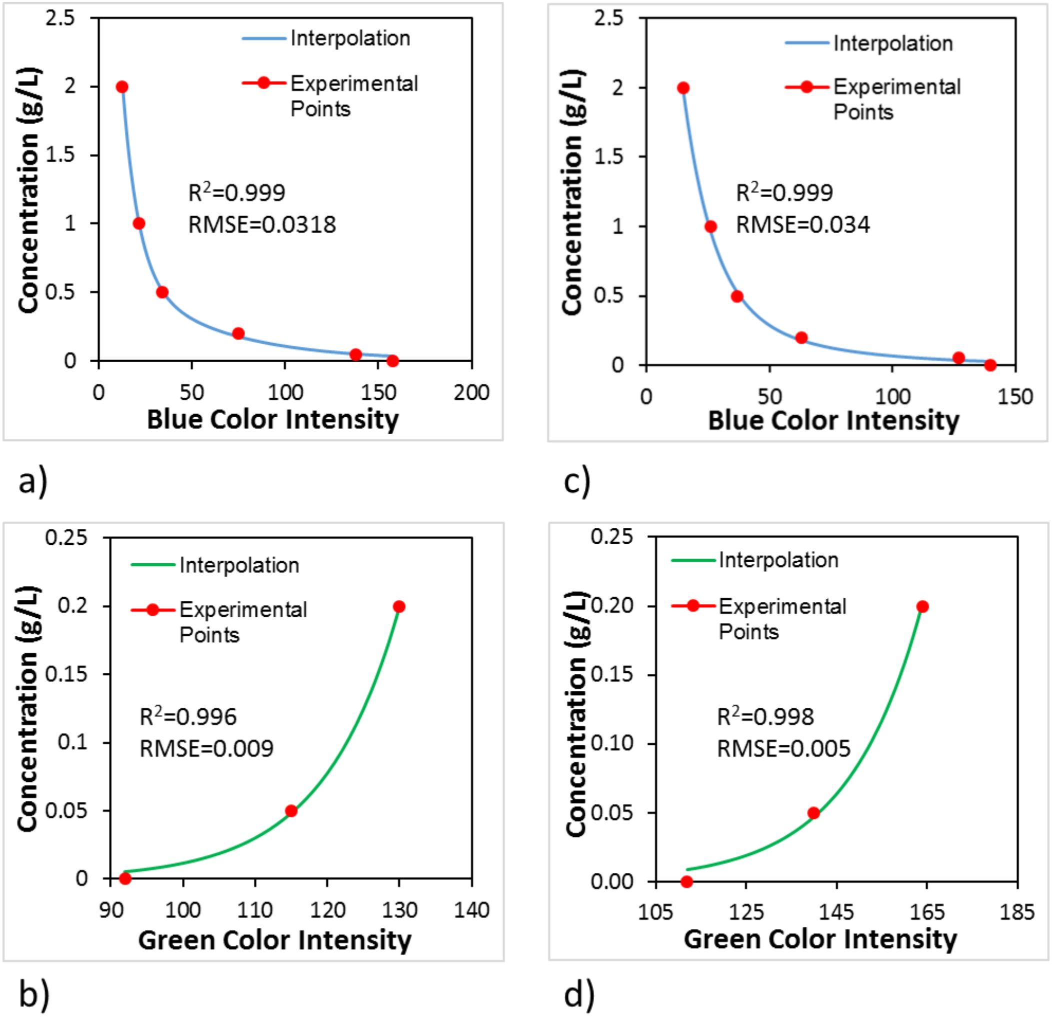

**Fig.10:** Analytical relations between Fluorescein concentration and colour intensity in the middle part of the box model (a, b) and in the outer part (d, c) (Tatti et al., 2016).

### *1.3.2 Effluent concentrations estimated by image analysis*

As reported above, pictures of the tank were collected during the daily water flushing. In each picture, the Blue and Green colour channels were separated and converted into grey scale images. The Fluorescein concentration was evaluated by image analysis at the control section positioned in the side part of the tank (Fig.11). In each image, the average colour intensity value of the control section was considered; next, using the functions obtained during the calibration phase, a concentration was assigned to that value. During the flushing, the tail of the first lens reaches the third lens. This fact is negligible for our purposes because we use image analysis to estimate the effluent concentration, which is the sum of the three tails. To evaluate the described procedure, the Fluorescein concentrations estimated by image analysis were compared to the concentrations of the effluent samples collected at the outlet of the box.

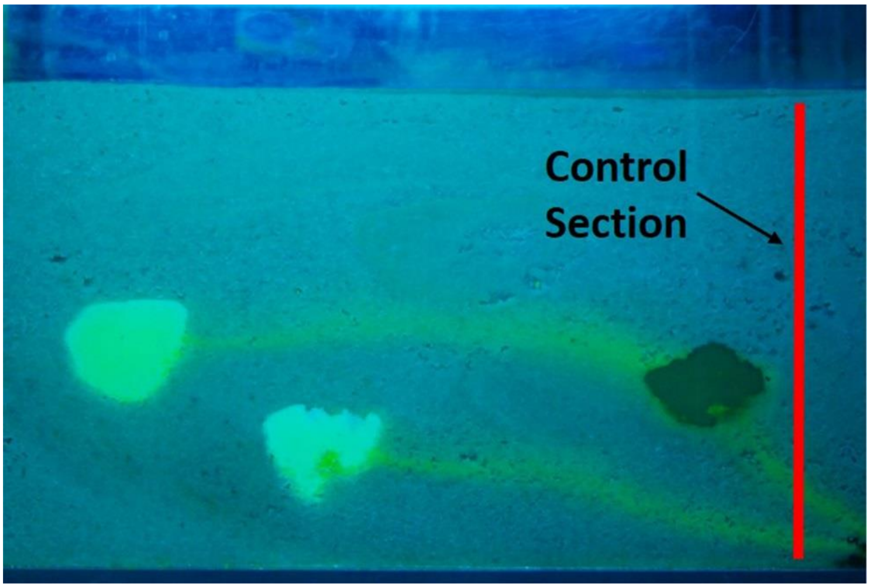

**Fig.11:** The control section analysed to estimate the Fluorescein concentration by image analysis.

An error value (E) was used to evaluate the agreement between the obtained and measured concentrations (Yang et al., 2014):

$$E = 1 - \frac{\sum_i (O_i - P_i)^2}{\sum_i (O_i - O)^2} \quad (4)$$

where $P_i$ is the calculated concentration using image analysis, $O_i$ and O are the measured concentration and the average concentration of the samples, respectively. The E values range from negative infinity to 1.0, with values closer to 1.0 indicating a better fit. As shown in Table 2, the E values obtained range from 0.9 to 0.3. These values were considered suitable for demonstrating the efficiency of the image analysis technique to estimate the Fluorescein concentration in the aquifer.

**Table 2:** Error value for Blue and Green colours calculated for the first 5th days (Tatti et al., 2016).

| Day | Coefficient of efficiency (E) for Blue color | Coefficient of efficiency (E) for Green color |
|---|---|---|
| 1 | 0.9 | -0.4 |
| 2 | -1.7 | 0.8 |
| 3 | - | 0.9 |
| 4 | - | 0.9 |
| 5 | - | 0.3 |

The error values suggest that the Green function is more suitable to describe the low concentration and the Blue function is more appropriated to estimate the high concentrations. In fact, during the first day, the effluent concentrations are higher than 0.1 g/L (Fig. 12a) and the E value for the Blue colour was 0.9, substantially larger than the value obtained for the Green function (-0.4).

On the second day, the trend changed drastically: the effluent concentrations are lower than 0.1 g/L (Fig. 12b), and the E value of Green function becomes larger than the Blue one. The decreased concentration value in the following days led to the use of only the Green function to estimate the trend of effluent concentration during this period (Fig.12c, d).

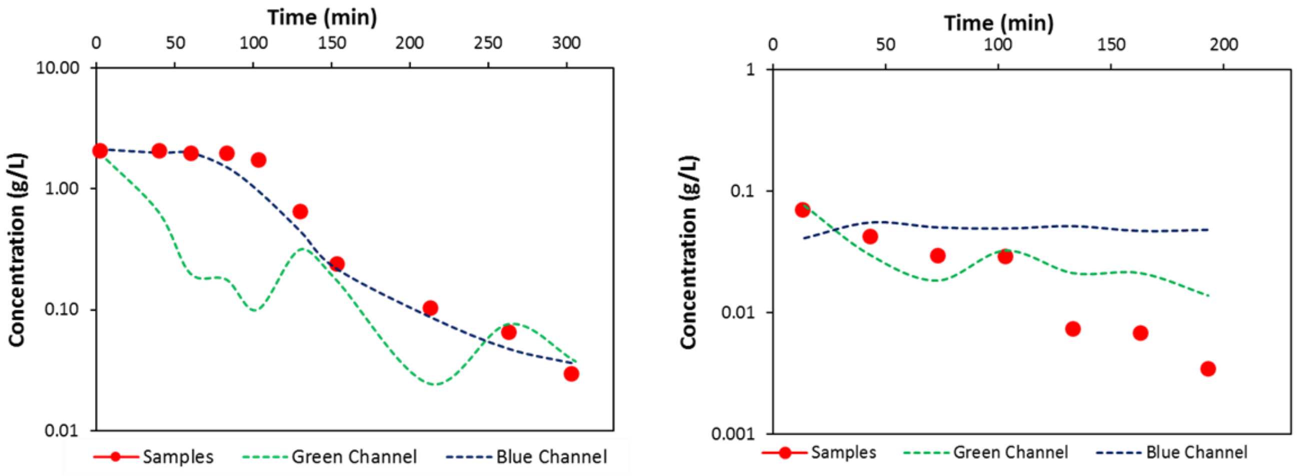

(a) - 1st day (b) - 2nd day

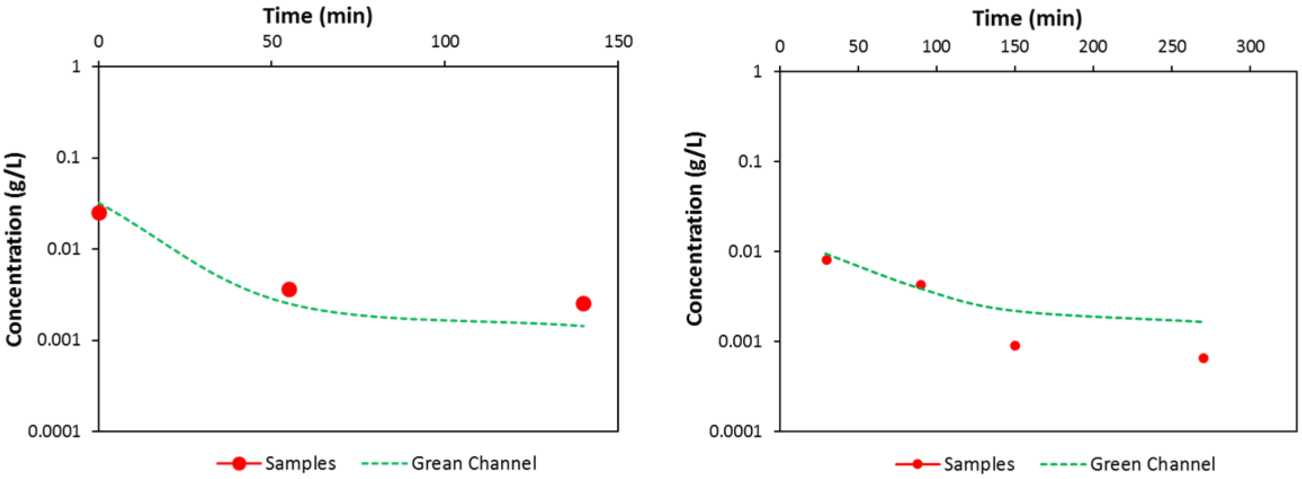

(c) - 3rd day (d) - 5th day

**Fig.12:** The trend of effluent concentration estimated by image analysis compared to the concentrations of water samples (Tatti et al., 2016).

The lowest E value was obtained on the 5th day; this value is due to the low concentration values of the Fluorescein, which determined the larger errors during the image analysis procedure. Difficulties in obtaining a constant light source caused variations in light intensity in the acquired images, which resulted in small fluctuations in the Fluorescein concentrations (Yang et al., 2014, Konz et al., 2008). However, their presence did not spoil the results; as a result, Fig. 8 shows the concentration trends after a smoothing procedure was applied.

### *1.3.4 Image analysis procedure to evaluate the Back- Diffusion process*

In the previous paragraph the suitability of the image analysis technique to estimate Fluorescein concentration in the aquifer was demonstrated. Based on this result, the image analysis technique was used to study the Back-Diffusion phenomenon, in particular it was applied to evaluate the diffusive flux of tracer released by lenses during the non flushing phase.

To achieve the goal, the image captured each day before the beginning of the flushing phase was analyzed. The area around each lens characterized by the presence of Fluorescein was examined (Fig.13a). For each area the three color channels were separated, transforming every picture into a grey scale image (Fig. 13b). The histogram representing the distribution of pixels for each gray level shows two distinct peaks representing the light intensity corresponding to the presence of the lens and of sand (background). The values between the two peaks represent the presence of Fluorescein (Fig. 13c) and they were selected using two thresholds (Fig. 13d, e). The number of pixels for each value of gray level contained in the selected range was determined using a specific image analysis program. Each group of pixels was associated with a value of the Fluorescein concentration and with a value of area. The value of concentration was determined using the relations between the Fluorescein concentrations and light intensity obtained during the calibration. The value of the area was obtained multiplying the pixel number of each group by the area of a single pixel ($2.83 \times 10^{-5}$ cm$^2$). In this way, the total mass of Fluorescein released from each lens was estimated. Dividing this value by both the perimeter of the lens and the non-flushing time, the values represent a diffusion flow per unit of time and per unit of length for every lens.

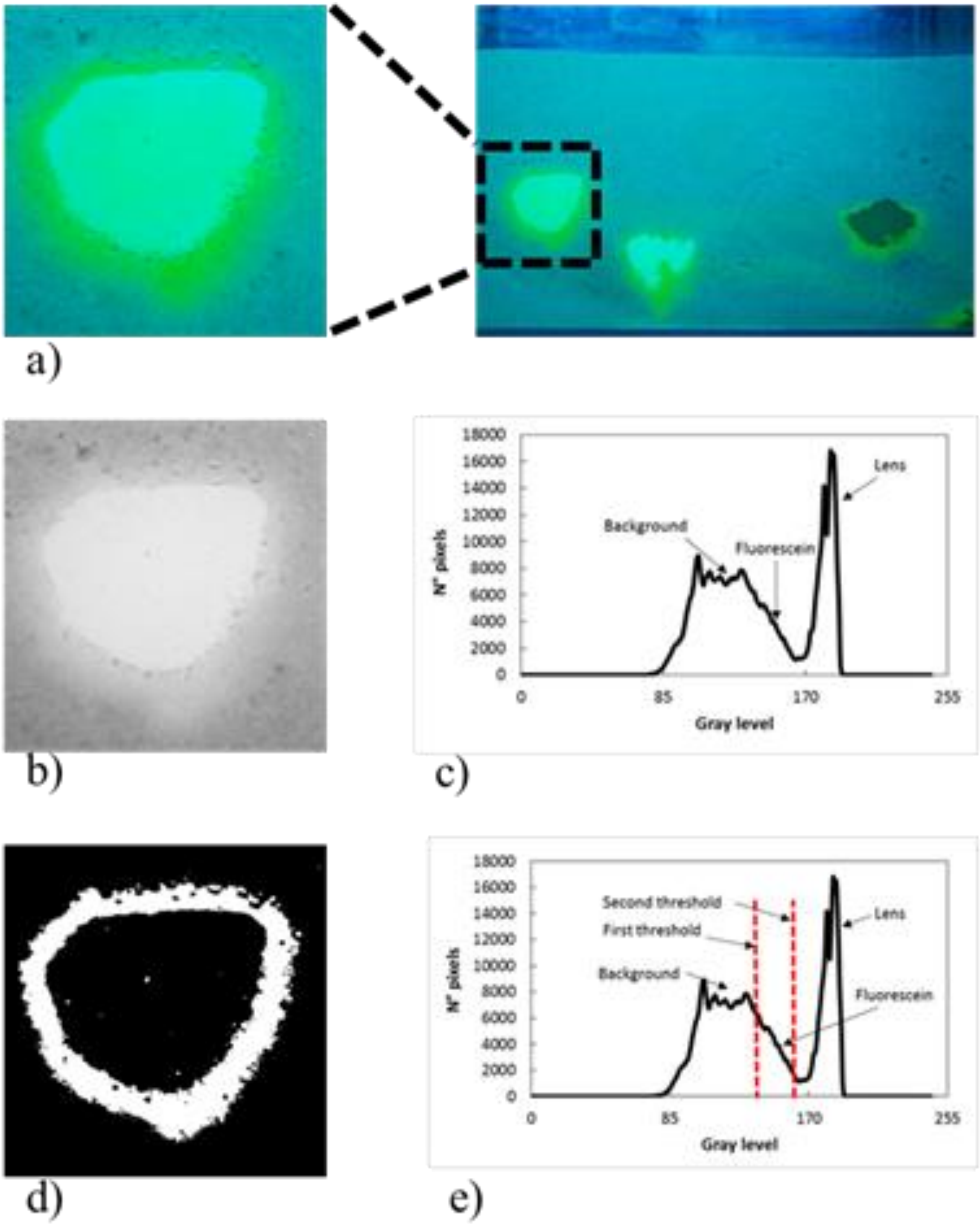

**Fig.13**: The image analysis procedure elaborated to evaluate the diffusive flux of Fluorescein released from the lenses during the non flushing phase. The area around each lens examined (a). The same area converted into a gray scale (b) and its histogram of pixel frequencies (c). The area around each lens showing Gray levels corresponding to the presence of Fluorescein (d) and the histogram of the Gray levels selected by application of two thresholds (e) (Tatti et al., 2016).

Lens 1, because of its circular shape, was chosen to validate the described image analysis procedure. For this lens, the value of diffusive flux was estimated by image analysis from 2nd until 14th day. The obtained values were compared with those calculated by the analytical solution of diffusive flux proposed by Yang et al., 2014.

$$J = C_0 * \eta \sqrt{\frac{D^*}{\pi * t}} \tag{5}$$

where J is the diffusive flux, $C_0$ is the constant solute concentration released into the sand, η is the porosity of low permeability zone (Table 1) and t is the time of diffusive flow. D* is the effective solute molecular diffusion coefficient, defined as:

$$D^* = \frac{D * \tau}{1 + \frac{k_d * \rho_b}{\eta}} \tag{6}$$

where $\tau$ is the metric tortuosity (Table 3), $\rho_b$ is the density and $k_d$ is the distribution coefficient. This analytical solution was obtained from Fick's first law of diffusion. It is effective at the interface between low and high-permeability porous media. The release of Fluorescein from the low-permeability lenses into the bulk is fundamentally based on the basic mechanisms of transport therefore mainly on Back Diffusion; thus, in the proposed analytical solution, the distribution coefficient ($k_d$) was considered equal to zero because it can influence only the lower or greater availability of the entrapped substance. As shown in Fig. 14, the fit between the numerical and experimental trends is rather good (E = 0.99). During the last four days, image analysis underestimated the medium diffusive flow values, mainly due to the low Fluorescein concentrations.

**Table 3:** Parameters used to calculate the effective molecular diffusion coefficient (D*) (Tatti et al., 2016).

| **Parameters** | **Values** | **Units** | **Notes** |
|---|---|---|---|
| $\tau$ | 0.6 | - | Chapman et al., 2012 |
| D | 13.0E-10 | $m^2/s$ | Chapman et al., 2012 |

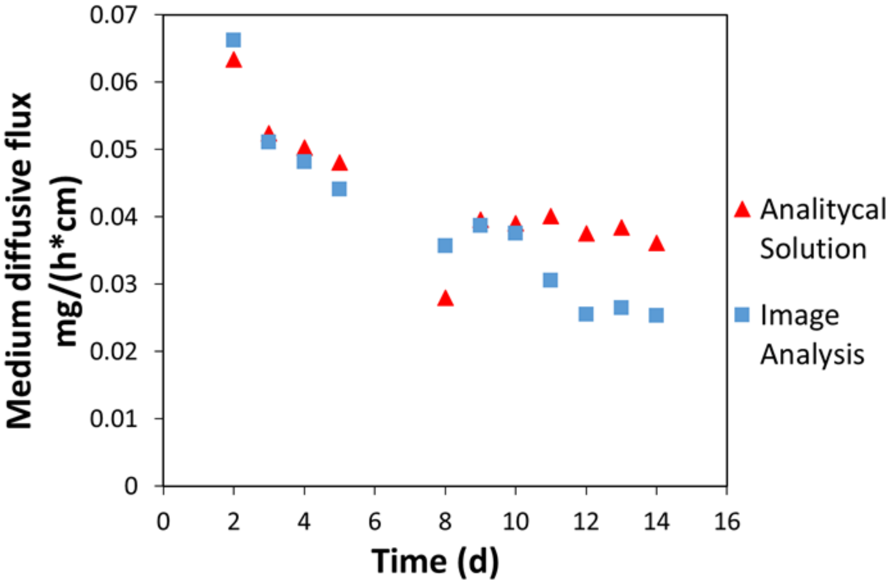

**Fig.14:** Comparison between the medium diffusive flux values estimated by image analysis procedure and the analytical solution proposed by Young et al., 2014 (Tatti et al., 2016).

## 1.4 Influence of grain size distribution on the Back-Diffusion process

To investigate how the grain size distribution of low permeability zones influence the Back-Diffusion process, the diffusive flow released by lenses during the non flushing phase was measured.

It was calculated using the image analysis procedure (reported in paragraph 1.3.4) for each lens from the 2nd until the 14th day. During the flushing, the tail of the first lens reaches the third lens. This fact is negligible for our purposes because we use image analysis to estimate the diffusive flux from the lenses during the no-flushing phase. As the Fig. 17 shows, the exponential function fits the experimental data with $R^2$ ranging from 0.92 to 0.97 for all lenses. The obtained trends clearly show an increase in medium diffusive flux from lens 1 to lens 3. This result can be directly linked to the grain size: the smaller the grain size is, the larger the diffusive flux is, presumably because of a greater storage capacity in the smaller medium grain size. Thus, according to Fig. 15, lens 3 is found to be able to store more diluted substance; as a result, its release is larger than that of the others. These results can be used to further confirm that low-permeability zones must be considered as a long-lasting contaminant source, recalling the behavior of other similar sources such as DNAPL and LNAPL. Furthermore, the different capacity of the low permeability zone to store contaminant causes grate implications for the remediation techniques, which must be chosen properly by carefully considering the soil texture.

The characteristics of the materials used in the tests allows for the comparison of obtained results at laboratory scale to possible field scenarios. The molecular diffusion coefficient of the Fluorescein presents an order of magnitude of $10^{-6}$ $cm^2/s$ (Sabatini, 2000), similar to the molecular diffusion coefficient of TCE and PCE (Liu and Ball, 2002), which are very commonly encountered contaminants. The low-permeability lenses used in our tests are characterized by hydraulic conductivity and porosity ranges that can be compared to the values of a silty loam.

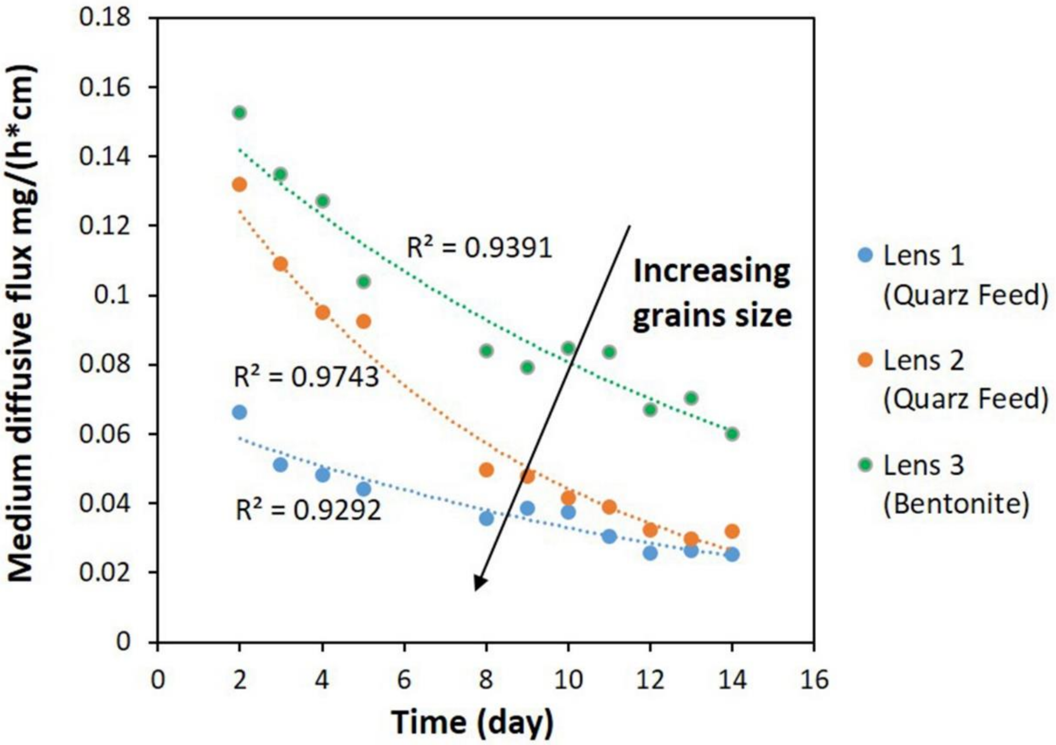

**Fig.15:** The trend in time of medium diffusive flux released by the lenses calculated by image analysis (Tatti et al., 2016).

# CHAPTER 2

# REMEDIATION OF CONTAMINATED LOW PERMEABILITY ZONES OF AQUIFERS: EFFECTS OF ENHANCED GROUNDWATER VELOCITY AND INFLUENCE OF LENS SHAPE

## 2.1 Laboratory tests

To investigate the effect of groundwater velocity on depletion time of the Back-Diffusion process, the test described in paragraph 1.2 was repeated three times using three different velocities of flushed water (U=5 m/s, U=10 m/s, U=20 m/s). In this way, the enhancement of groundwater velocity due to the use of pumping technologies was simulated (Fig.16).

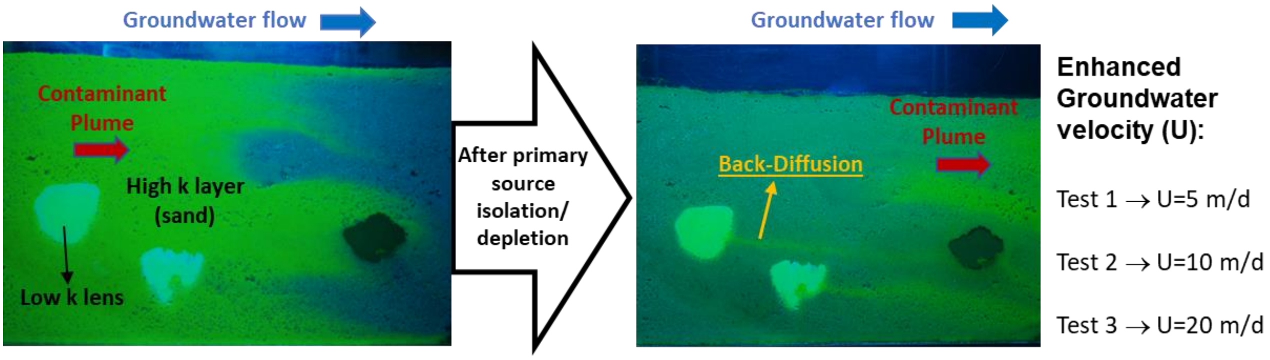

**Fig.16:** Laboratory tests carried out flushing clean water at three different velocities to simulate the enhanced groundwater velocity due to application of pumping technologies.

Briefly, in the first step of the experiment the aquifer was saturated by a 2 g/L Sodium Fluorescein solution. When that concentration was achieved in all zones of the aquifer, it was kept in saturated condition with null velocity for three weeks. During this period, dissolved Fluorescein advanced in the low permeability lenses by molecular diffusion. At the end of three weeks, clean water was flushed into the aquifer for 10 days allowing a slow re-distribution of tracer from the lenses to the high permeability zone. The first test was carried out flushing water with U=5 m/d, the second with U=10 m/d and the third with U=20 m/d. The daily amount of flushed water was the same in each test: two pore volumes for the first 5 days and only one pore volume for the remaining days. When the daily amount of water was flushed, the flow was stopped and then re-started the following day. During the tests images of the aquifer were captured using the experimental apparatus described in paragraph 1.1.

## 2.2 Image analysis procedure used to evaluate the Back-Diffusion process in the case of enhanced groundwater velocity

To investigate the effect of enhanced groundwater due to the application of pumping technologies, the mass of tracer released from the low permeability lenses during the tests was estimated.

The image analysis procedure described in paragraph 1.3.4 was applied to calculate the mass of tracer released from the three lenses during the non flushing phases of the tests. To evaluate the diffusive flux of Fluorescein released by lenses during the flushing phase, a specific image analysis procedure was applied to each image captured during this phase of the tests. In every collected picture three plume tails released from the lenses were clearly visible. For each lens a specific section crossing the plume tail and characterized by a known length was considered (Fig. 17).

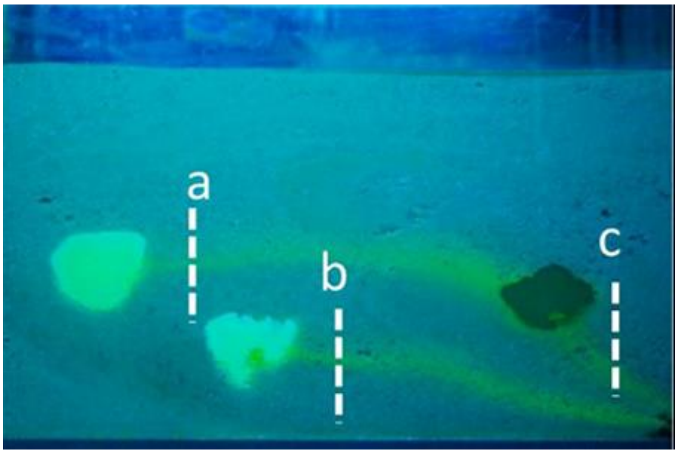

**Fig. 17:** The sections considered to estimate the diffusive flux of Fluorescein released from the lenses during the flushing phase of the test (Tatti et al., 2018).

The color intensity over the sections were measured. Using the relations obtained during the calibration phase, an average Fluorescein concentration was assigned to the analyzed segments. For each lens a diffusive flow per unit of time (J) was calculated by means of the relation (5):

$$J = C * L * U \tag{7}$$

where C is the average concentration calculated using image analysis over the section length L (cm) at a fixed instant and U (cm/s) the bulk average Darcy velocity. The obtained value of diffusive flux divided by the perimeter of the lens (P) furnished the diffusive flux value for units of time and of length.

As Figure 15 shows, the tail of lens 1 interacts with lens 3. Therefore, to correctly quantify the Fluorescein released from lens 3, the solute mass estimated to be released by lens 1 was subtracted from the solute mass released from lens 3.

The described procedure was validated performing a mass balance of a circular lens in a specific test. The experimental apparatus described in paragraph 1.1 was used to reconstruct an aquifer composed of a sand layer containing a low permeability lens inside. The lens was saturated with a known quantity of dissolved Fluorescein (0.1 g) and then clean water was flushed continuously inside the aquifer until all tracer was released by the lens. During the test images of aquifer were collected with a prefixed time interval. For each picture the diffusive flux was calculated using the image analysis procedure reported in this paragraph. The tracer mass released from the lens was obtained multiplying the diffusive flux value by the lens perimeter and by the time interval between the capture of one image and the next, assuming the flux condition is steady (the gradient value and the molecular diffusion coefficient being constant). Fig. 18 shows the suitability of the proposed image analysis procedure to estimate the diffusive flux of tracer released by low permeability lenses during water flushing.

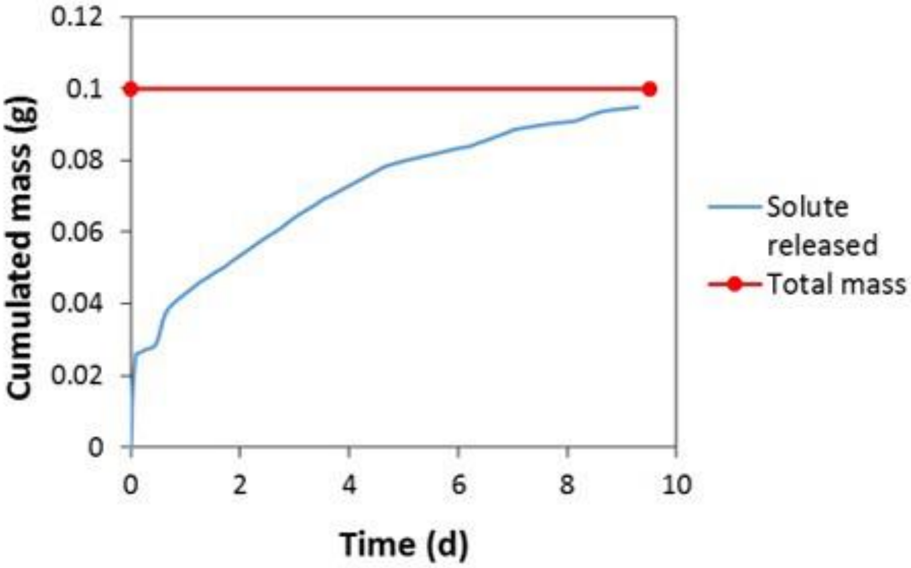

**Fig. 18:** Comparison between the initial mass of Fluorescein inside the lens and the released mass of tracer calculated using the proposed image analysis procedure (Tatti et al., 2018).

## 2.3 Influence of groundwater velocity on the Back-Diffusion process

For each lens the diffusive flows of Fluorescein released during the flushing and non flushing phases were measured by image analysis. As shown in Fig. 19, the diffusive flux of the tracer released by lenses during the flushing phase is higher than the diffusive flux released during the non flushing phase. This result is probably related to the effects of the water convective motion. It removes the solute released from the lenses from the interface between the zones at a different permeability level, therefore maintaining the concentration gradient at the interface always high.

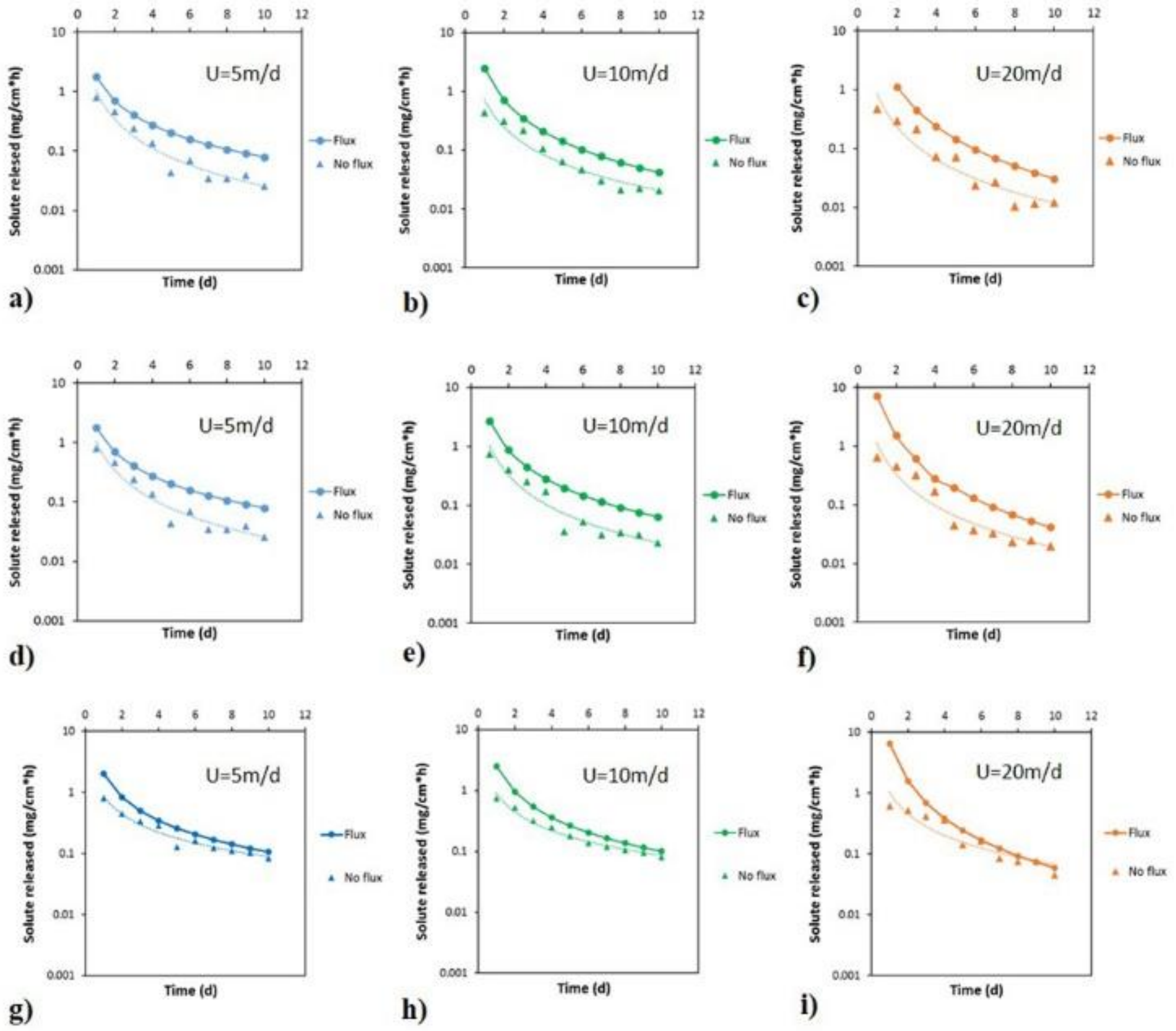

**Fig.19:** Comparison between diffusive flux of Fluorescein released during the flushing and non flushing phases of three tests. Fig. 19a-c show the comparison for lens 1, Fig. 19d-f for lens 2 and Fig. 19g-i for lens 3 (Tatti et al., 2018).

To investigate if hydraulic gradient between the lenses and the sand layer induces a consistent advective flow inside the lenses during the flushing phase, the distribution of pressure on the surface of the lenses was estimated. Considering the lenses as a sphere in a laminar flow (Fig. 20), the pressure was calculated using the relation:

$$p = -\frac{3}{2}\frac{\mu U cos\theta}{R} \qquad (8)$$

where p is the pressure, $\mu$ the dynamic viscosity of water, U the groundwater velocity, R the radius of the sphere and $\theta$ the angle measured around the sphere from 0° at the rear point (P1) and 180° at the front point (P2).

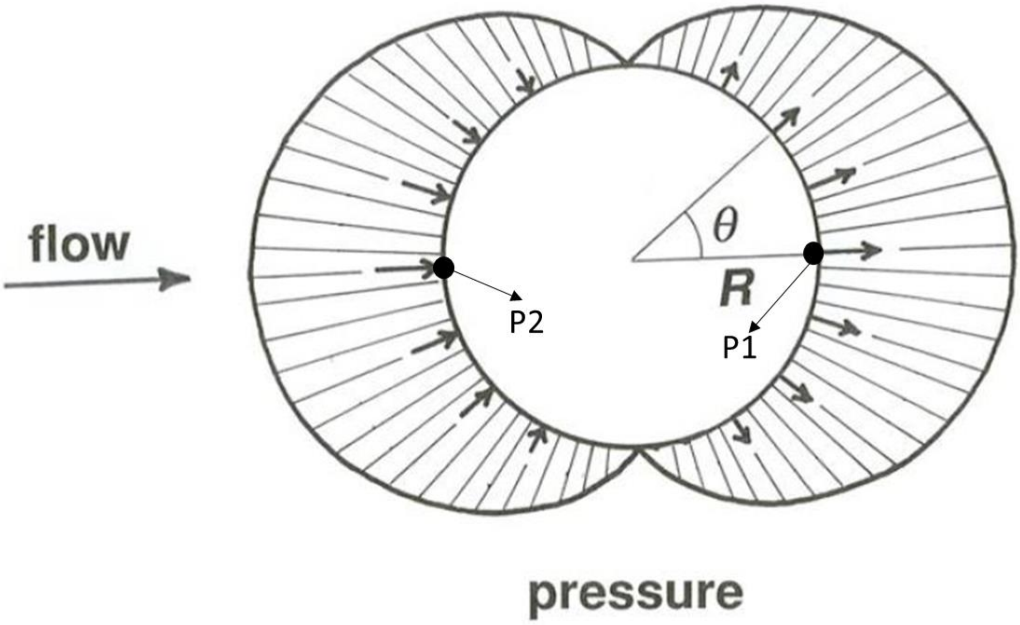

**Fig. 20:** Distribution of pressure on the surface of a sphere in laminar flow (Southard, 2006).

The Δp calculated between the front and rear points of the lenses is around $1*10^{-5}$ Pa. Therefore, the hydraulic gradient between the lenses and the main body of the experiment can be considered numerically negligible. It is reasonable to assume that this slight difference in the pressure values can influence the position of the beginning Fluorescein tail, but it does not develop a consistent advective flow internal to the lenses to be coupled to the diffusional one.

For each lens the diffusive flows released during the flushing phase of the three tests were compared (Fig. 21). The comparison shows that higher fluxes correspond to higher velocities, but only at the beginning of the Back-Diffusion process. This behavior can be explained by considering the tracer distribution inside the lenses. The lenses act as homogeneous layered bodies, so initially the outer layers loose tracer (Fig. 22) and the water advective flow helps maintain high concentration gradient, resulting in more effective depletion.  By diminishing the tracer concentration in the outer layers, the content of the inner layers is transported by the diffusive flux at a molecular level. This process is extremely slow and dominated by the molecular diffusion at pore scale, thus depending on grain size distribution. In these conditions the effect of water motion involves such small-time scales as to be considered negligible if compared with those regarding transport from the inner layers.

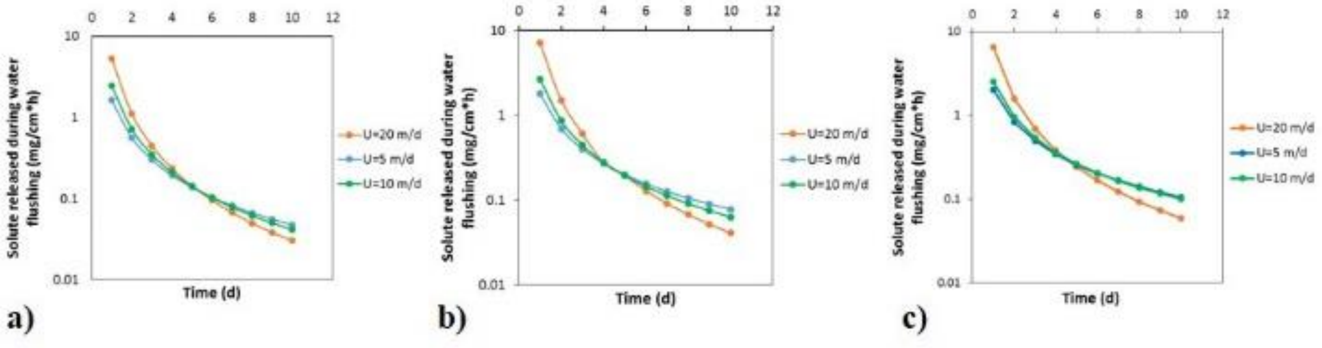

**Fig. 21:** Comparison between diffusive flux of Fluorescein released from the lenses during the flushing phase carried out at different velocities. Fig.21a shows the comparison for the first lens, Fig. 21b for the second lens and Fig. 21c for the third lens (Tatti et al., 2018).

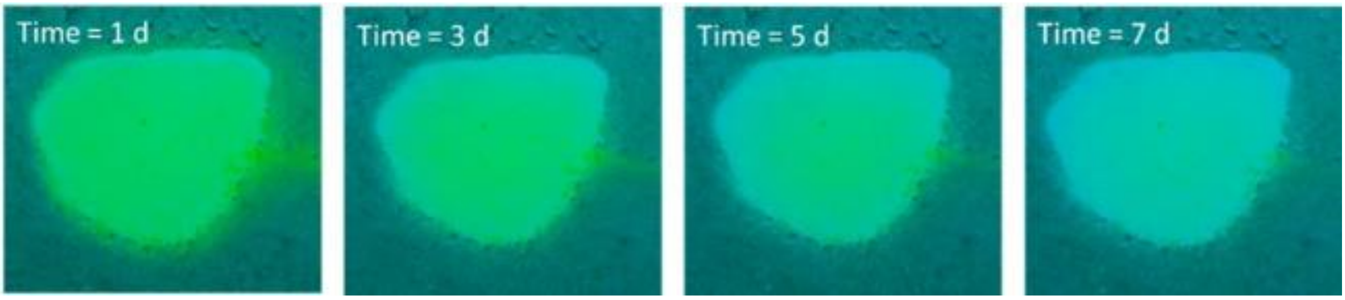

**Fig. 22:** Fluorescein distribution inside the lens 1 during the Back-Diffusion process (Tatti et al., 2018).

## 2.4 The effect of groundwater velocity on timeframe remediation of contaminated low permeability zones

The considerations reported in the above paragraph influence the remediation timeframes in the presence of contaminated low permeability lenses. This was analysed for the three tests presented. The remediation timeframes are defined as the interval time between the beginning of the flushing phase and the emptying of all the low permeability lenses. The evaluation of the released mass from the lenses during the flushing and non flushing phases is carried out using the aforementioned procedures. The object was to rate the remediation strategy that uses the enhanced flow velocity in this kind of contamination source. The images collected were used to evaluate the values of Fluorescein mass and diffusive fluxes released during the flushing and the non flushing phases for each lens. Consequently, the total solute mass contained inside each low permeability zone could be estimated. Clearly, this value is different for each lens. Thus, the average daily diffusive flux measured during the flushing phase can be associated with the value of the tracer mass contained inside the lens deducted from the calculated tracer mass based on the diffusive flux during no-flushing periods. The diffusive flux values vs the respective Fluorescein mass trends are interpolated to determine analytical relations between the Fluorescein mass and the diffusive flux under flow conditions.

These relations were used to estimate the remediation timeframe of the lenses simulating constant groundwater velocity with values of 5, 10 and 20 m/d. A time step ($\Delta$t=1 hour) was chosen and the diffusive flux value corresponding to the initial Fluorescein mass inside the lens was multiplied by $\Delta$t and by the perimeter of the lens. The calculated solute mass was subtracted from the initial value of the Fluorescein mass. Using the relation between the tracer mass and the diffusive flux the new value of diffusive flux was calculated. This procedure is repeated until the residual mass inside the lens could be considered null. In Fig. 23a, b and c trends for the solute amount released during three simulations are compared. For each lens, it is possible to observe an increase of tracer release following the increase in the groundwater velocity which reduced the time interval necessary for emptying. The estimated timeframes necessary for each lens are interpolated to obtain a relation between the remediation timeframe and the groundwater velocity. As shown in Fig. 23d the data for each lens was fitted according to exponential functions ($\alpha$*$e^{\beta x}$) with satisfactory precision. Coefficients $\alpha$ and $\beta$ appear to be related to the grain size of the low permeability layer (Fig. 23e and f) and thus restoration time is a function of groundwater velocity and lens granulometry. The analytical relations obtained can be considered to be an initial approach to investigate the trend of remediation time, knowing the grain size of the contaminated layer and varying groundwater velocity. Results shown in Fig. 23d show a decrease of restoration time which is correlated with an increase of the U, especially in lens 1 and 2 and this is more evident between U=5 m/d and U=20 m/d. This is probably correlated by the lower permeability of lens 3 and would appear to prove the low efficiency of aggressive pumping treatments for the remediation of less permeable zones. This idea is evident if the small reduction in the timeframe remediation is compared with the high energy costs of pumping and the efforts needed to treat the extracted water.

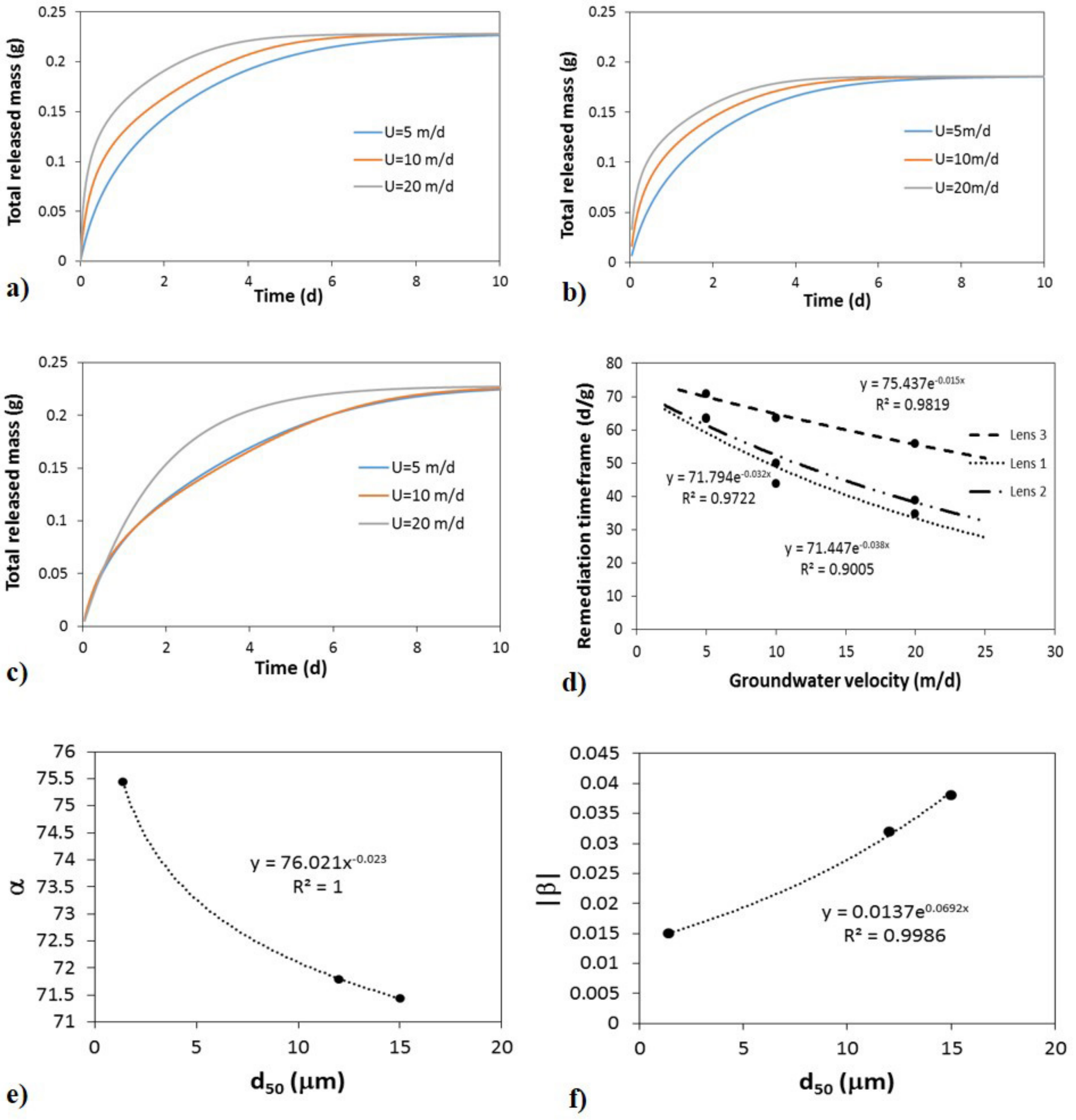

**Fig. 23:** Trend of Fluorescein release using different groundwater velocities for lens 1 (a), lens 2 (b) and lens 3 (c). Trend of remediation timeframes vs groundwater velocity for the three lenses (d). Relation between the coefficients $\alpha$ and $\beta$ and the grain size of the lenses (e, f) (Tatti et al., 2018).

## 2.5 The influence of lens shape on the Back-Diffusion depletion time

A laboratory test was performed to investigate the influence of lens shape on the Back-Diffusion phenomenon. The test was carried out using the experimental setup described in paragraph 1.1. The aquifer model mainly consists of a high permeability layer with two low permeability lenses characterized by the same grain size, but different geometry (Fig. 24). The lenses were previously saturated with a known quantity of Fluorescein and then they were inserted in the sand layer. Aquifer was saturated and clean water was flushed for 5 weeks with U=0.2 m/d. The flushing phase was conducted continuously, without stopping the flux during the night-time hours. During the test images were collected continuously with a prefixed time interval.

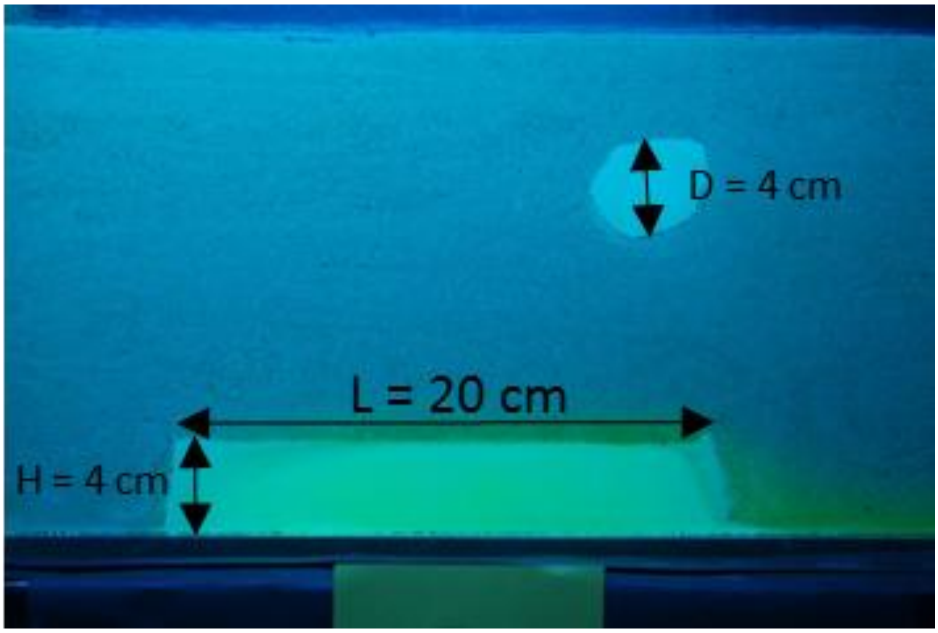

**Fig. 24:** The aquifer model.

The high permeability aquifer zone was composed of sand and the two low permeability lenses of quartz flour. Particle size and porosity of each material used to reproduce the aquifers were defined by the laboratory measurements described in paragraph 1.1. The sand and the lenses hydraulic conductivities were estimated by Hazen and Kozeny equations (2, 3), respectively (Tab. 4).

**Table 4:** The characteristics of the materials used to reproduce the aquifer.

| | **Materials** | **$\gamma s$ (kg/dm$^3$)** | **D$_{50}$ (µm)** | **D$_{10}$ (µm)** | **Porosity** | **Hydraulic Conductivity (m/s)** |
|---|---|---|---|---|---|---|
| Sand | Quartz | 2.65 | 700 | 430 | 0.40 | 3*10$^{-3}$ |
| Lens 1 | Quartz Flour | 2.65 | 12 | 1.4 | 0.42 | 5*10$^{-7}$ |
| Lens 2 | Quartz Flour | 2.65 | 12 | 1.4 | 0.42 | 5*10$^{-7}$ |

The first low permeability lens is characterized by a cylindrical shape with a diameter (D) of about 4 cm and a thickness of 7 cm. Lens 2 can be considered a layer of parallelepiped shape with a length L>>D, a high (H) equal to the diameter of the first lens and a thickness of 7 cm. The low permeability layer is positioned on the bottom of the box model. From Fig. 25 it is possible to observe the different behaviour of Fluorescein inside the two lenses during the test. Inside the second lens, the tracer flux comes from the layers more exposed to the water flow, comprising therefore also the top part of the lens. The release is therefore not symmetric and contrary to what was the effect in the case of the cylindrical lens which had shown an isotropic loss of tracer. (Fig.25).

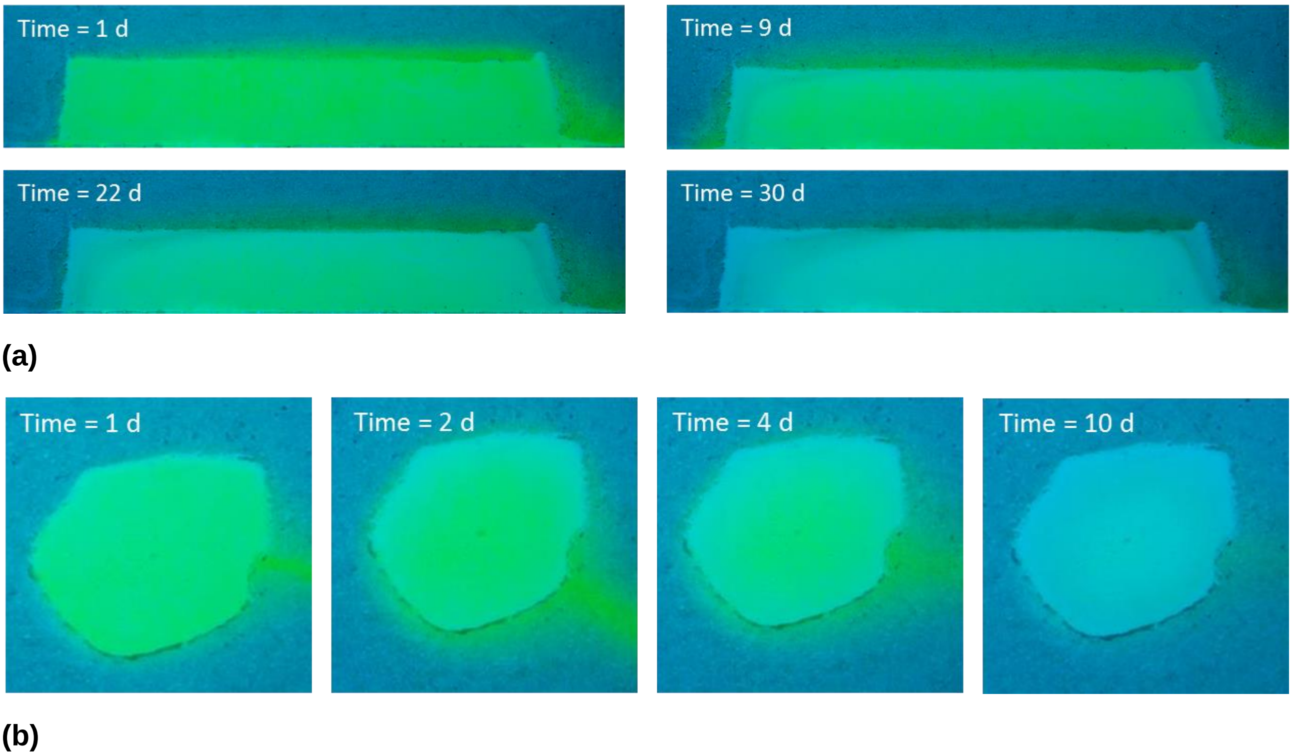

**Fig.25:** Comparison between the distribution of Fluorescein inside the layer (a) and inside the lens (b) during the test.

To investigate how the lens shape influences the Back-Diffusion depletion time, the Fluorescein mass released from the two lenses during the test was estimated using the image analysis procedure previously reported on paragraph 2.2. For each lens and for each collected picture a specific section crossing the plume tail was considered. The average color intensity of the analyzed sections was obtained using a suitable software and using the relations obtained during the calibration phase, a Fluorescein concentration (C) was assigned to the sections. Equation 7 allows for the calculation of a value of diffusive flux of Fluorescein released by each lens per unit of time. Multiplying the obtained value by the time interval between one image and the next, the tracer mass released by the lenses was estimated. As reported previously, the lenses were reproduced using the same materials and they were saturated with a solution containing 2 g/L of dissolved Fluorescein. Thus, we can consider that the unit of volume of each lens contains the same quantity of tracer (about 1 mg). Comparing the trend of cumulated Fluorescein mass per unit of volume of each lens, the release of tracer appears slower for the second lens (Fig. 26). In particular, the lens characterized by a cylindrical shape released the total Fluorecein storage inside its structure during the first 10 days of the test. The layer, instead, continued to release tracer even after the thirtieth day. The laboratory test was stopped after 5 weeks because the concentration of tracer released by the layer after the thirtieth day was too low to be estimated using image analysis. The slower release of Fluorescein from the second lens is probably due to the absence of water motion at the bottom layer. In this way, the area of the second lens available for the release of tracer was reduced and the ratio between Fluorescein mass and the area exposed to the water motion increased. The results of the described laboratory experiment demonstrate the importance of lens shape in relation to the Back-Diffusion process. In particular, contaminated low permeability layers can release contaminats through molecular diffusion for a longer period of time than the lenses, neutralizing the remediation efforts for a complete groundwater restoration.

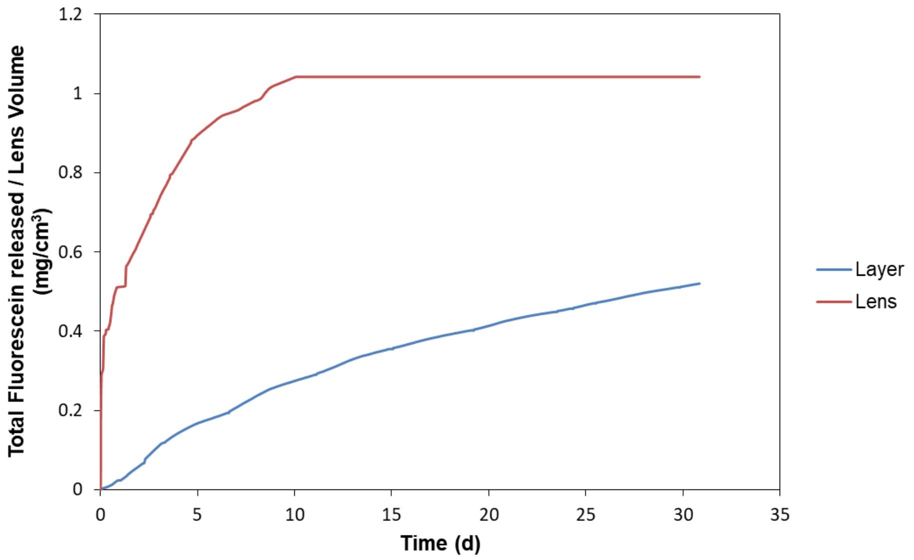

**Fig. 26:** Trend of solute released from the layer and compared with the trend of Flurescein released from the cylindrical lens.

# CHAPTER 3

# APPLICATION OF GROUNDWATER CIRCULATION WELL (GCW) AS AN ALTERNATIVE TECHNOLOGY TO RESTORE CONTAMINATED LOW PERMEABILITY LAYER OF AN AQUIFER

## 3.1 Laboratory investigation: Experimental set-up

The experimental apparatus used to perform the test consisted of a box model, a Groundwater Circulation Well (GCW) with three screen sections, two peristaltic pumps connected to the well, four UV lamps positioned in front of the tank and a 3CCD camera (Fig. 24).

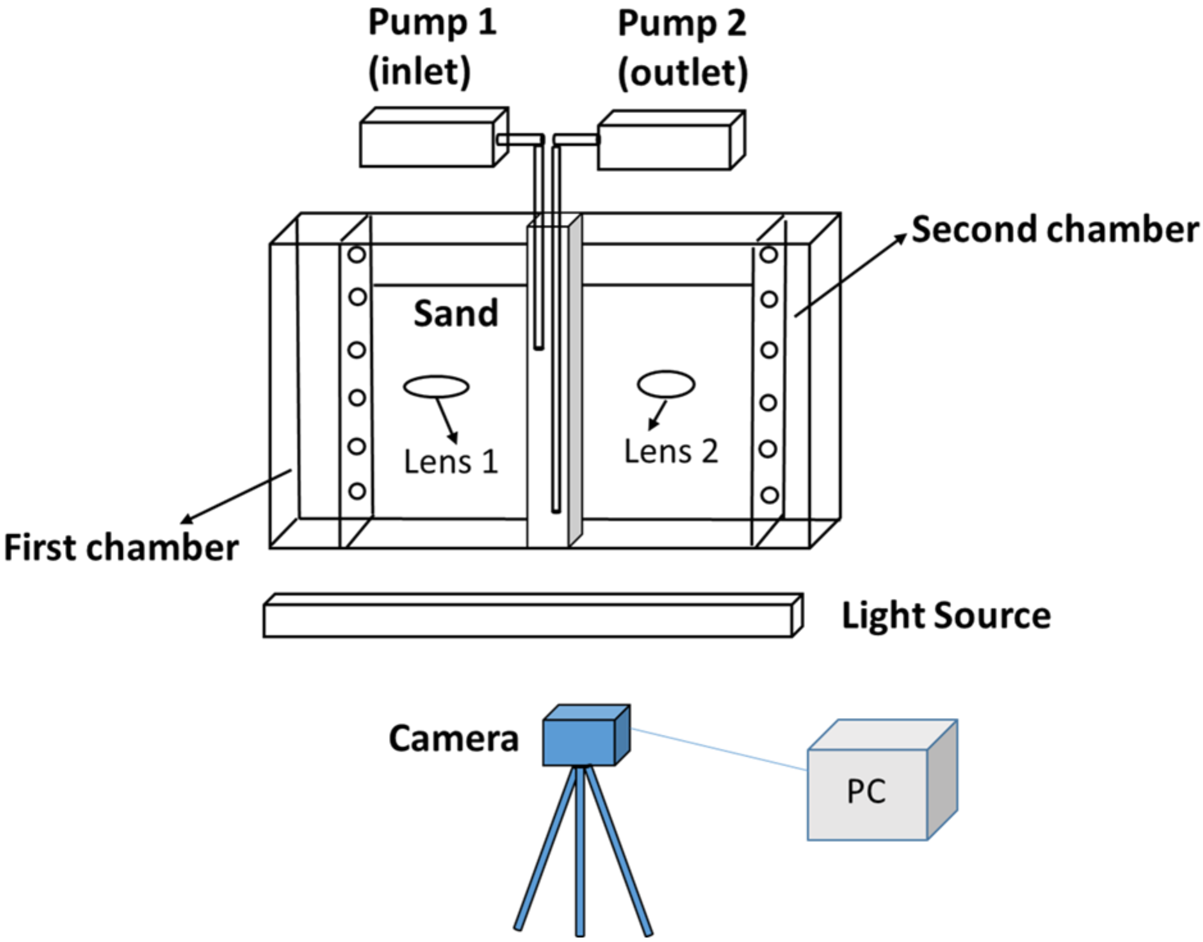

**Fig. 24:** The experimental apparatus used to carry out the test.

An aquifer was reconstructed inside the box model with length 1 m, high 0.7 m and depth 0.12 m. The box is divided in three parts: a central part used to reconstruct the aquifer and two small chambers on the side. The chambers were collected to the central part by punched plates and they were utilized to control the water head. Similarly to the previous described tests, the model of the reconstructed aquifer consists of a high permeability layer and two low permeability lenses with different grain size and hydraulic conductivities. The high permeability layer was reproduced using quartz sand and the two lenses utilizing quartz flour. The grain size of the materials was estimated by the laboratory measurements described on the paragraph 1.1 The sand and the lenses hydraulic conductivities were estimated using the formula proposed by Hazen (equation 2) and by Kozeny and Carman (equation 3), respectively. The properties of the materials are reported in Table 5 and, as it shows, lens 1 is characterized by bigger grain size and by higher permeability than lens 2.

**Table 5:** Characteristics of the reconstructed porous media.

| | **Materials** | **$\gamma$s (kg/dm$^3$)** | **Medium Grain Size $D_{50}$ (µm)** | **$D_{10}$ (µm)** | **Specific surface (cm$^2$/g)** | **$D_{60}$ (µm)** | **Hydraulic Conductivity (m/s)** |
|---|---|---|---|---|---|---|---|
| Sand | Quartz | 2.65 | 700 | 450 | - | 800 | $3.0*10^{-3}$ |
| Lens 1 | Quartz Flour | 1.2 | 35 | 4 | 1900 | 55 | $1.6*10^{-6}$ |
| Lens 2 | Quartz Flour | 0.5 | 3 | 0.8 | 12000 | 3 | $9.2*10^{-7}$ |

In the middle section of the sand layer, between the two low permeability lenses, a GCW model was located (Fig. 25). The GCW was characterized by 1 m of high and 0.11 m of diameter. It had three screen sections and the boreholes between the screen sections were impermeable. Gravel was positioned near the screens to prevent sand from escaping into the well. The first screen was located at the top of the aquifer, the second at the middle part of the sand layer and the third at the aquifer bottom. Sodium Fluorescein was used as tracer due to its property to emit light ranging from green to orange as a function of its concentration when it is excited by UV light. This property allows for the use of the image analysis technique to estimate the tracer concentration during the test. In the reported experiment Fluorescein was excited using 4 UV lamps positioned in from of the box model. A 3CCD camera connected to a computer was located behind the UV lamps in order to acquire images of the aquifer.

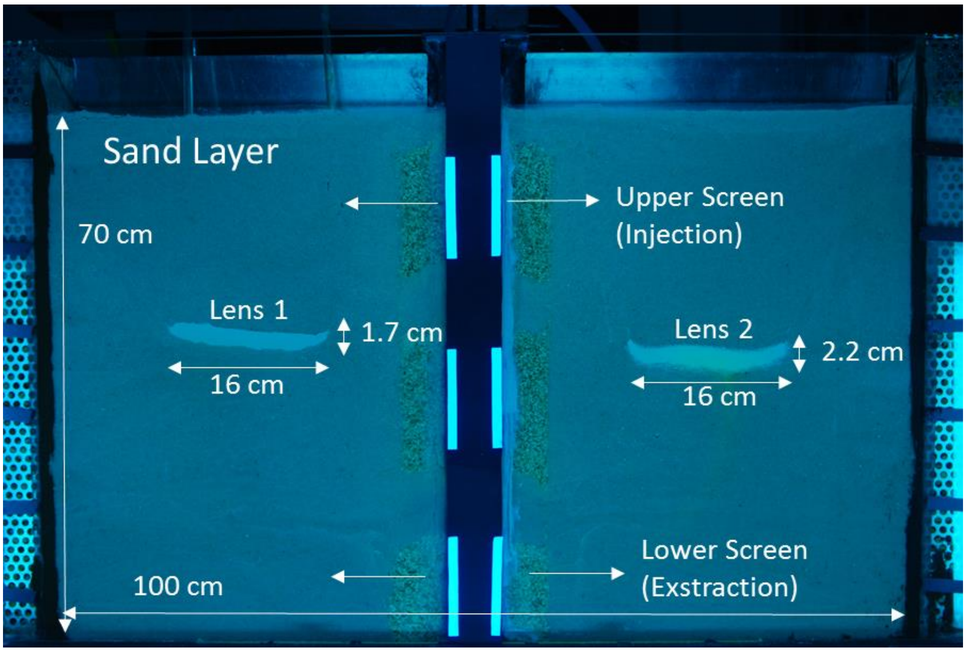

**Fig. 25:** The reconstructed aquifer with two low permeability lenses inside.

## 3.2 Test procedure

The Groundwater Circulation Well was tested in a homogeneous sand aquifer reconstructed inside the middle section of the box model. Aquifer was saturated with clean water and then the tank was sealed to keep the water head constant. Two peristaltic pumps working at a fixed flow rate were connected to the upper screen of the GCW and to the lower screen respectively. Water was introduced into the aquifer from the upper screen and extracted from the lower. In this way, the GCW system created a flow field characterized by circular pathlines with a radius dependent on the circulation flow rate. Tests were carried out to choose the optimum value of circulation flow rate based on the box model's dimensions and on the velocity of water circulation. To visualize the pathlines of the flow and to estimate their radius, Fluorescein was injected in different points of the aquifer during the tests (Fig. 26).

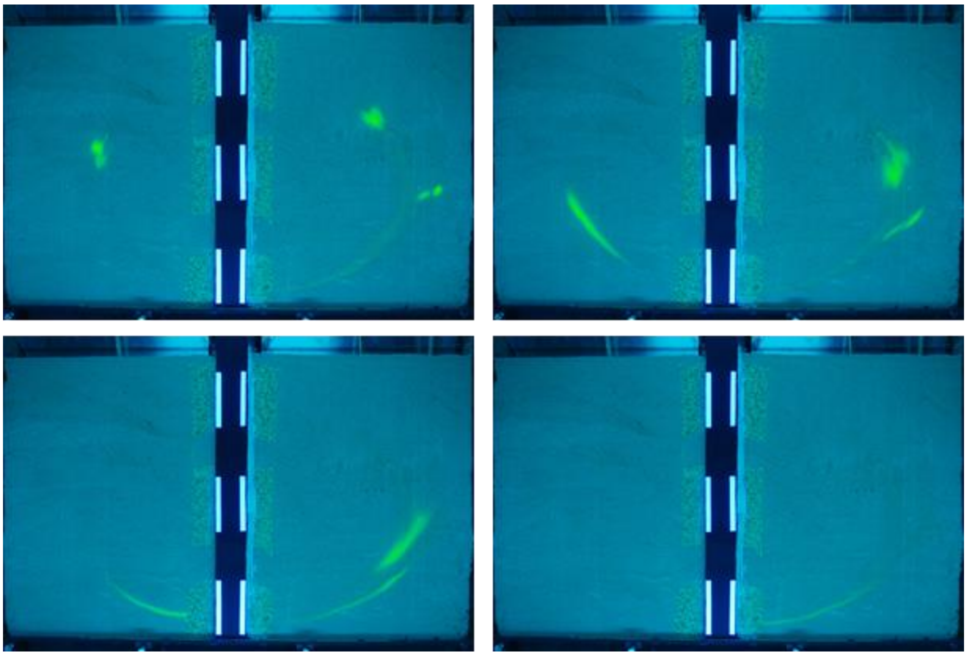

**Fig.26:** Flow pathlines visualized by injection of Fluorescein in different point of the sand aquifer.

The optimum value of the circulation flow rate was estimated around 120 L/h and it was used during the test carried out to investigate the effect of GCW on Back-Diffusion process.

The Back-Diffusion process from the low permeability zone of the aquifer was simulated by saturating the two reconstructed lenses with a solution containing 2 g/L of dissolved Fluorescein. Lens 1 and lens 2 were filled with an amount of about 0.1 g and 0.2 g of tracer, respectively. The second lens contained more Fluorescein than the first one due to its higher porosity and dimensions (Fig. 25).

The saturated lenses were inserted into the sand layer, the aquifer was saturated with clean water and then water was circulated for 8 days. During this phase the Back-Diffusion process was clearly visible (Fig. 27). The tracer released by the lenses generates Fluorescein tails. During the test images of the aquifer were collected continuously with a prefixed time interval from an automatic acquisition system and stored on a computer. To improve the clarity of the pictures, a UV filter (Hoya Pro1 Digital Filter UV) was applied to the camera lens.

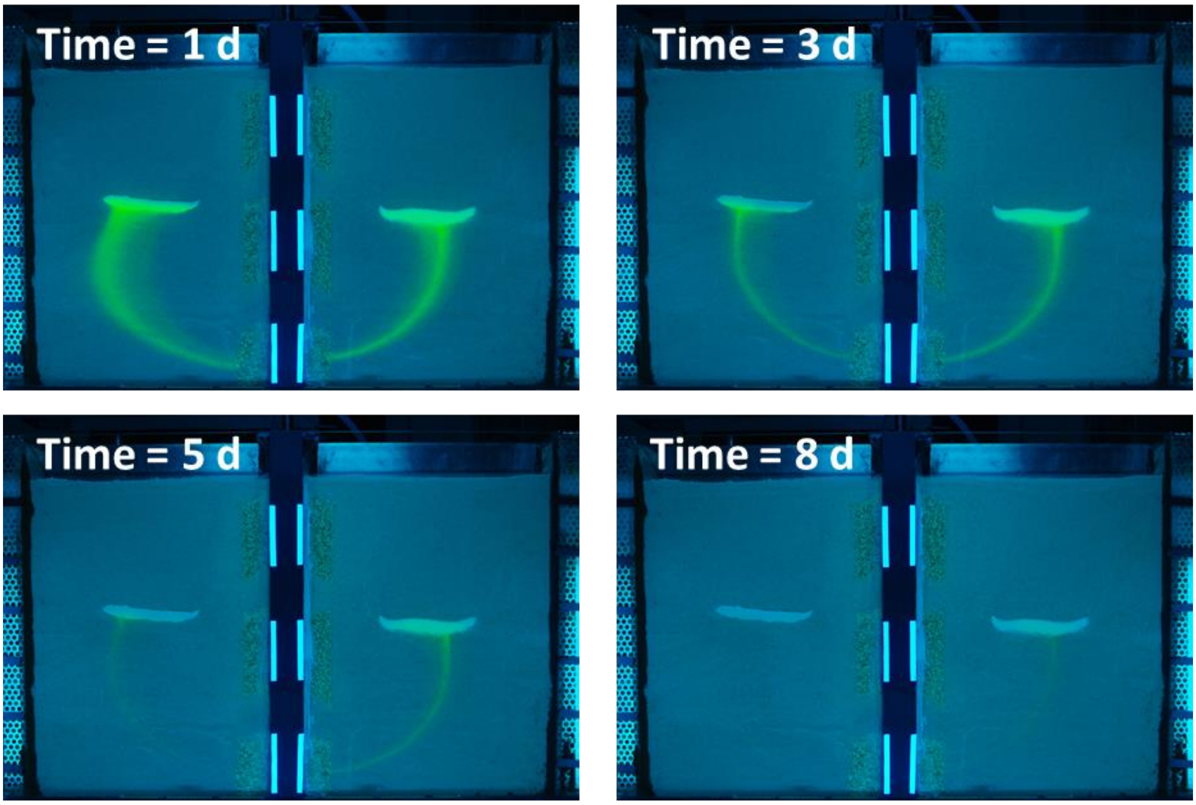

**Fig.27:** The Back-Diffusion process from the low permeability lenses during water circulation.

### 3.3 Image analysis procedure

To evaluate the Fluorescein concentration inside the aquifer, a calibration procedure was used. Briefly, an aquifer was saturated with solutions at different known concentrations of Fluorescein and for each solution images of a saturated box model were collected (Fig.28).

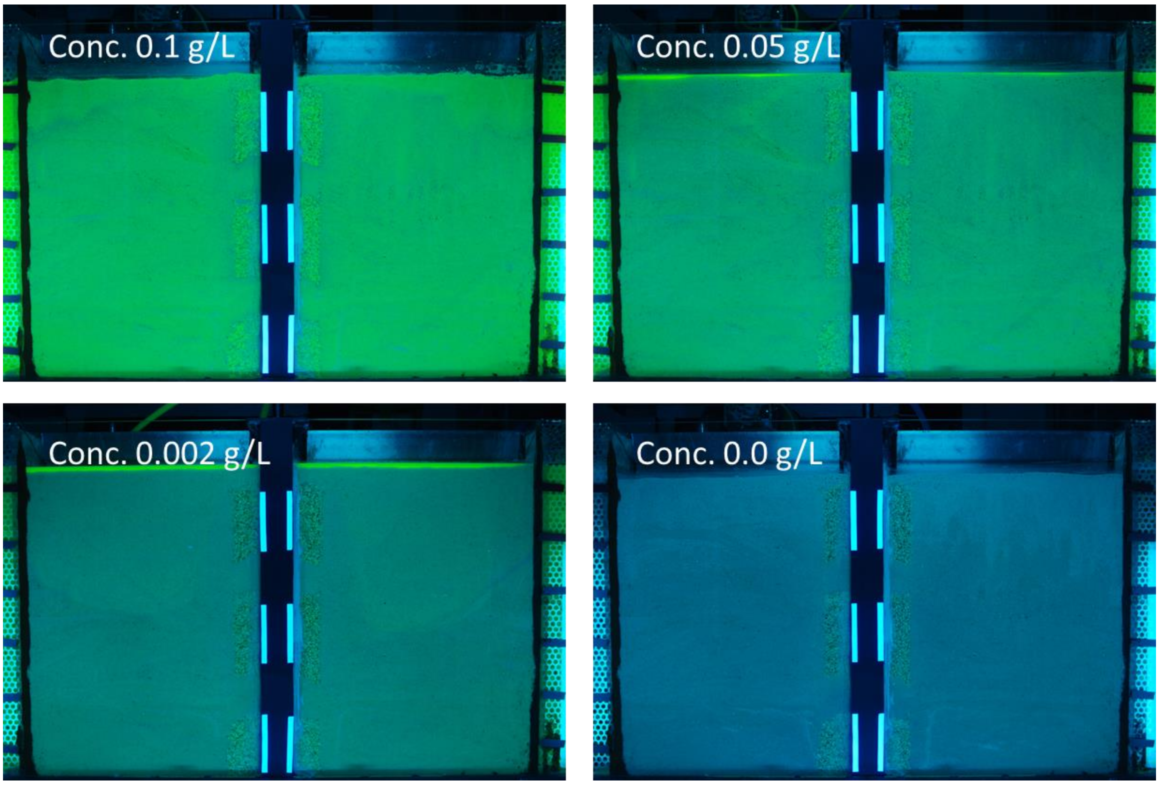

**Fig.28:** Images of aquifer saturated with Fluorescein solutions at known concentrations.

For every picture the three color channels were split and using a suitable software the average intensity of the Green color was measured.

Color intensity values obtained by image elaboration coupled with the respective concentrations were interpolated to determine the analytical relations between the Fluorescein concentration and the Green light intensities. As Fig. 29 shows, an exponential function fits the relation between the Green color intensity and the concentrations, according to the results reported on paragraph 1.3.1. The satisfying agreement between the experimental data and the interpolating relations is demonstrated by the high value of correlation coefficient ($R^2$) and by the low value of the Root Mean Square Error (RMSE).

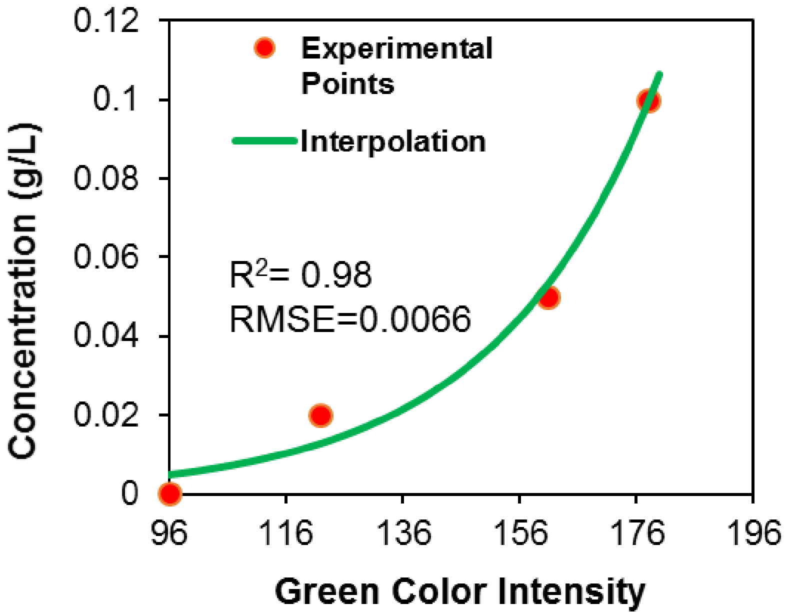

**Fig.29:** Relation between Green color intensity and Fluorescein concentration.

To investigate the effect of water circulation on the Back-Diffusion process the mass of Fluorescein released during the test from the low permeability lenses was estimated. To achieve the goal, the diffusive flux of tracer released by the two lenses was calculated adopting the image analysis procedures described in paragraph 2.2. For each lens a specific section crossing the plume tail was considered (Fig. 30) and using the relations obtained during the calibration phase, a Fluorescein concentration (C) was assigned to the analyzed sections.

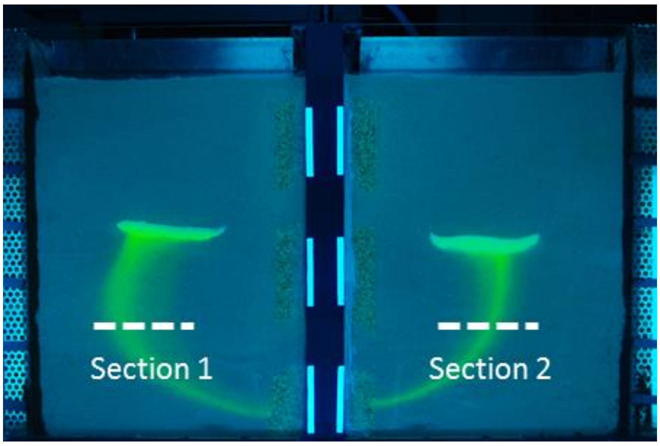

**Fig.30:** The sections considered to estimate the Fluorescein mass released from the two lenses during the test using the image analysis technique.

The obtained concentration values were used in equation (7) to calculate the diffusive flow per unit of time (J) released by each lens.

The Darcy velocity (U) was estimate by image analysis technique considering the position of the Fluorescein tail in images captured with a fixed time interval. This method was validated using the theoretical approach proposed by Ros and Gary, 1993:

$$U_x = -\frac{k}{n} * \frac{\partial h}{\partial x} \tag{9}$$

$$U_z = -\frac{k}{n} * \frac{\partial h}{\partial z} \tag{10}$$

$$\frac{\partial h}{\partial x} = -\frac{Q(x-x_0)}{8\pi kL} * \left| \frac{1}{\sqrt{(x-x_0)^2+(y-y_0)^2+(z-z_0+L)^2}} - \frac{1}{\sqrt{(x-x_0)^2+(y-y_0)^2+(z-z_0-L)^2}} \right| \tag{11}$$

$$\frac{\partial h}{\partial z} = -\frac{Q}{8\pi kL} * \left| \frac{1}{\sqrt{(x-x_0)^2+(y-y_0)^2+(z-z_0+L)^2}} - \frac{1}{\sqrt{(x-x_0)^2+(y-y_0)^2+(z-z_0-L)^2}} \right| \tag{12}$$

where Ux and Uz are the components of velocity vector, k is hydraulic conductivity, n porosity, h hydraulic head, Q flow rate of injected/extracted water, ($x_0$, $y_0$, $z_0$) and 2L coordinates are the center point and the length of the well screen respectively.

The diffusive flux (J) was calculated for each lens and for each image captured during the test. The Fluorescein mass released from low permeability lenses was obtained multiplying every value of J by the time interval between the capture of the images. In this way, the values of Fluorescein mass in each lens vs time were obtained (Fig. 31). As the results show, the depletion time of the mass contained in the lenses due to the Back-Diffusion phenomenon is larger for the second lens, because of its major dimensions and of its lower permeability. This result agrees with data obtained during the previous tests that show an increase of the remediation time correlated to the decrease of grain size (Fig.23d).

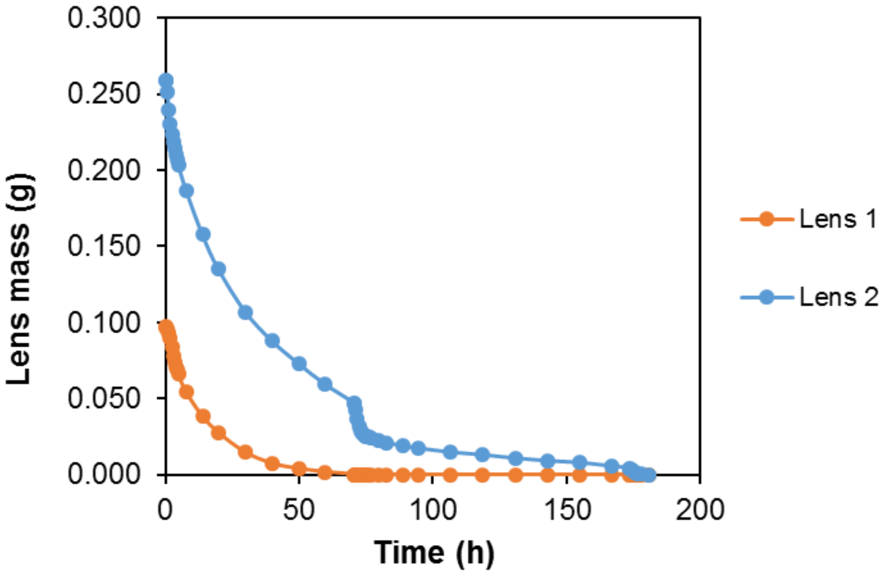

**Fig.31:** Fluorescein mass contained into the two lenses during the test.

## 3.4 Numerical model

A numerical model was developed to reproduce the Back-Diffusion process and to evaluate the effects of pumping technologies on the contaminant redistribution process from low to high-permeability zones of an aquifer.

Considering a heterogeneous and anisotropic aquifer, the fluid flow was simulated numerically using the groundwater flow equation:

$$s_s \frac{\partial h}{\partial t} = \frac{\partial}{\partial x_i}(k_{ii} \frac{\partial h}{\partial x_j}) + q_s \qquad (13)$$

where h is the hydraulic head [L], $k_{ii}$ the principal component of the hydraulic conductivity tensor [$LT^{-1}$], $S_s$ the specific storage of the porous media [$L^{-1}$] and $q_s$ the volumetric flux of water extracted/injected per unit of aquifer volume [$T^{-1}$].

Groundwater velocity was described by the Darcy equation:

$$U_i = -\frac{k}{n} * \frac{\partial h}{\partial x_i} \tag{14}$$

where hydraulic head was obtained from the solution of equation (13).

The numerical simulation of non-reactive contaminants transported in an aquifer was carried out using the transport and diffusion equation:

$$\frac{\partial C}{\partial t} + u_i \frac{\partial C}{\partial x_i} = D_{idr} \frac{\partial^2 C}{\partial x_i^2} \tag{15}$$

where C [$ML^{-3}$] is the solute concentration, $u_i$ are the components of velocity vector and $D_{idr}$ [$L^2T^{-1}$] is the hydrodynamic dispersion coefficient. The equations used in the model were numerically solved in two dimensions using the finite difference method. For the bottom and for the side boundaries of the domain the Neumann condition was used.

The model was validated reproducing the laboratory test described in paragraph 3.2 and comparing the experimental results with the numerical ones. The calibration phase was carried out by varying the values of the hydrodynamic dispersion coefficient and the hydraulic conductivity of the media. Table 6 reports the input data used in the model.

**Table 6:** Model input data.

| Parameter | Value | Units |
|---|---|---|
| Sand hydraulic conductivity | $8*10^{-4}$ | m/s |
| Lens1 hydraulic conductivity | $2*10^{-6}$ | m/s |
| Lens 2 hydraulic conductivity | $6*10^{-7}$ | m/s |
| Sand hydrodynamic dispersion | $5*10^{-9}$ | $m^2/s$ |
| Lenses hydrodynamic dispersion | $1*10^{-10}$ | $m^2/s$ |
| Injection/Extraction flow rate | 120 | L/h |
| Initial Fluorescein mass inside Lens 1 | 1.0 | g |
| Initial Fluorescein mass inside Lens 2 | 0.26 | g |

To validate the model, the Fluorescein mass contained inside the lenses determined numerically was compared to the one estimated by image analysis (Fig. 32). The agreement between the values can be considered satisfactory to demonstrate the model suitability to reproduce the investigated process.

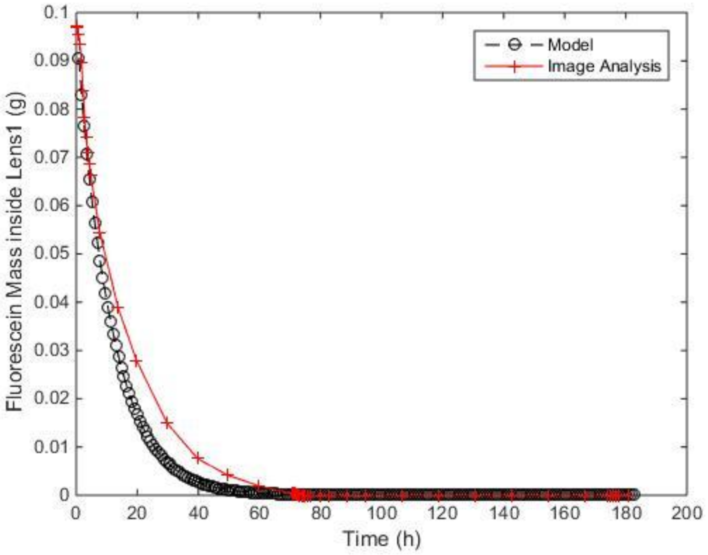

**(a)**

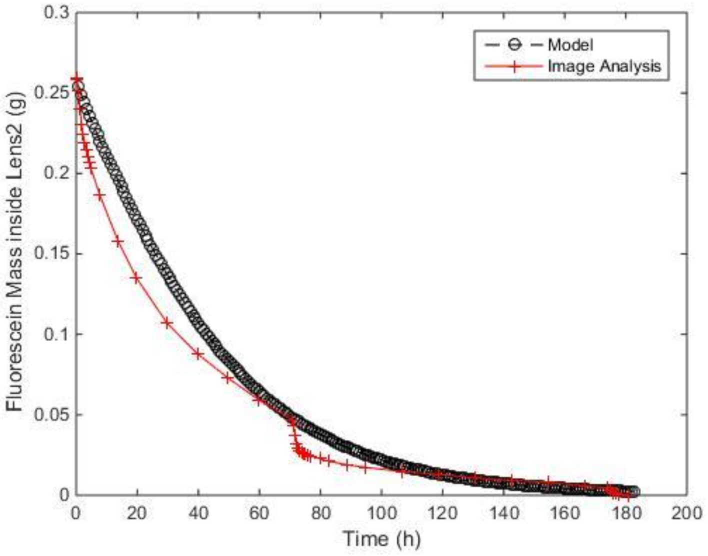

**(b)**

**Fig.32:** The comparison between the experimental data and those obtained by numerical simulation for lens 1 (a) and lens 2 (b).

## 3.5 Results of numerical simulations

The numerical model was used to investigate the effects of the GCW technology and of a classic Pump and Treat system on the contaminant redistribution process from low-permeability layers of an aquifer. To achieve this goal, the laboratory test was numerically simulated varying injection/extraction water flow rate and considering different positions of the polluted low-permeability layers inside the aquifer.

The numerical simulation of the Groundwater Circulation Well was carried out pumping contaminated water from the lower screen and injecting clean water from the upper screen section (Fig. 33a and Fig. 34a). The traditional well, characterized by only one screen section, was simulated extracting water from a lower screen (Fig. 33b and Fig. 34b), as generally used at the field scale. To investigate the effect of the injection/extraction water flow rate (Q) on the Back-Diffusion process, three flow rates were simulated (Q=60 L/h, Q=120 L/h and Q=150 L/h). As Figures 35a and b show, enhancing the flow rate of water circulation the tracer depletion time decreased for both the two lenses. This effect appears valid for both remediation technologies investigated, however the decrease of the Back-Diffusion depletion time is more evident in case of GCW (Fig. 35a and b). This result depends on the different effects generates by the two considered types of well. Both the remediation technologies develop a flow field that removes the contaminant at the interface between the high and the low-permeability zones increasing the diffusive flux of contaminant released by the lenses. The GCW develops also a hydraulic gradient orthogonal to the main axis of the low-permeability layers that generates a small flow into the lenses supporting the contaminant diffusive flow.

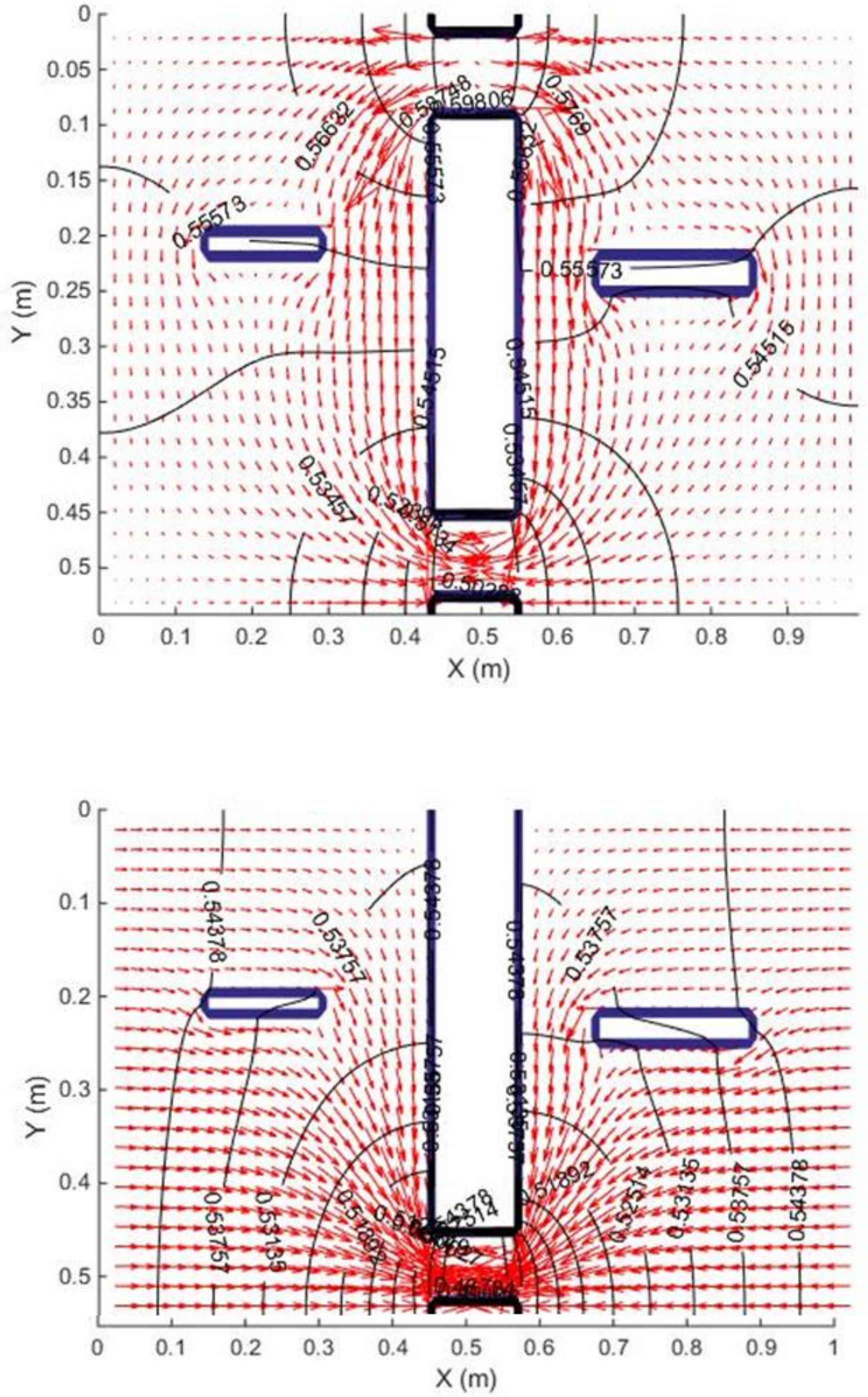

(a)

(b)

**Fig. 33:** The hydraulic head and the flow field simulated numerically using a GCW (a) and a standard well (WS) (b).

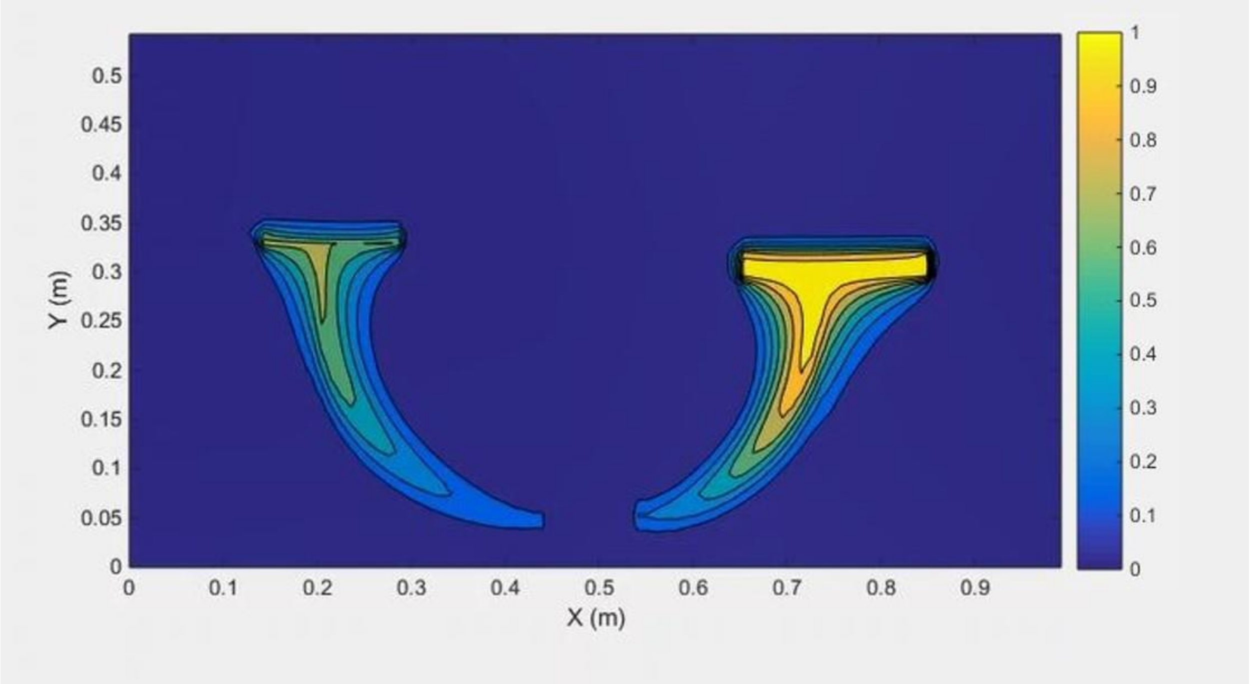

**(a)**

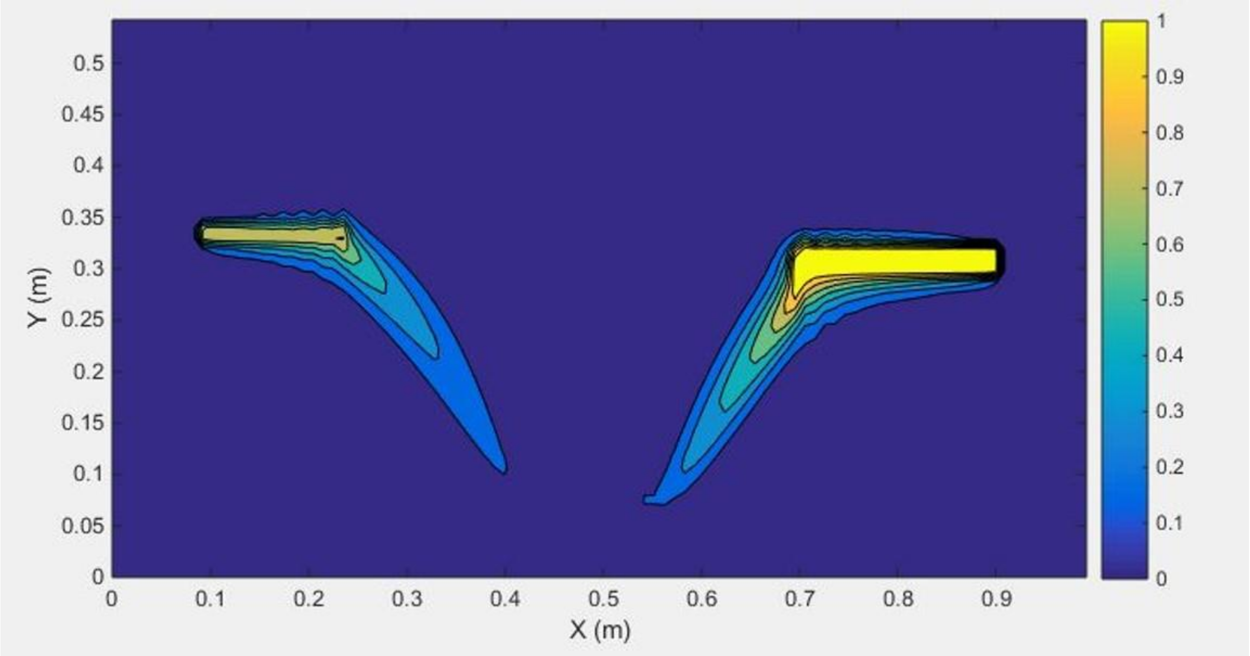

**(b)**

**Fig.34:** The concentration field simulated numerically using a GCW (a) and a standard well (WS) (b).

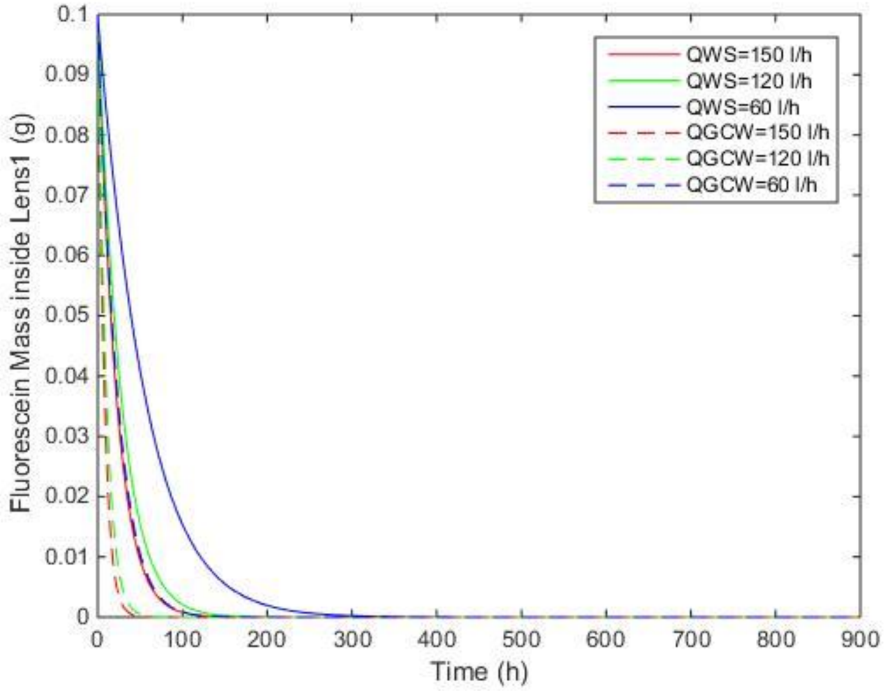

**(a)**

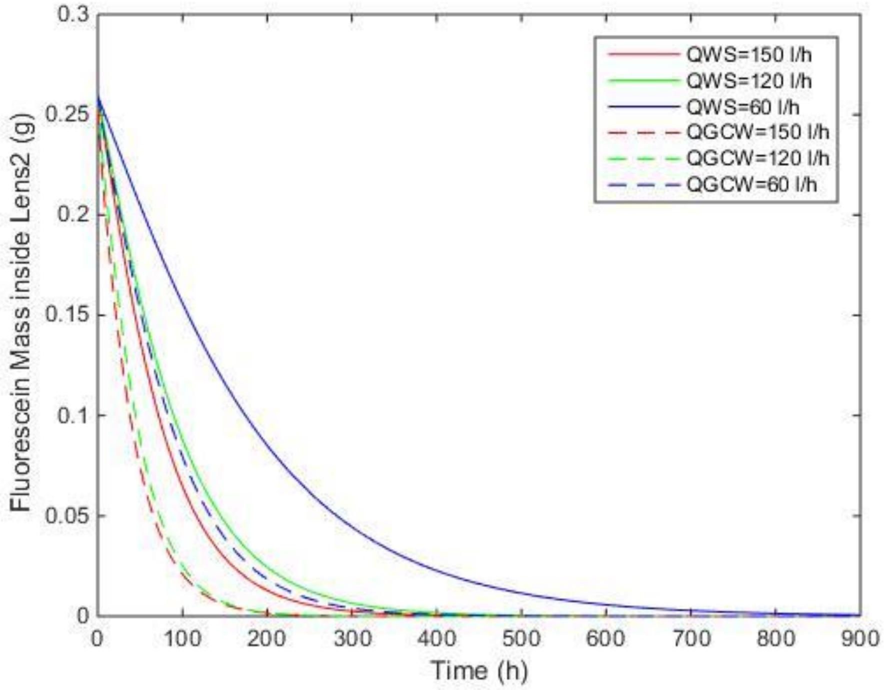

**(b)**

**Fig. 35:** The trend of Fluorescein mass contained into the lens 1 (a) and the lens 2 (b) simulating the use of a GCW and of a standard well (WS) with different injection/extraction water flow rates.

The efficiency of the Groundwater Circulation Well was evaluated varying also the position of the low permeability lenses. In particular, the lenses were positioned near the top and close to the bottom of the aquifer (Fig. 36), reproducing therefore situations in which it is not clearly known the low permeability layer position. For both cases, three numerical simulations were carried out using different water circulation flow rates (60 L/h, 120 L/h and 150 L/h). The results obtained for each position were compared to those obtained for the central position (the real position of the lenses in the reconstructed aquifer at laboratory scale). As Figures 37 and 38 show, for both positions of the lenses the Back-Diffusion depletion time increases if compared to those obtained with the central position. This result is correlated to the flow field developed by the GCW. The lenses located at the top and at the bottom of the aquifer are close to the upper and the lower GCW screen respectively and thus the main component of the water flow is parallel to the main axis of the low permeability layers. The results obtained using a GCW were then compared to those obtained simulating the remediation of the lens positioned at the top and at bottom of the aquifer using a traditional well (Fig. 39). Three simulations were performed pumping water at Q=60 L/h, Q=120 L/h and Q=150 L/h. Comparing the trends of Fluorescein mass released from the lenses using a GCW and a traditional well, the Back-Diffusion depletion appears faster using the GCW scheme (Fig. 40-41). This result is valid for both the lenses and for both the considered positions.  Taking into account the results of all numerical simulations performed, the Groundwater Circulation Well technology appears more suitable to be used in the contest of presence of contaminated low permeability lenses rather than the traditional well, but as verified its efficiency depends on the position of the lenses.

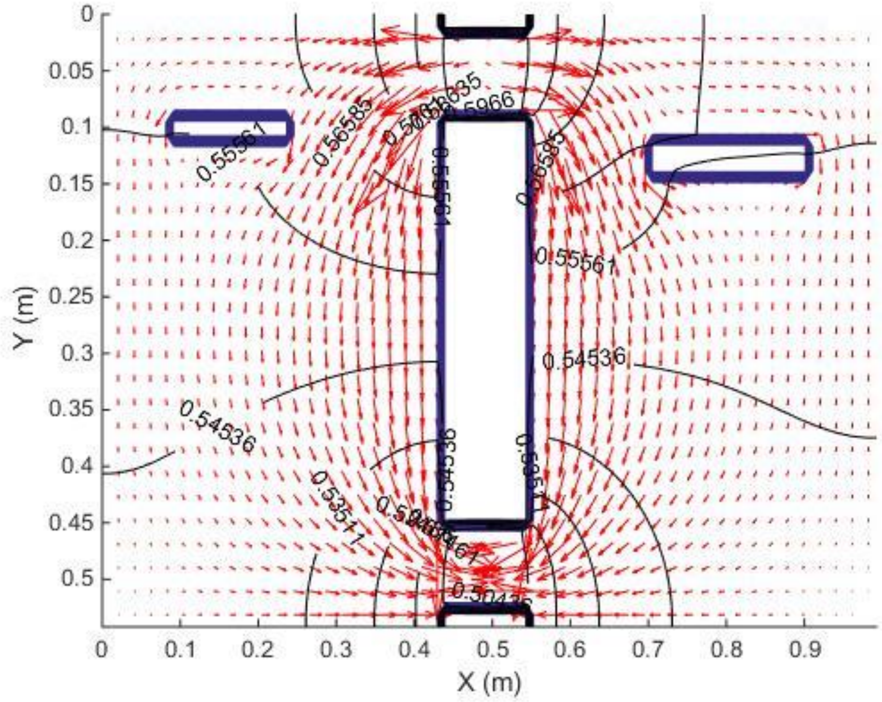

(a)

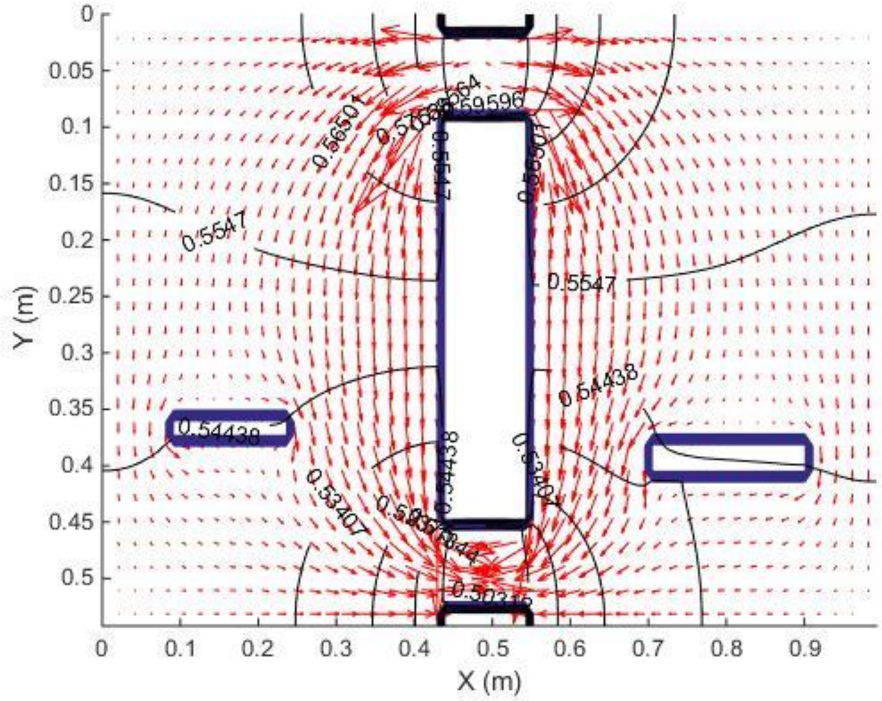

(b)

**Fig. 36:** The hydraulic head and the flow field simulated numerically using a GCW for the lenses positioned at the top (a) and at the bottom (b) of the acquifer.

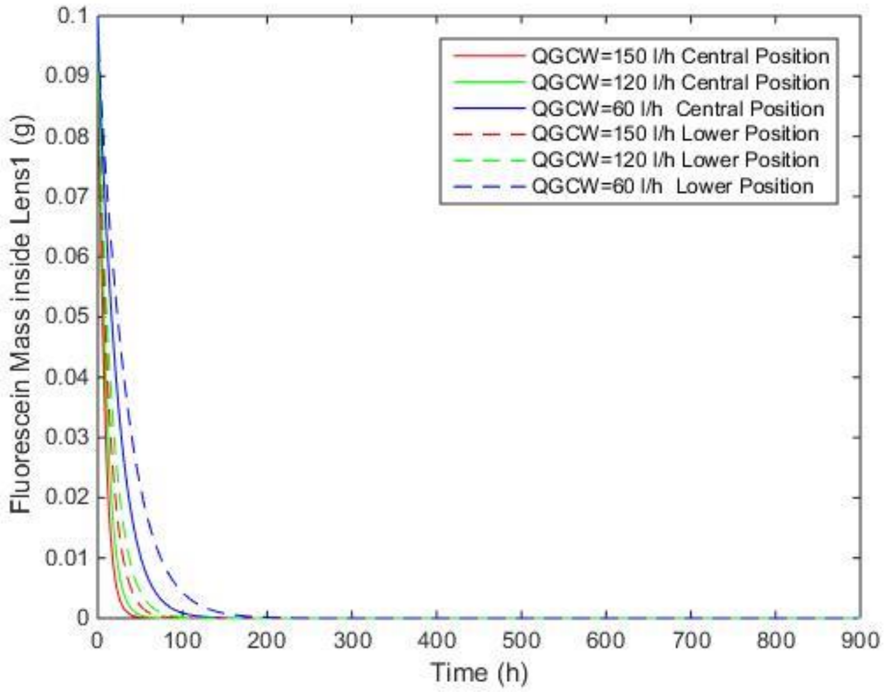

**(a)**

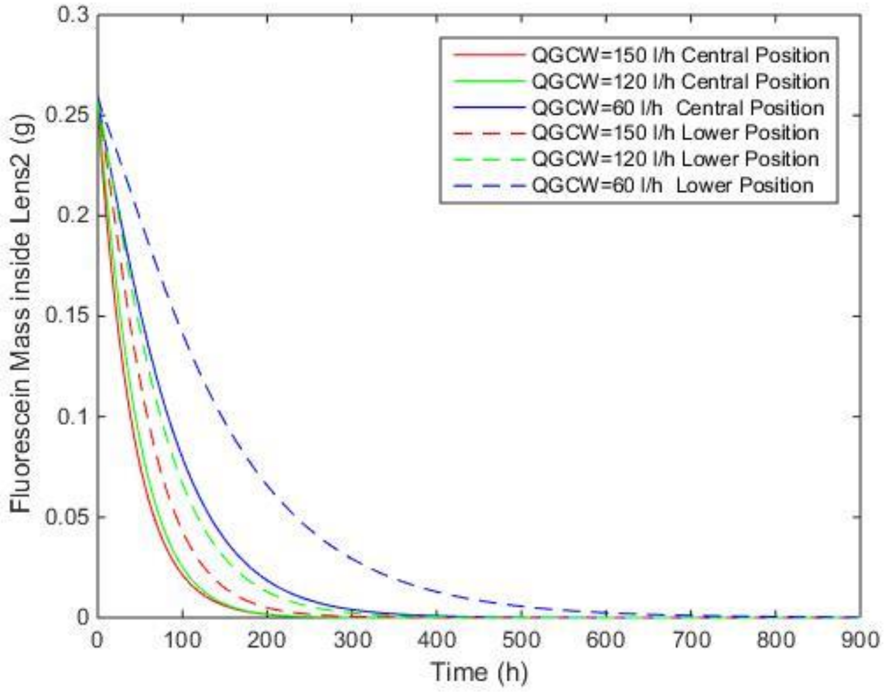

**(b)**

**Fig. 37:** The trend of Fluorescein mass contained into the lens 1 (a) and the lens 2 (b) positioned near the bottom and in the middle part of the aquifer simulating the use of a GCW.

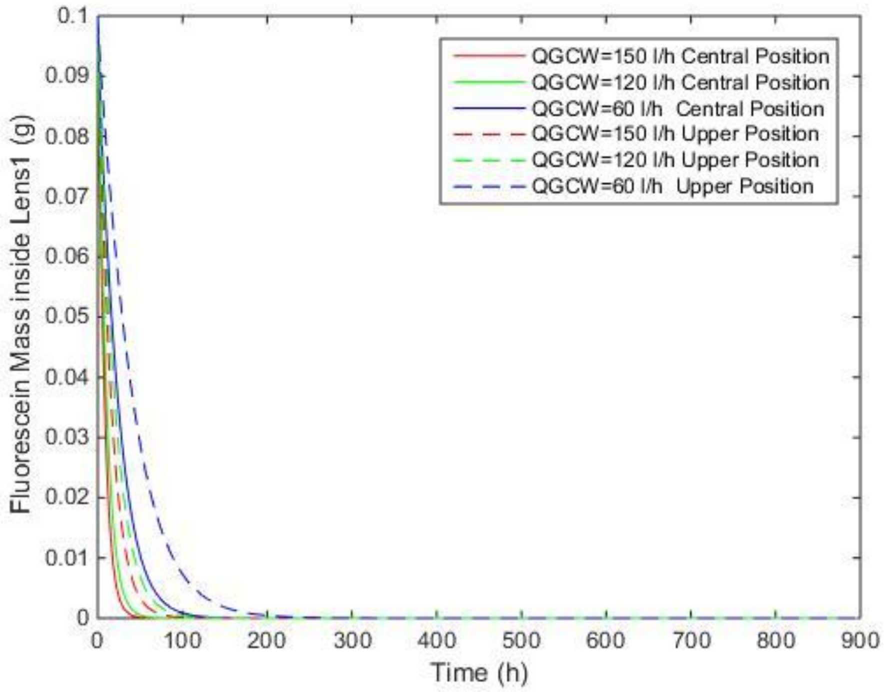

**(a)**

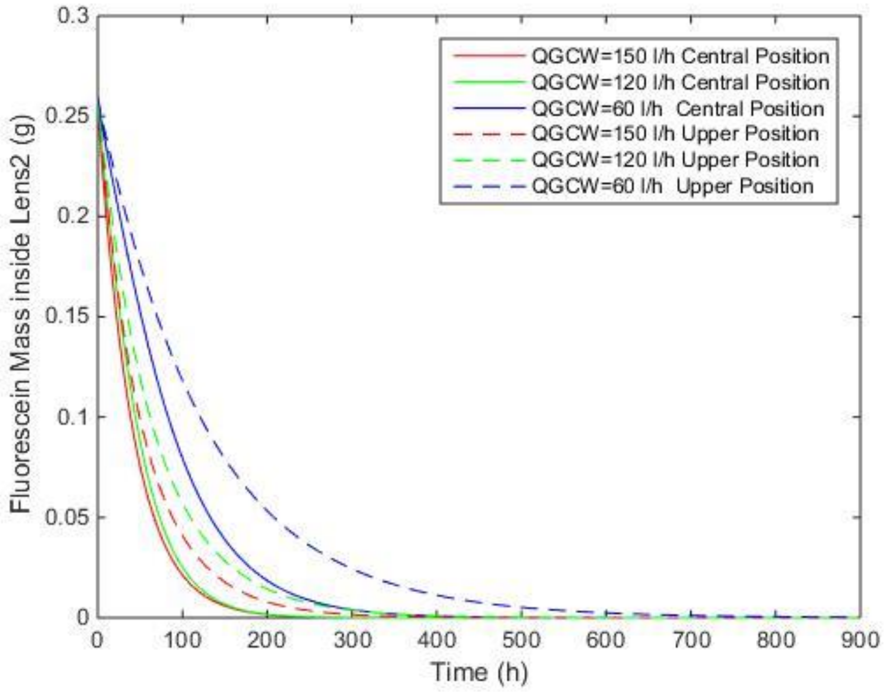

**(b)**

**Fig. 38:** The trend of Fluorescein mass contained into the lens 1 (a) and the lens 2 (b) positioned near the top and in the middle part of the aquifer simulating the use of a GCW.

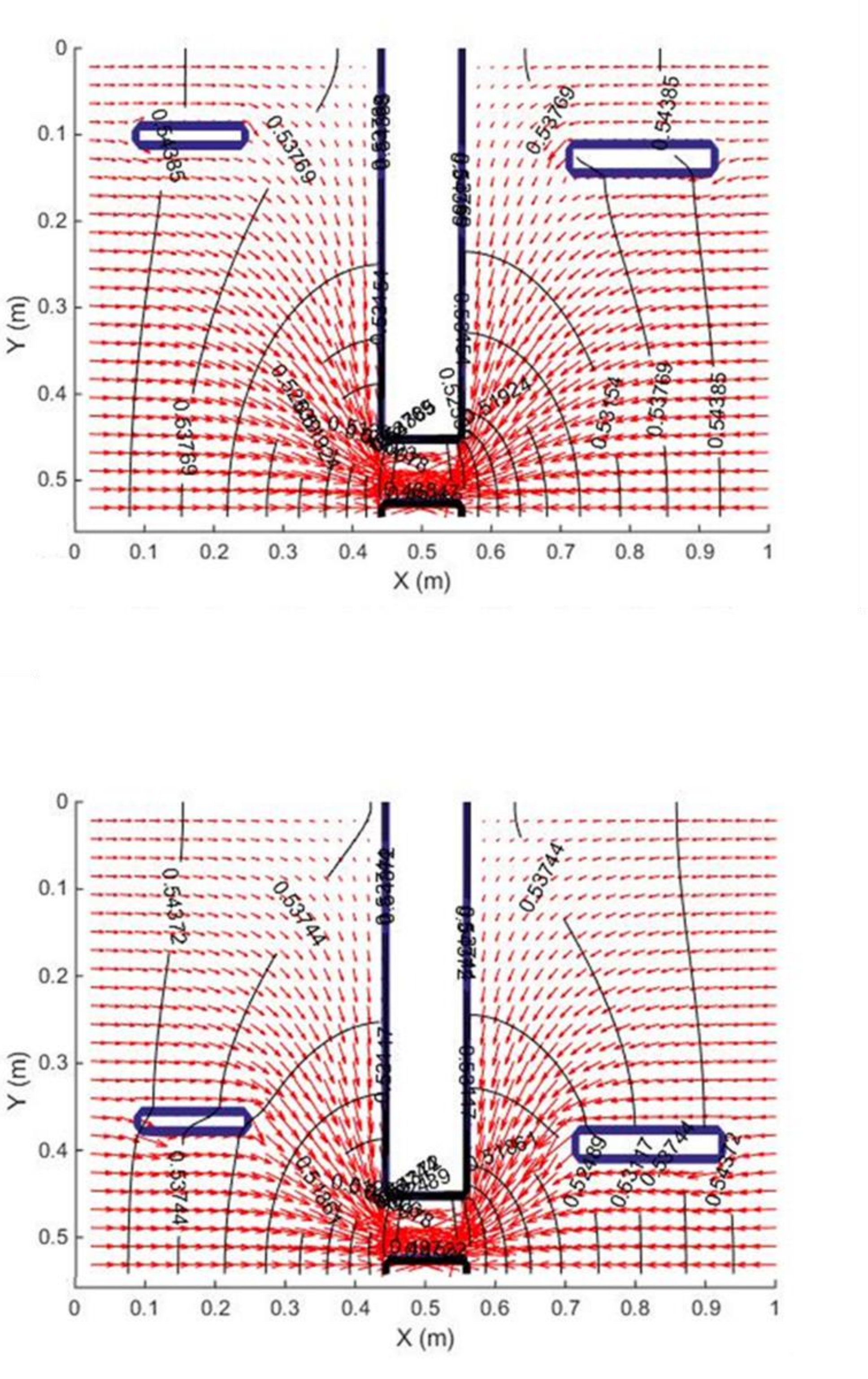

(a)

(b)

**Fig. 39:** The hydraulic head and the flow field simulated numerically using a standard well for the lenses positioned at the top of the acquifer (a) and at the bottom (b).

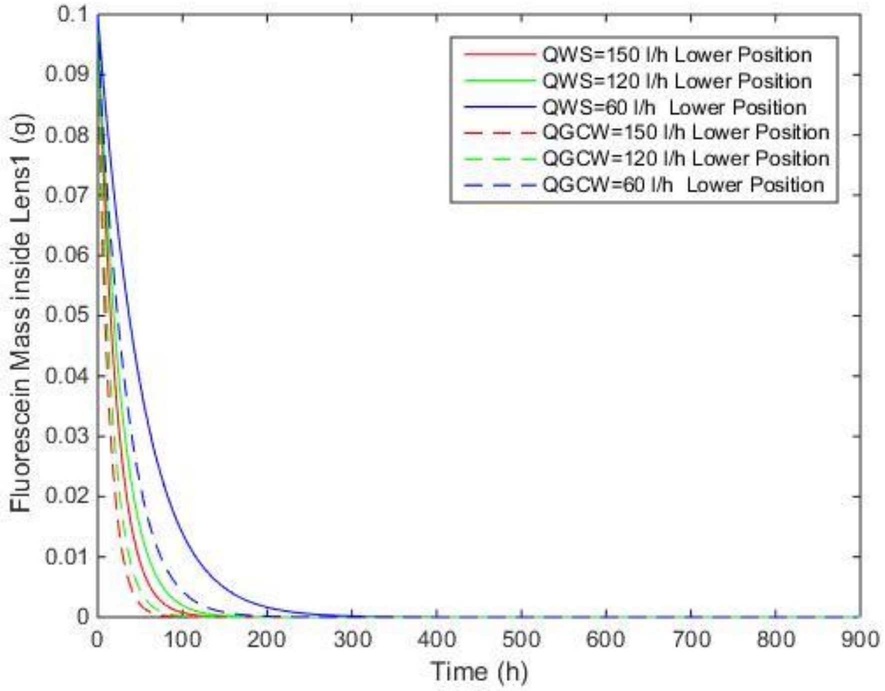

**(a)**

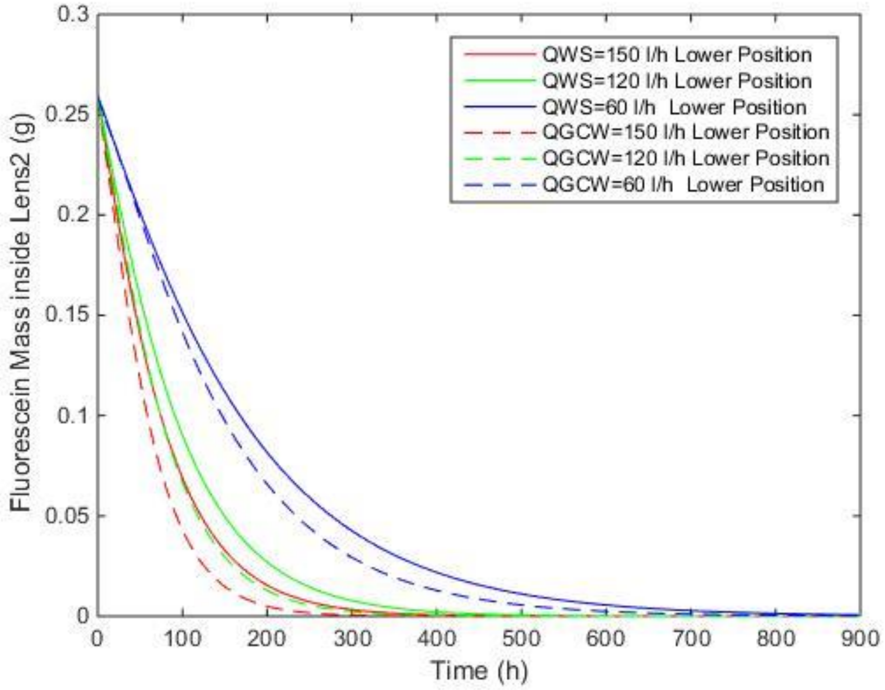

**(b)**

**Fig. 40:** Comparison between the trend of Fluorescein mass contained into the lens 1 (a) and the lens 2 (b) positioned near the bottom of the aquifer simulating the use of a GCW and of a standard well.

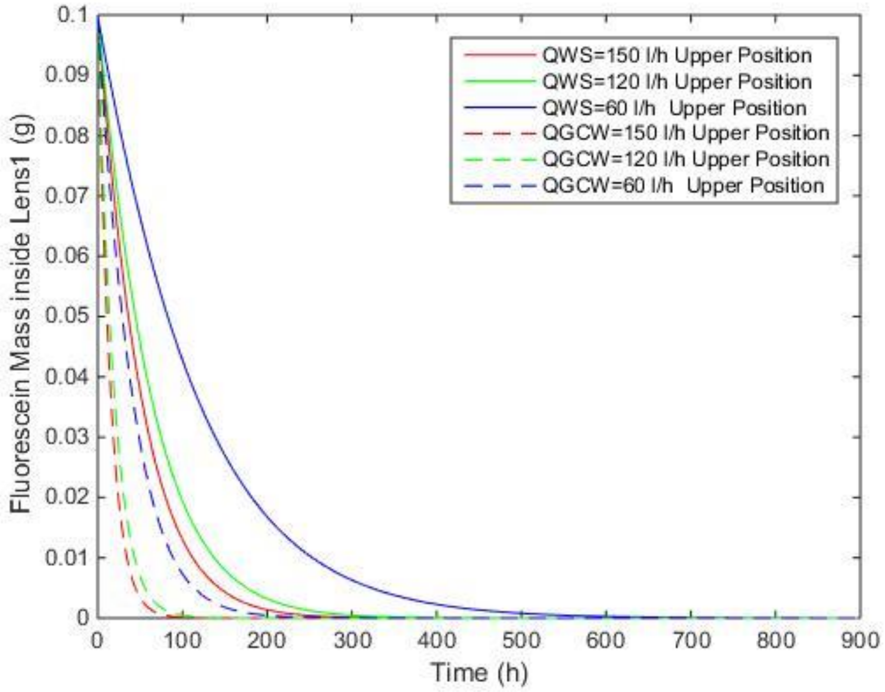

**(a)**

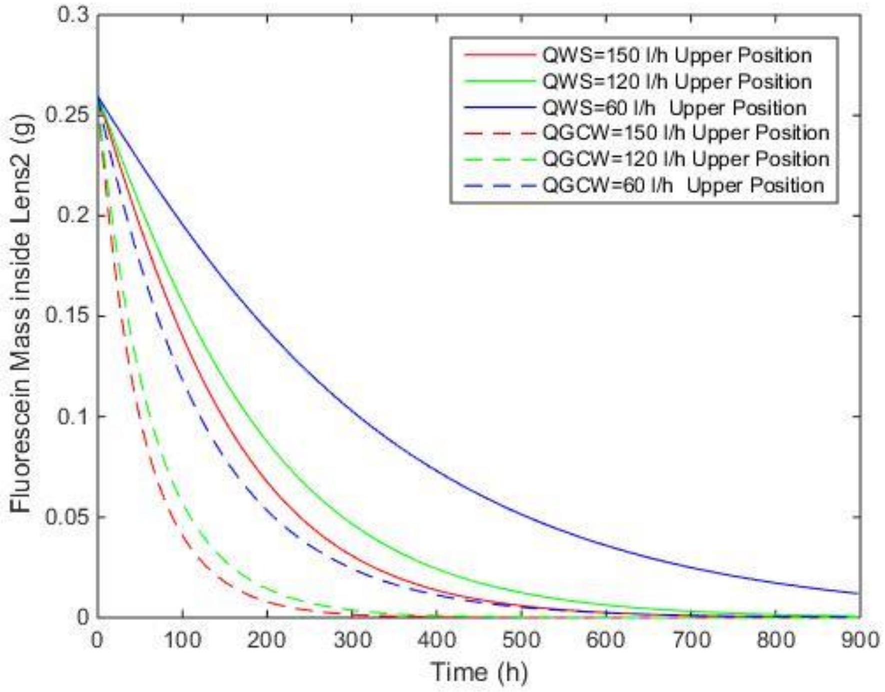

**(b)**

**Fig. 41:** Comparison between the trend of Fluorescein mass contained into the lens 1 (a) and the lens 2 (b) positioned near the top of the aquifer simulating the use of a GCW and of a standard well.

The GCW technology can be applied extracting/injecting water from two or more screen sections. In this study we have investigated the efficiency of a GCW characterized by three screen sections. In particular, we numerically simulated the laboratory test extracting contaminated water from the middle section of the GCW and injecting clean water from the lower and the upper screens.  In this way, the GCW develops two circulation patterns inside the aquifer (Fig. 42). As described for the previously tests, three simulations were carried out using different values of injected flow rate (Q=60 L/h, Q=120 L/h and Q=150 L/h). The numerical results were compared in Fig. 43 and they demonstrate a decrease in mass depletion time enhancing the circulation flow rate. This result agrees with the results obtained for the traditional well and for the GCW characterized by two screen sections. However, comparing the trend of Fluorescein released from the lenses using the two different models of GCW, the restoration of the low permeability lenses appears faster using a GCW characterized by two screen intervals. This result is correlated with the flow field developed by the Groundwater Circulation Well. The two circulation patterns developed using a GCW with three screen sections are characterized by a radius of influence smaller than that of the circulation pattern generated by a GCW with two screen sections. The low permeability lenses are close to the middle screen of the well and thus the principal component of the velocity field is parallel to the main axis of the lenses. To verify the efficiency of a GCW with three screen sections, the lenses were located at the bottom and at the top of the aquifer and their restoration was simulated (Fig.44). For both positions water was circulated using Q=60 L/h, Q=120 L/h and Q=150 L/h. For each lens and for each position the obtained results were compared with the corresponding results calculated using a GCW with two screen sections. As the Fig. 45 and the Fig. 46 show the remediation times of the two lenses result higher using a GCW with three screen sections. This result appears valid for both lenses and for both positions. Considering the small influence radius of the circulation pattern, the efficiency of a GCW with three screen sections was investigated locating the first lens closer to the well (Fig. 47). As the Fig. 48 shows, the remediation time of the first lens decreased and it appears similar than the corresponding time calculated using the GCW with two screen sections. The performed study demonstrates that the efficiency of the GCW characterized by three screen sections is generally lower than the efficiency of a GCW with two screen sections, because it is closely dependent on the position and on the orientation of the contaminated low permeability lenses.

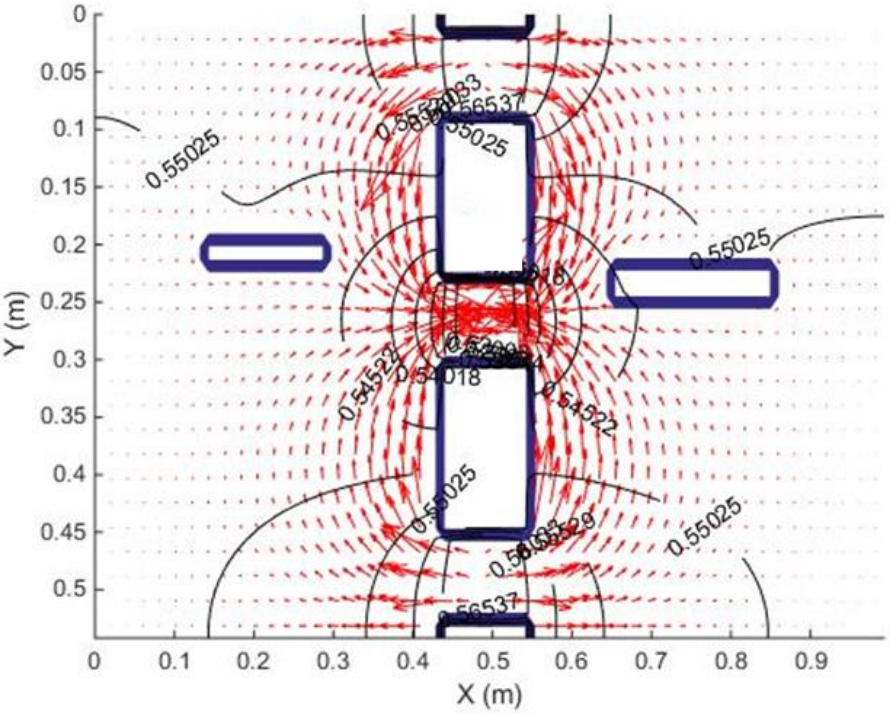

**(a)**

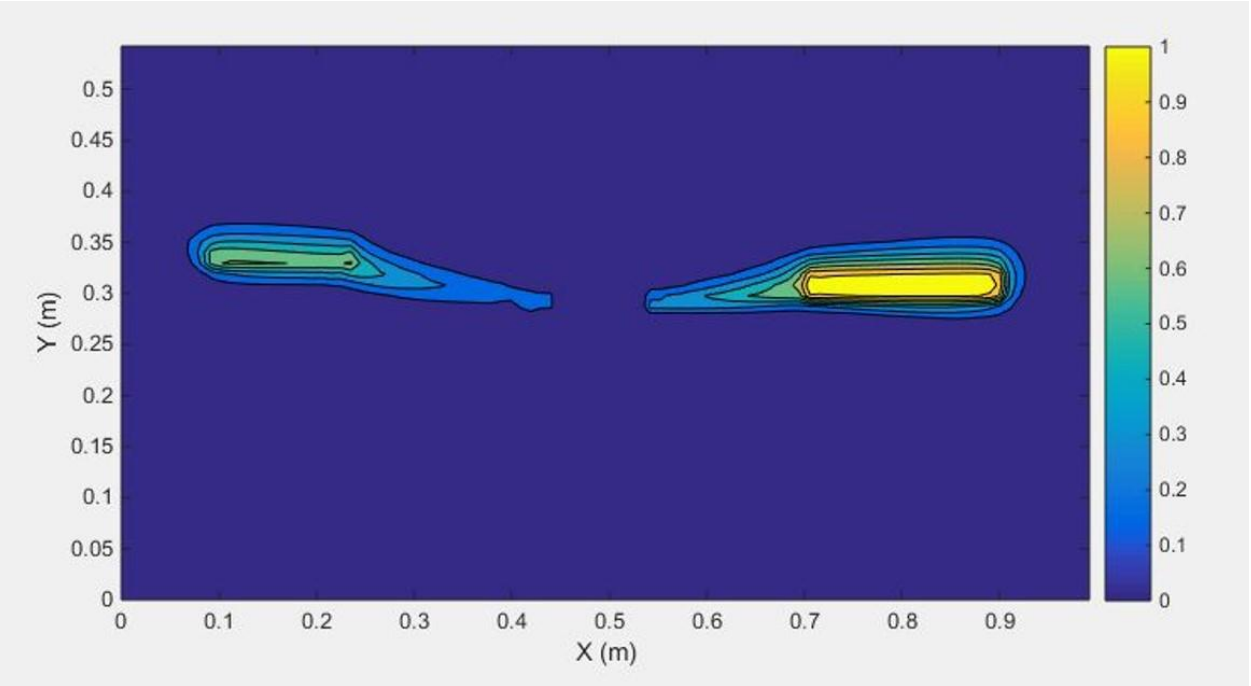

**(b)**

**Fig. 42:** The hydraulic head and the flow field simulated numerically using a GCW with three screen sections (GCW3) for the lenses positioned in the middle part of the aquifer (a). The corresponding concentration field obtained by the nemurical model (b).

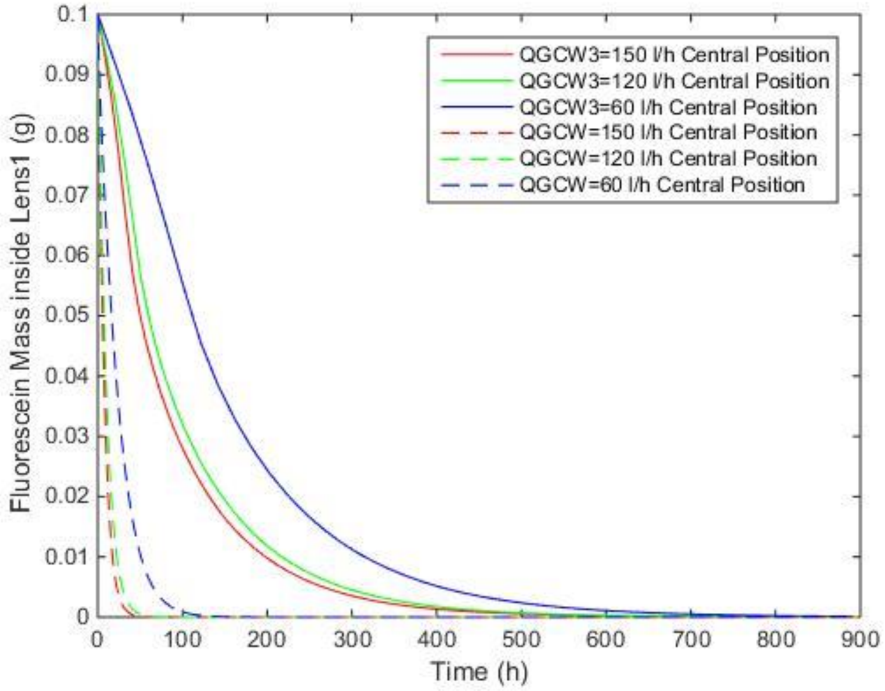

**(a)**

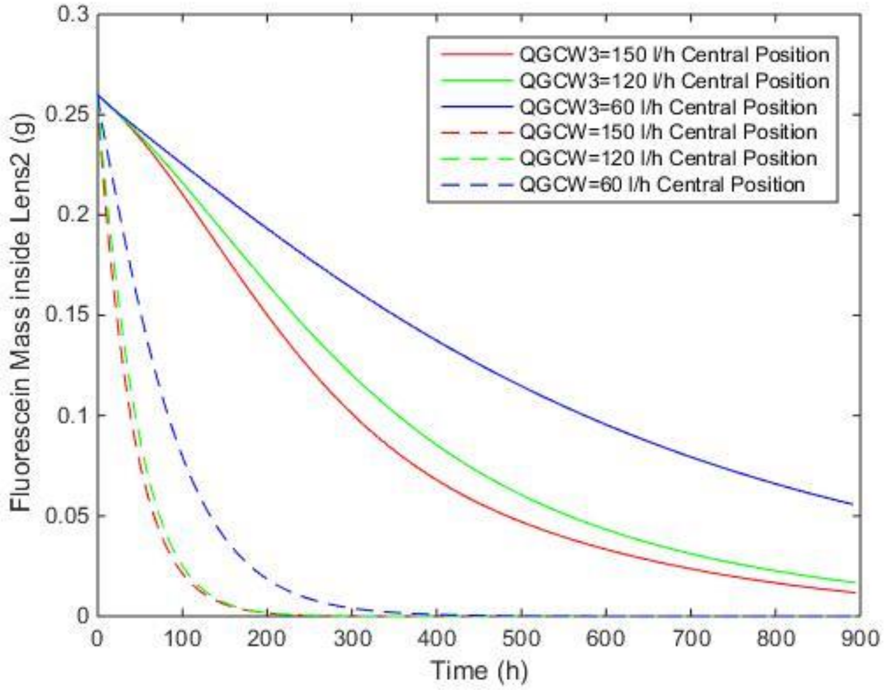

**(b)**

**Fig. 43:** Comparison between the trend of Fluorescein mass contained into the lens 1 (a) and the lens 2 (b) positioned in the middle part of the aquifer simulating the use of a GCW with two and three screen sections (GCW3).

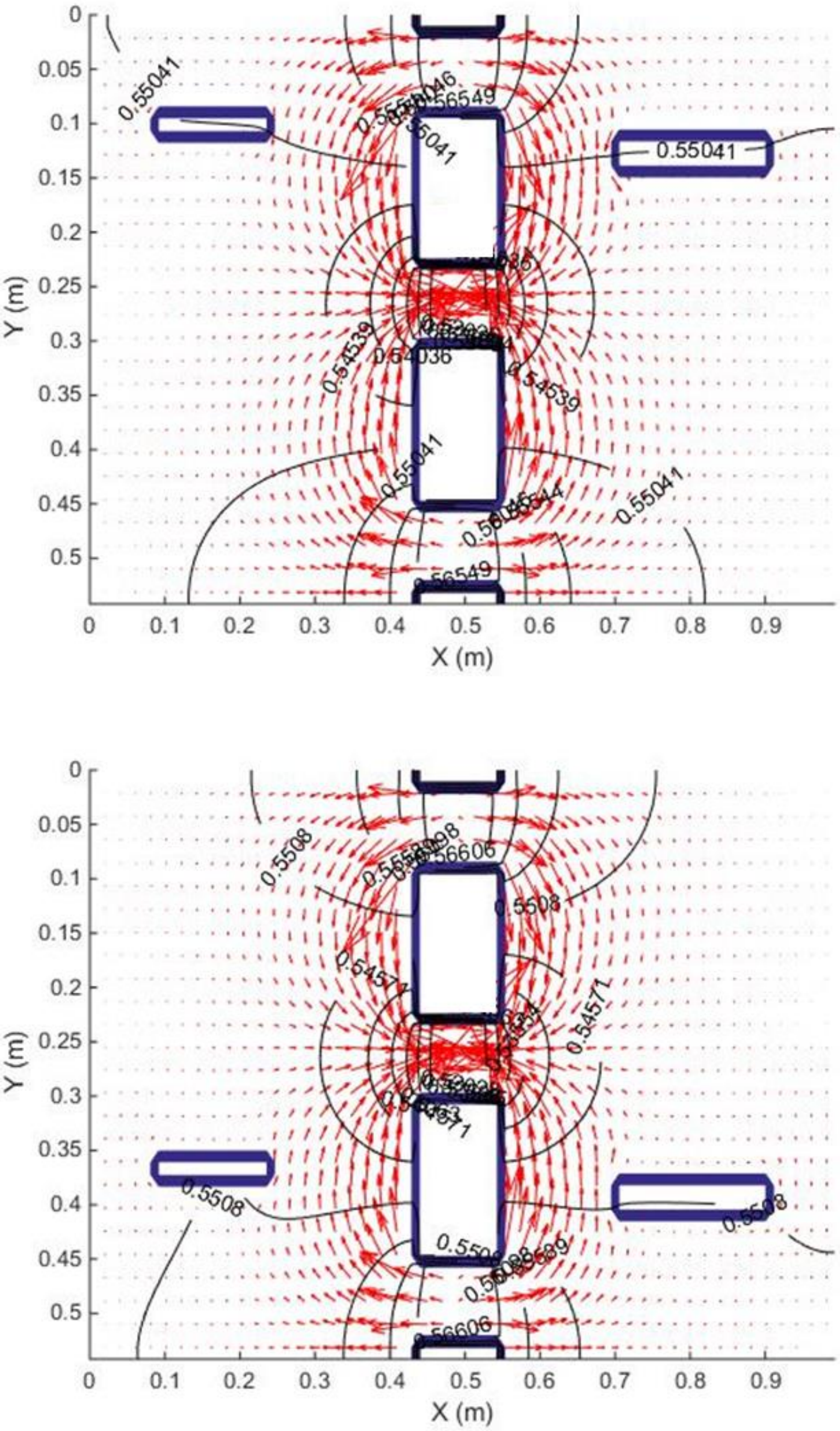

(a)

(b)

**Fig. 44:** The hydraulic head and the flow field simulated numerically using a GCW with three screen sections (GCW3) for the lenses positioned near the top (a) and bottom (b) part of the aquifer.

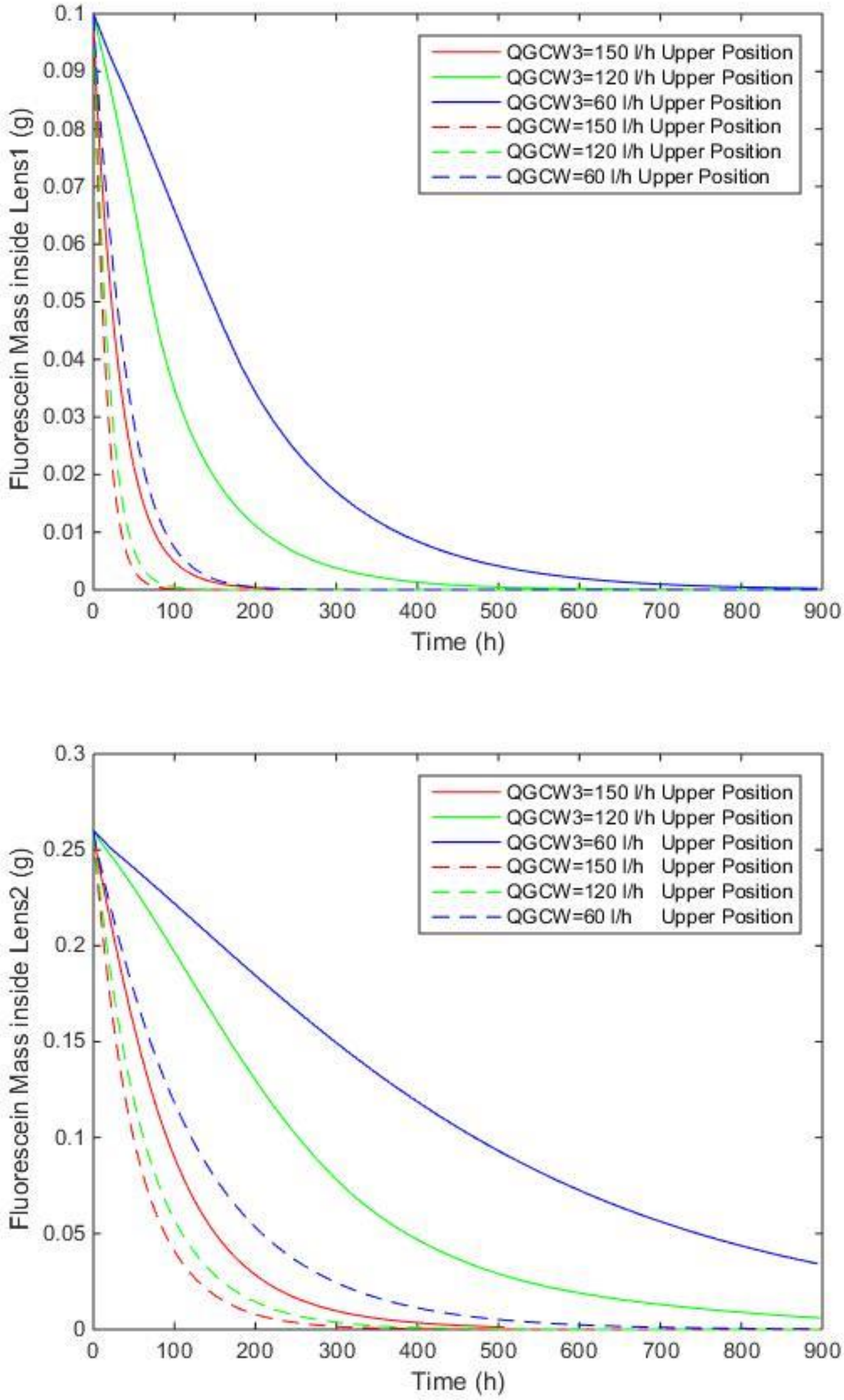

**(a)**

**(b)**

**Fig. 45:** The trend of Fluorescein mass contained into the lens 1 (a) and the lens 2 (b) positioned near the top of the aquifer simulating the use of a GCW with two and three screen sections (GCW3).

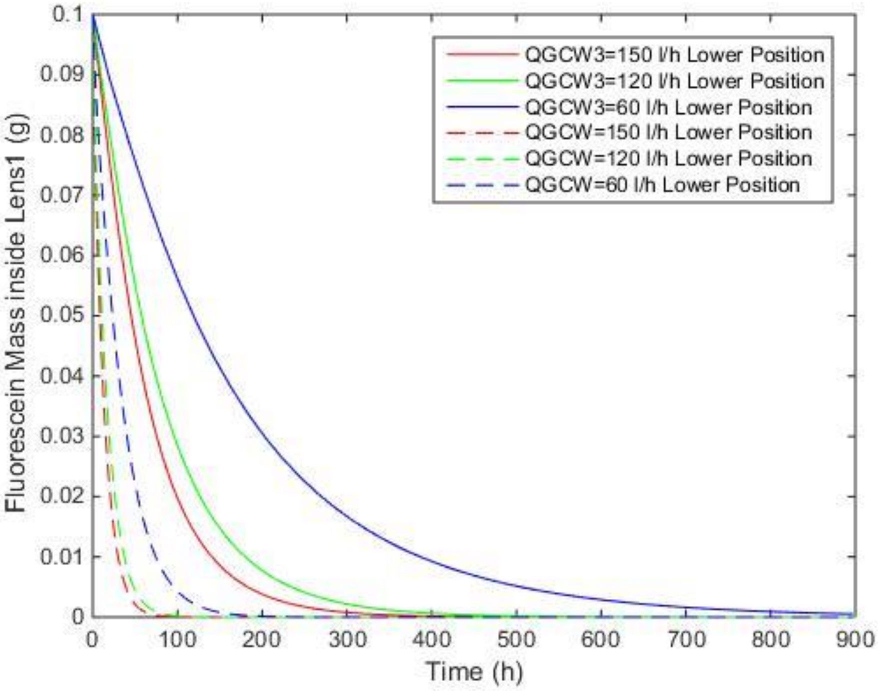

**(a)**

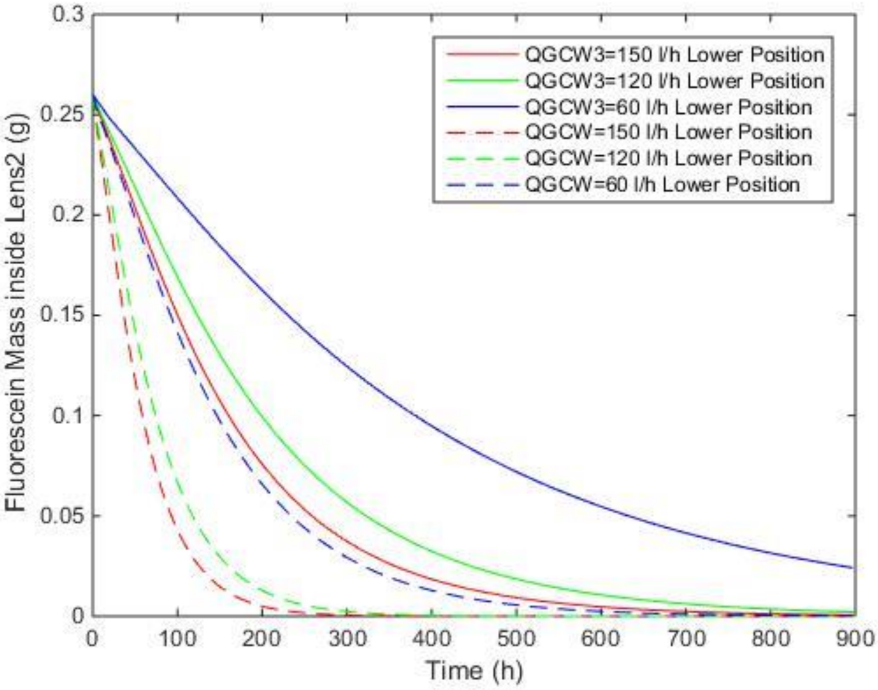

**(b)**

**Fig. 46:** The trend of Fluorescein mass contained into the lens 1 (a) and the lens 2 (b) positioned near the bottom of the aquifer simulating the use of a GCW with two and three screen sections (GCW3).

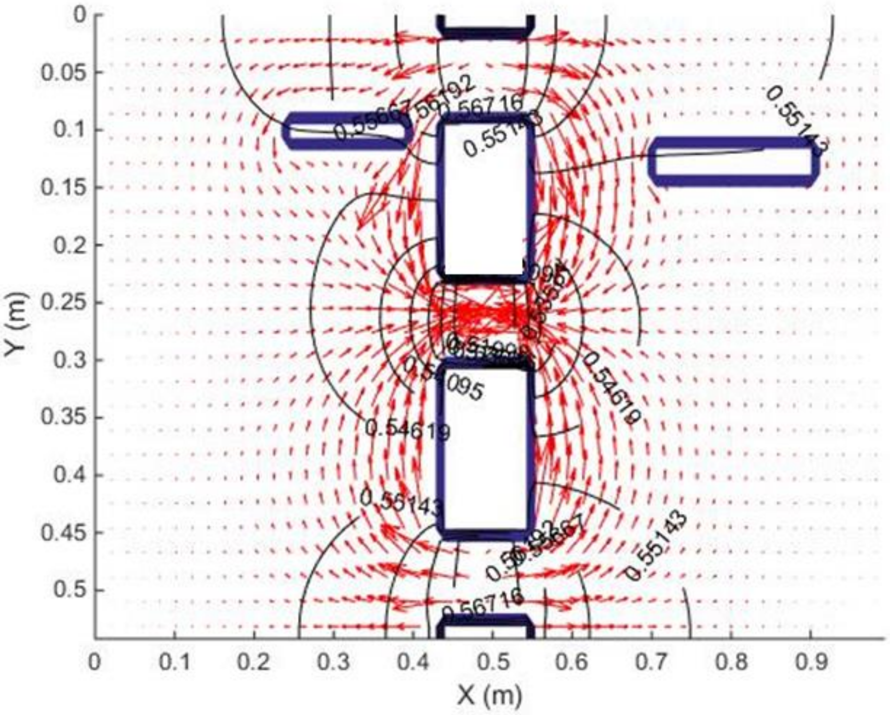

**Fig. 47:** The hydraulic head and the flow field simulated numerically using a GCW with three screen sections moving the first lens closer the GCW.

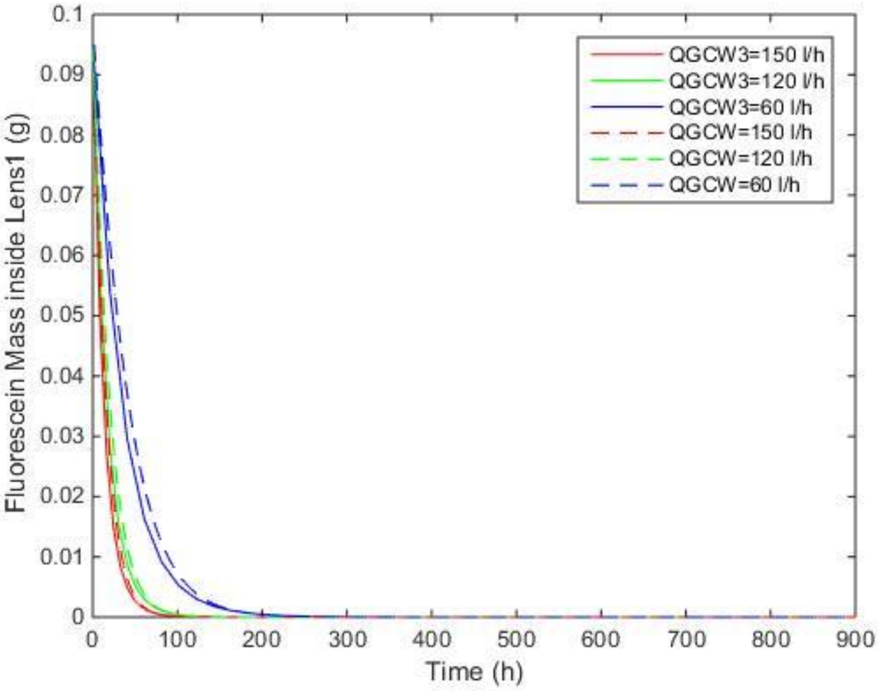

**Fig. 48:** The trend of Fluorescein mass contained into the lens 1 positioned close the well simulating the use of a GCW with two and three screen sections (GCW3).

# Conclusion

The aim of this thesis was to study the Back-Diffusion process from the lower permeability zones of aquifers in order to evaluate the best remediation strategies for these zones. The process is dominated by molecular diffusion and caused a long plume tail, today regarded as one of the main obstacles to effective groundwater remediation.

In the first chapter, the described laboratory test clearly showed the Back-Diffusion phenomenon and demonstrated the importance of aquifer heterogeneities during groundwater restoration. They can be considered long-lasting secondary sources of contamination, as observed in NAPLs sources. The measurement of contaminant fluxes released from the low permeability lenses permitted the analysis of the relation between the granulometry of the lenses and the Back-Diffusion process. The results show that the lower the average grain dimension of the formation is, the higher the flux is and the longer the time for which the values of the released concentration can constitute a source of contamination. This observation causes strong implications for the choice of remediation techniques, because they must be chosen by carefully considering the soil texture.

In the second chapter, the efficiency of the traditional pumping technology to restore contaminated low permeability zones of aquifer was investigated by laboratories tests. The results showed that enhancing groundwater velocity, the diffusive fluxes released by the lenses increase, but only during the first days of the redistribution process. This observation is related to the tracer distribution inside the lenses. At the beginning of the Back-Diffusion process, the tracer is present homogeneously inside the lenses and, when the concentration gradient between the low and high permeability zones is established, the outer layers of the lenses start to release contaminant. During this phase the impact of groundwater motion increases the concentration gradient at the interface thus facilitating the tracer flux released by the lenses. The decrease in tracer concentration in the outer layers establishes a concentration gradient inside the lens which by diffusive flux transports Fluorescein from the inner to the outer areas of the low-permeability zone. This process depends on grain size and its transport rate is generally lower if compared with the purely advective transport. Thus, the effect of enhanced groundwater velocity is negligible when low-permeability zones begin to release the tracer stocked in the inner part of their structure. This behavior is the main cause of Pump and Treat inefficiency to restore contaminated low-permeability zones in a short time. The traditional pumping technology also appear unable to treat NAPLs sources. Luciano et al., (2012) and Erning et al., (2011) observed only a moderate increase in the DNAPL dissolution rate due to enhanced groundwater velocity. These results demonstrate that the contamination tail due to long-lasting sources cannot be remediated solely by the mechanical enhancement of the flow velocity and therefore they prove the need to use alternative technologies.

In the third chapter, the Groundwater Circulation Well system was investigated as an alternative technology to improve the remediation of the contaminated low permeability zone of aquifers. The suitability of this system was studied using laboratory tests and numerical simulations. Results show that GCW develops a hydraulic gradient inside the aquifer which supports the diffusive flow into the lenses and removes the contaminant at the interface between the high and the low-permeability zones, increasing the flux of contaminant released by the lenses. The efficiency of the GCW system appears dependent on the position of the low permeability zones, but it seems always higher than traditional pumping technology one. The GCW performance results higher if water was extracted and injected using only two screen sections, because the developed circulation pattern appears to affect a larger zone of aquifers.

Further investigation can be performed regarding the use of a Groundwater Circulation Well in conjunction with other remediation technologies. Considering the importance of diffusive transport, the increase in temperature using electrical resistance can be shown to be an alternative technology to restore the low-permeability zones. In fact, it improves the diffusive flux released by low-permeability zones and, if the contaminant is biodegradable, it enhances the bioremediation of released pollutants in high-permeability aquifer layers (Beyke and Fleming 2005). These technologies have been widely used for in situ groundwater remediation and several studies were carried out concerning the enhanced bioremediation of chlorinated solvents and hydrocarbons (Scow and Hicks, 2005, Hood et al., 2008, Aulenta et al., 2005).

# References

Adamson, D. T., De Blanc, P. C., Farhat, S. K., Newell, C. J., 2016. Implications of matrix diffusion on 1,4-dioxane persistence at contaminated groundwater sites. J. of the Total Environment 562, 98-107.

ASTM D. Standard test method for particle-size analysis of soils. Annual Book of ASTM Standards, (2007).

Aulenta, F., Bianchi, A., Majone, M., Petrangeli Papini, M., Potalivo, M., Tandoi, V., 2005. Assessment of natural or enhanced in situ bioremediation at a chlorinated solvent-contaminated aquifer in Italy: a microcosm study. Environment International 3, 185-190.

Beyke, G., Fleming, D., 2005. In Situ Thermal Remediation of DNAPL and LNAPL Using Electrical Resistance Heating. Remediation DOI: 10.1002/rem.20047.

Brown, G. H., Brooks, M. C., Wood, A. L., Annable, M. D. & Huang, J., 2012. Aquitard contaminant storage and flux resulting from dense nonaqueous phase liquid source zone dissolution and remediation. Water Resource Research 48, W06531.

Carey, G. R., Chapman, W. S., Parker, B. L., McGregor, R., 2015. Application of an Adapted Version of MT3DMS for Modeling Back-Diffusion Remediation Timeframes. Remediation DOI: 10.1002/rem.

Carey, G. R., McBean, E. A., Feenstra, S., 2014. DNAPL Source Depletion: 2. Attainable Goals and Cost–Benefit Analyses. Remediation DOI: 10.1002/rem.

Catania, F., Massabo, M., Valle, M., Bracco, G. & Paladino O., 2008. Assessment of quantitative imaging of contaminant distributions in porous media. Exp. Fluids 44(1), 167–177.

Cavanagh, B. A., Johnson, P. C., Daniels, E. J., 2014. Reduction of Diffusive Contaminant Emissions from a Dissolved Source in a Lower Permeability Layer by Sodium Persulfate Treatment. Environ. Sci. Technol. 48, 14582−14589.

Cenedese, A., Viotti, P., 1996. Lagrangian analysis of nonreactive pollutant dispersion in porous media by means of the particle image velocimetry technique. Water Resour. Res. 32, 2329-2343.

Chapman, S. W., Parker, B. L., Sale, T. C. & Doner, L. A., 2012. Testing high resolution numerical models for analysis of contaminant storage and release from low permeability zones. Journal of Contaminant Hydrology 136–137, 106–116.

Chokejaroenrat, C., Comfortc, S., Sakulthaew, C., Dvoraka, B., 2014. Improving the treatment of non-aqueous phase TCE in low-permeability zones with permanganate. J. of Hazard. Mater. 268, 177–184.

Chowdhury, A. I. A., Gerhard, J. I., Reynolds, D., Sleep, B. E., O'Carroll, D. M., 2017. Electrokinetic-enhanced permanganate delivery and remediation of contaminated low-permeability porous media. Water Res. 113, 215-222, http://dx.doi.org/10.1016/j.watres.2017.02.005.

Citarella, D., Cupola, F., Tanda, M. G., Zanini, A., 2015. Evaluation of dispersivity coefficients by means of a laboratory image analysis. J. of Contam. Hydrol. 172, 10–23.

Clifton, L. M., Dahlen, P. R., Johnson, P. C., 2014. Effect of Dissolved Oxygen Manipulation on Diffusive Emissions from NAPL-Impacted Low-permeability Soil Layers. Environ. Sci. Technol. 48, 5127−5135.

Cupola, F., Tanda, M. G., Zanini, A., 2015. Laboratory Estimation of Dispersivity Coefficients. Procedia Environmental Sciences 25, 74–81.

Elmore, A. C., P.E., Member, ASCE, Hellman, J. B., 2001. Model-Predicted Groundwater Circulation Well Performance. Pract. Period. Hazard. Toxic Radioact. Waste Manage., 5 (4).

Erning, K., Schäfer, D., Dahmke, A., Luciano, A., Viotti, P., Petrangeli Papini, M., 2011. Simulation of DNAPL distribution dependings on groundwater flow velocities using TMVOC. IAHS Publ 342.

Falta, R. W., Basu, N. & Rao, P. S., 2005. Assessing impacts of partial mass depletion in DNAPL source zone: II. Coupling source strength functions to plume evolution. Journal of Contaminant Hydrology 79, 45–66.

Gill, R. T., Thornton, S. F., Harbottle, M. J., Smith, J. W. N., 2015. Electrokinetic Migration of Nitrate Through Heterogeneous Granular Porous Media. Ground Water. Monit. Rem. 35, 46–56.

Hadley, P., Newel, C., 2014. The New Potential for Understanding Groundwater Contaminant Transport. Groundwater, 52 (2),174-186.

Hood, E. D., Major, D. W., Quinn, J.W., Yoon, W.-S., Gavaskar, A., Edwards, E. A., 2008. Demonstration of Enhanced Bioremediation in a TCE Source Area at Launch Complex 34, Cape Canaveral Air Force Station. Ground Water. Monit. Rem. 28, 98-107.

Huang, W.E., Smith, C. C., Lerner, D. N., Thornton, S. F., Oram, A., 2002. Physical modelling of solute transport in porous media: evaluation of an imaging technique using UV excited fluorescent dye. Water Res. 36, 1843–1853.

Jaeger, S. et al., 2009. CCD camera Image Analysis for mapping solute concentrations in saturated porous media. Analalytical Bioanalytical Chemistry 395, 1867–1876.

Jones, E. H. & Smith, C. C., 2015. Non-equilibrium partitioning tracer transport in porous media: 2-D physical modelling and imaging using a partitioning fluorescent dye. Water Research 39, 5099–5111.

Johnson, R. L., Simon, M. A., 2007. Evaluation of groundwater flow patterns around a dual-screened groundwater circulation well. Journal of Contaminant Hydrology, 93, 188-202.

Konz, M. et al., 2008. On the measurement of solute concentrations in 2-D flow tank experiments. Hydrology and Earth System Sciences 12, 727–738.

Konz, M., Ackerer, P., Huggenberger, P. & Veit, C., 2009. Comparison of light transmission and reflection techniques to determine concentrations in flow tank experiments. Exp Fluids 47, 85–93.

Liu, C., Ball, W. P., 2002. Back Diffusion of chlorinated solvent contaminants from a natural aquitard to a remediated aquifer under well controlled filed conditions: predictions and measurements. Ground Water 40(2), 175–184.

Luciano, A., Viotti, P., Petrangeli Papini, M., 2012. On Morphometric Properties of DNAPL Sources: Relating Architecture to Mass Reduction. Water, Air, & Soil Pollut. DOI 10.1007/s11270-011-1071-7.

Luciano, A., Viotti, P., Petrangeli Papini, M., 2010. Laboratory investigation of DNAPL migration in porous media. J. of Hazard. Mat. 176, 1006–1017.

Mackay, D. M., Cherry, J. A., 1989. Groundwater contamination: pump-and treat remediation. Environ. Sci. Technol. 23 (6), 630–636.

McNeil, J. D., Oldenborger, G. A. & Schincariol, R. A., 2006. Quantitative imaging of contaminant distributions in heterogeneous porous media laboratory experiments. Journal of Hydrology 84, 36–54.

Miller, G. R., ASCE, A. M., Elmore, A. C., 2005, Modeling of a Groundwater Circulation Well Removal Action Alternative. Pract. Period. Hazard. Toxic Radioact. Waste Manage., 9(2), 122-129.

Mohrlok, U., Kirubaharan, C. S., Eldho, T. I., 2010. Transport characteristic in a 3D groundwater circulation flow field by experimental and numerical investigation. Practice periodical of hazardous, toxic, and radioactive waste management 14 (3), 185-194.

Parker, B. L., Chapman, S. W., Guilbeault, M. A., 2008. Plume persistence caused by back diffusion from thin clay layers in a sand aquifer following TCE source-zone hydraulic isolation. J. of Contam. Hydrol. 102, 86–104.

Parker, B. L., Chapman, S. W., Guilbeault, M. A., 2005. Plume persistence due to aquitard back diffusion following dense nonaqueous phase liquid source removal or isolation. Water Resour. Res. 41.

Rolle, M., Chiogna, G., Hochstetler, D. L. & Kitanidis, P. K., 2013. On the importance of diffusion and compound-specific mixing for groundwater transport: An investigation from pore to field scale. Journal of Contaminant Hydrology 153, 51–68.

Ross, D., Gary, R. W., 1992. Prediction of Flow and Hydraulic Head Fields for Vertical Circulation Wells. Ground Water, 30 (5).

Sabatini, D. A., Al Austin, T., 1991. Characteristics of Rhodamine WT and Fluorescein as Adsorbing Ground-Water Tracer. Ground Water 29(3), 341–349.

Sabatini, D. A., 2000. Sorption and Intraparticle Diffusion of Fluorescent Dyes with Consolidated Aquifer Media. Ground Water 38, 651-656.

Sale, T. C., Zimbron, J. A., Dandy, D. S., 2008. Effects of reduced contaminant loading on downgradient water quality in an idealized two-layer granular porous media. J. of Contam. Hydrol. 102, 72-85.

Scholz, M., Weber, O., Mohrlok, U., Eldho, T. I., 1998. Large scale experiments for in situ flushing using groundwater circulation wells: identification of processes and limiting parameters. Groundwater Quality: Remediation and Protection (Proceedings of the GQ'98 Conference held at Tubingen, Germany, September 1998). IAHS Publ. no. 250, 1998.

Scow, K. M., Hicks K. A., 2005. Natural attenuation and enhanced bioremediation of organic contaminants in groundwater. Current Opinion in Biotechnology 16, 246–253.

Seyedabbasi, M. A., Newell, J. C., Adamson, D. T., Sale, T. C., 2012. Relative contribution of DNAPL dissolution and matrix diffusion to the long-term persistence of chlorinated solvent source zones. J. of Contam. Hydrol. 134–135, 69–81.

Simon, F. G., Meggyes T., Tünnermeier, T. Groundwater remediation using active and passive processes. Federal Institute for Materials Research and Testing (BAM), Unter den Eichen 87, D-12205 Berlin, Germany.

Southard, J., 2006. Introduction to Fluid Motions, Sediment Transport, and Current-Generated Sedimentary Structures. Massachusetts Institute of Technology: MIT OpenCourseWare, https://ocw.mit.edu. License: Creative Commons BY-NC-SA.

Tatti, F., Petrangeli Papini, M., Raboni, M., Viotti, P., 2016. Image analysis procedure for studying Back-Diffusion phenomena from low-permeability layers in laboratory tests. Sci. Rep. 6, 30400; doi: 10.1038/srep30400.

Tatti, F., Petrangeli Papini, M., Sappa, G., Raboni, M., Arjmand, F., Viotti, P., 2018. Contaminant back-diffusion from low-permeability layers as affected by groundwater velocity: A laboratory investigation by box model and image analysis. Science of the Total Environment 622–623, 164–171.

Theodoropoulou, M. A., Karoutsos, V., Kaspiris, C. & Tsakiroglou, C. D., 2003. A new visualization technique for the study of solute dispersion in model porous media. Journal of Hydrology 274(1–4), 176–197.

United States Environmental Protection Agency, 1998. Field Applications of In Situ Remediation Technologies: Ground-Water Circulation Wells. EPA-542-R-98-009.

Wang, H., Chen, X. & Jawtz, W., 2008. Locally-calibrated light transmission visualization methods to quantify nonaqueos phase mass in porous media. Journal of Contaminant Hydrology 102, 29–38.

Werth, C. J., Zhang, C., Brusseau, M. L., Oostrom, M. & Baumann, T., 2010. A review of non-invasive imaging methods and applications in contaminant hydrogeology research. Journal of Contaminant Hydrology 113, 1–24.

Wilking, B. T., Rodriguez, D. R. & Illangasekare, T. H., 2013. Experimental Study of the Effects of DNAPL Distribution on Mass Rebound. Ground Water 51(229), 236.

Wilson, J. L., 1997. Removal of aqueous phase dissolved contamination: Non-chemically enhanced pump and treat, in Subsurface Restoration. CRC Press, Boca Raton, 271-285.

Yang, M., Annable, M. D., Jawitz, J. W., 2014. Light reflection visualization to determinate solute diffusion into clays. J. of Contam. Hydrol. 161, 1-9.

Zinn, B., Meigs, L. C., Harvey, C. F., Haggerty, R., Peplinski, W. J., Freiherr Von Schwerin, C., 2004. Experimental Visualization of Solute Transport and Mass Transfer Processes in Two-Dimensional Conductivity Fields with Connected Regions of High Conductivity. Environ. Sci. Technol. 38, 3916-3926.